TÉCNICO LISBOA

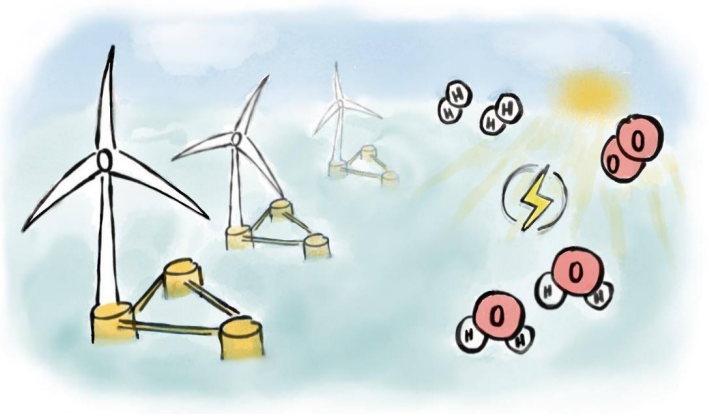

Feasibility of Wind Energy for Hydrogen Production: the WindFloat Atlantic case-study

Tiago José Rosário Lucas

Thesis to obtain the Master of Science Degree in

Mechanical Engineering

Supervisors: Dr. Ana Filipa da Silva Ferreira
Prof. Ricardo Balbino Santos Pereira

Examination Committee

Chairperson: Prof. Edgar Caetano Fernandes
Supervisor: Prof. Ricardo Balbino Santos Pereira
Member of the Committee: Dr. Rui Pedro da Costa Neto

January 2021

Acknowledgments

First, I want to thank Prof. Ricardo Pereira for having embraced the supervision of my dissertation. I had opportunity to have him as Professor in the course of Offshore Wind Energy, one of the most interesting courses I had in IST, where I learnt more about the emergent topic of floating wind technology. The chosen subject was suggested by Dr. Marco Alves from WavEC, who also agreed to supervise and whom I also thank for the important feedback he gave.

Then, I also want to thank Prof. Ana Filipa Ferreira, who enthusiastically accepted to supervise my dissertation on the topic of green hydrogen. Week by week, during an atypical year characterized by the lock-down months and Zoom meetings, together with Prof. Ricardo, Prof. Ana was always there to give her feedback and to share her knowledge, contributing to the best dissertation course.

I really appreciate the time they dedicated to me, and I wish the very best for them, academic and personally.

Last, but not the least, I want to thank all my family, friends, colleagues and Professors that contributed to what I am today, over these academic years in IST.

Abstract

Green hydrogen production is regarded as a promising solution to solve some of the main challenges of energy transition. Additionally, floating offshore wind market has been deployed unveiling a window for the growth of wind energy. In 2020, WindFloat Atlantic, a floating wind farm, was commissioned in Portugal. In this study two scenarios are considered to analyse the feasibility of this wind farm for hydrogen production considering a PEM electrolyzer system (*Siemens* Silyzer-300). The first scenario assumes the current farm's load capacity of 25.2 MW with a 17.5 MW electrolyzer module. The second considers a long-term commercial phase of 150 MW with an electrolyzer system of 140 MW, integrated in a developed hydrogen economy with pipelines for H_2 distribution. The study considers the production either during nights (Case A), or nights and afternoons (Case B), considering the wholesale electricity market of 2019. Case B and oxygen sales contribute to a more feasible project. Considering only Case B, H_2 selling price of 8 €/kg, discount rate (10%) and corporate tax (21%), results show that scenario 2, due to the long-term lower costs, is the only feasible solution. Scenario 1 could be suitable with governmental incentives. Different plant power ratios (PPRs), *i.e.* different ratios between the H_2 plant and wind farm load capacities, are compared and show that PPR is a significant parameter on H_2 production cost. This study also analyzes the influence of wind turbulence in the generated power of IEA-15 MW wind turbine on a semi-submersible platform using openFAST software.

Keywords: hydrogen production feasibility, PEM electrolysis, wind energy, WindFloat Atlantic

Resumo

A produção de hidrogénio verde é considerada uma solução promissora para resolver alguns dos principais desafios da transição energética. Ademais, o mercado eólico *offshore* flutuante surge como uma porta para o crescimento da energia eólica. Em 2020, o parque eólico flutuante *WindFloat Atlantic* foi construído em Portugal. Nesta dissertação, dois cenários são considerados para estudar a viabilidade deste parque para a produção de hidrogénio, considerando um sistema de eletrólise *PEM* (*Siemens* Silyzer-300). O primeiro cenário assume a capacidade de carga do actual parque ($25.2\ \mathrm{MW}$) com um módulo de electrólise de $17.5\ \mathrm{MW}$. O segundo considera uma fase comercial a longo prazo de $150\ \mathrm{MW}$ com um sistema de electrolisadores de $140\ \mathrm{MW}$, integrado numa economia de hidrogénio mais desenvolvida onde existem condutas para distribuição. É considerada a produção quer durante as noites (Caso A), quer durante as noites e tardes (Caso B), assumindo o mercado grossista de electricidade de 2019. O Caso B e a venda de oxigénio contribuem para um projecto mais viável. Considerando apenas o Caso B, o preço de venda de $8\ €/\mathrm{kg}$, a taxa de actualização (10%) e o IRC (21%), os resultados mostram que o Cenário 2, devido aos custos mais baixos a longo prazo, é a única solução viável. O Cenário 1 poderia ser lucrativo com incentivos governamentais. Diferentes *plant power ratios* (PPRs), *i.e.* diferentes rácios entre as capacidades de carga da central de H_2 e do parque eólico, são comparados e mostram que o PPR é um parâmetro significativo no custo da produção de hidrogénio. Esta dissertação também analisa a influência da turbulência do vento na potência gerada pela turbina eólica *IEA*-$15\ \mathrm{MW}$ numa plataforma semi-submersível, utilizando o *software openFAST*.

Palavras-chave: eletrólise *PEM*, energia eólica, produção de hidrogénio, WindFloat Atlantic

Contents

List of Tables

List of Figures

Nomenclature

Acronyms

AC	Alternate Current.
AE	Alkaline Electrolyzer.
AEM	Anion Exchange Membrane.
ATR	Autothermal Reformer.
BEM	Blade Element Momentum.
CAPEX	Capital Expenditure.
CCS	Carbon Capture and Storage.
CCUS	Carbon Capture, Utilization and Storage.
DC	Direct Current.
DOF	Degree of Freedom.
EAT	Earnings after taxes.
EBT	Earnings before taxes.
EN-H_2	*Estratégia Nacional para o H_2.*
EU	European Union.
FAST	Fatigue, Aerodynamics, Structures and Turbulence.
FCEV	Fuel Cell Electric Vehicle.
FF	Full-Field.
FOWT	Floating Offshore Wind Turbine.
FWT	Floating Wind Turbine.
GWA	Global Wind Atlas.
GWEC	*Global Wind Energy Council*.

HDPE	High Density Polyethylene.
HHV	High Heating Value.
HVAC	High-Voltage Alternating Current.
IEA	International Energy Agency.
IRC	*Imposto sobre o Rendimento de Pessoas Colectivas*.
IRENA	*International Renewable Energy Agency*.
JONSWAP	Joint North Sea Wave Observatory Project.
LCOE	Levelized Cost of Energy.
LCOH	Levelized Cost of Hydrogen.
LFL	Lower Flammable Limit.
LHV	Low Heating Value.
MD	Membrane Distillation Process.
MEA	Membrane Electrode Assembly.
MIBEL	*Mercado Ibérico de Electricidade*.
NL	Nominal Load.
NPV	Net Present Value.
NREL	National Renewable Energy Laboratory.
OMIE	*Operador de Mercado Ibérico Espanhol*.
OPEX	Operational Expenditure.
P-M	Pierson-Moskowitz.
PEM	Proton Exchange Membrane Electrolyzer.
PNEC2030	*Plano de Energia e Clima 2030*.
POR	Partial Oxidation Reformer.
PPR	Plant Power Ratio.
REN	*Redes Energéticas Nacionais*.
RNC2050	*Roteiro para a Neutralidade Carbónica 2050*.
SMR	Steam Methane Reformer.
SOEC	Solid Oxide Electrolyzer.

SPE	Solid Polymer Electrolyte.
T&D	Transmission and Distribution.
TDS	Total Dissolved Solid Units.
TLP	Tension Leg Platform.
TSR	Tip Speed Ratio.
UF	Ultrafiltration Process.
UFL	Upper Flammable Limit.
UV	Ultraviolet.

Symbols

Greek symbols

ΔG	Gibb's free energy variation.
ΔH	Enthalpy variation.
ΔS	Entropy variation.
η_E	Electrolyser efficiency.
η_F	Faraday or current efficiency.
ρ	Density.

Roman symbols

$\dot{C}_{\mathrm{stack}}$	Stack replacement cost per operating hour.
$\mathrm{C1}_{5h}$	Five hours night interval (Case 1).
$\mathrm{C2}_{4h}$	Four hours afternoon interval (Case 2).
C_p	Power coefficient.
C_t	Difference between inflows and cash out.
$c_{\mathrm{H_2}}$	Hydrogen production cost.
$c_{\mathrm{O_2}}$	Impact of O_2 sales in the hydrogen production cost.
C_{E}	Electrolyser energy consumption per unit volume of H_2.

$c_{\mathrm{H_2O}}$	Water cost.
$c_{\mathrm{H_2/O_2}}$	Hydrogen production cost including oxygen sales.
$e_{\mathrm{cons.}}$	Electricity consumption power.
e_{comp}	Compressor specific energy consumption.
e_{Silyzer}	Electrolyser Silyzer 300 specific energy consumption.
F	Faraday constant.
$f_{\mathrm{H_2}}$	Hydrogen production rate.
H_s	Significant wave height.
h_{min}	Hour with the minimum average electricity price.
I_{cell}	Cell current.
N_{cell}	Number of cells.
P	Power.
$P_{\mathsf{H_2}}$	Hydrogen production power.
$p_{\mathsf{O_2}}$	Oxygen selling price.
p_{elec}	Electricity price.
Q	Thermal energy.
$Q_{\mathrm{H_2}}$	Quantity of produced H_2.
$\%\,\mathrm{Ren}$	Percentage of renewable production under all electricity demand.
r	Rate of discount.
R_w	Wind farm's rate of capacity.
T	Process temperature.
T_p	Wave peak period.
u_w	Longitudinal wind component.
u_{hub}	Wind velocity at hub height.
$V_{\Delta H}$	Enthalpy voltage.
$v_{\mathrm{H_2O}}$	Volume of water consumption per kg of hydrogen.
V_{act}	Activation overvoltage.
V_{cell}	Cell voltage.

V_{con}	Concentration overvoltage.
V_{ohm}	Ohmic overvoltage.
V_{rev}	Reversible cell voltage.
V_{tn}	Thermo-neutral voltage.

Chapter 1

Introduction

This first chapter describes the circumstances that motivated the thesis' main objectives. In the end an overview of the work is provided.

1.1 Motivation

The European Union has different energy sources for energy production: solid fossil fuels, natural gas , crude oil, nuclear energy and renewable energy (such as hydro, wind and solar energy). Fig. 1.1 shows that renewable energy held the largest share ($34.3\ \%$) of energy production of EU in 2018 [1].

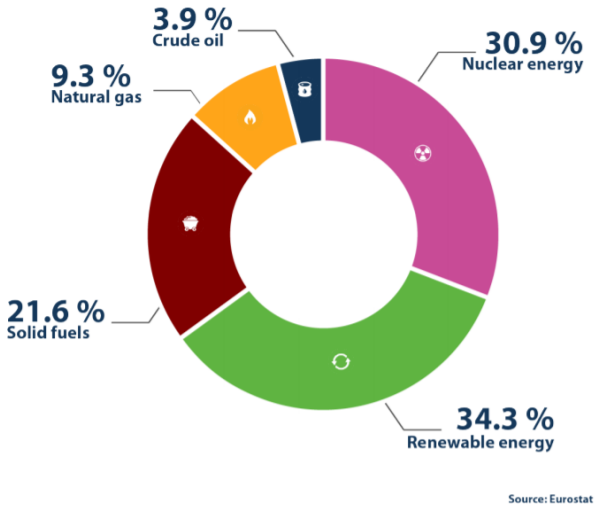

Figure 1.1: Share of EU energy production by source, 2018, from [1].

Energy sector of renewable sources is growing further and a big effort has been done either to correspond the energy transition goals or to decrease the energy dependence. In the case of Portugal, taking advantage of the natural resources it has, such as wind, sun and ocean, shall be part of the solution.

Currently, Portugal is one of the EU Member States with the biggest share of renewable production [1]. The evolution of energy production in mainland Portugal is presented in the next Fig. 1.2. In 2019,

$56\ \%$ of the electricity production corresponded to renewables [2].

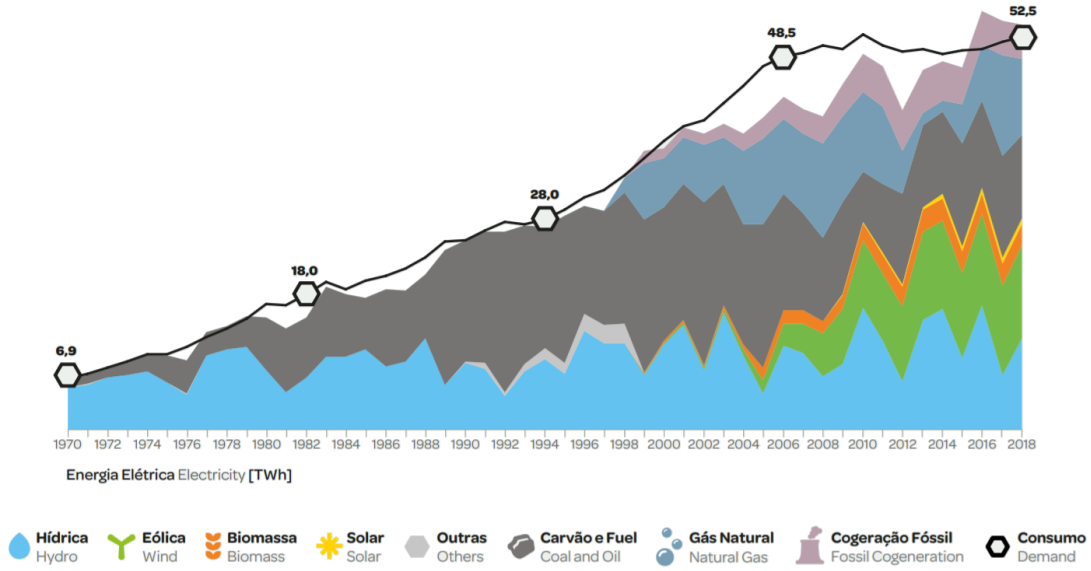

Figure 1.2: Evolution of the electricity production in mainland Portugal, from [3].

Energy transition urgency is mainly due to the accelerating climate change in the recent years. The average global temperature has been increasing, surpassing the value of the pre-industrial baseline by $1.04\,^{\circ}\mathrm{C}$ [4]. To avoid the emission of greenhouse gases, under the Paris Agreement of keeping the global temperature increase below $2\,^{\circ}\mathrm{C}$, the European Union implemented a long-term strategy of total decarbonization by 2050 – the European Green Deal [5]. Within this strategy, there are seven main building blocks [6]:

- Maximize the benefits of energy efficiency, including zero emission buildings;
- Maximize the deployment of renewables and the use of electricity to fully decarbonize European energy supply;
- Embrace clean, safe and connected mobility;
- A competitive EU industry and the circular economy as a key enabler to reduce GHG emissions;
- Develop an adequate smart network infrastructure and interconnections;
- Reap the full benefits of bio-economy and create essential carbon sinks;
- Tackle remaining CO_2 emissions with Carbon Capture and Storage (CCS).

Within the deployment of renewables, wind technology has evolved and new offshore sites have appeared as better places to produce electricity with wind energy. The most convenient sites to explore wind energy from onshore and shallow-water offshore conditions in Europe have been already explored [7] [8]. Thus, for deeper waters sites, floating offshore wind technologies are the solution to unlock the full potential of the offshore wind market [8]. Consequently, some floating prototypes have been

developed to validate and prepare a possible future FOWT farm, such as the WindFloat, Hywind and Blue H [9].

Since 2013, the global offshore market grew on average $24\ \%$ each year, reaching $6.1\ \mathrm{GW}$ of new installations in 2019 (Fig. 1.3), although only $11.4\ \mathrm{MW}$ of this value represented the installed floating wind technology ($8.4\ \mathrm{MW}$ from Portugal and $3\ \mathrm{MW}$ from Japan) [10]. Globally, until 2019, $65.9\ \mathrm{MW}$ of floating wind were already installed, $32\ \mathrm{MW}$ of which are located in the UK, $10\ \mathrm{MW}$ in Japan, $10.4\ \mathrm{MW}$ in Portugal, $2.3\ \mathrm{MW}$ in Norway and $2\ \mathrm{MW}$ in France [10].

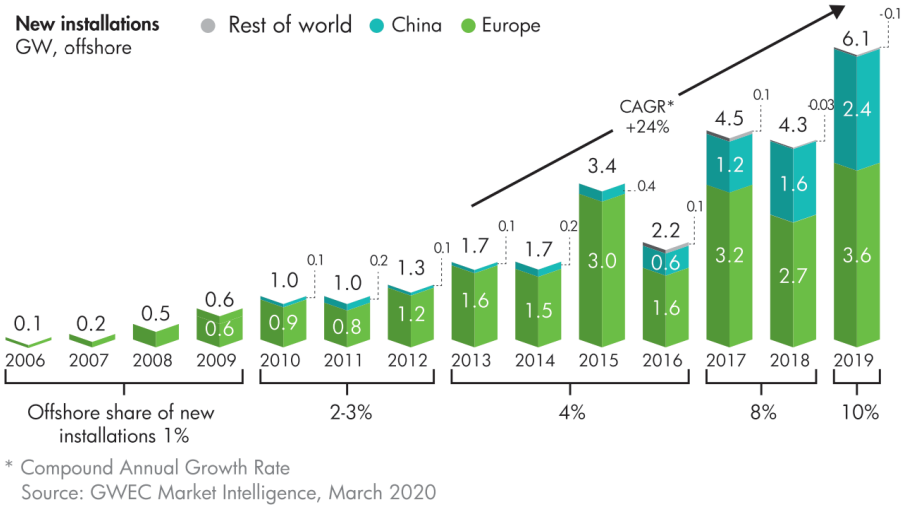

Figure 1.3: New offshore wind installations until 2019, from [10].

The Global Wind Energy Council [10] presents the expected growth for the next ten years. It is expected that over $205\ \mathrm{GW}$ of new offshore wind capacity will be added. In 2019, the offshore wind corresponded to $10\ \%$ of the new wind power installations, while in 2025 is expected to represent more than $20\ \%$ of the new installations. Figs. 1.4 and 1.5 show the outlook of the market growth until 2030 for both global offshore wind and floating offshore wind specifically.

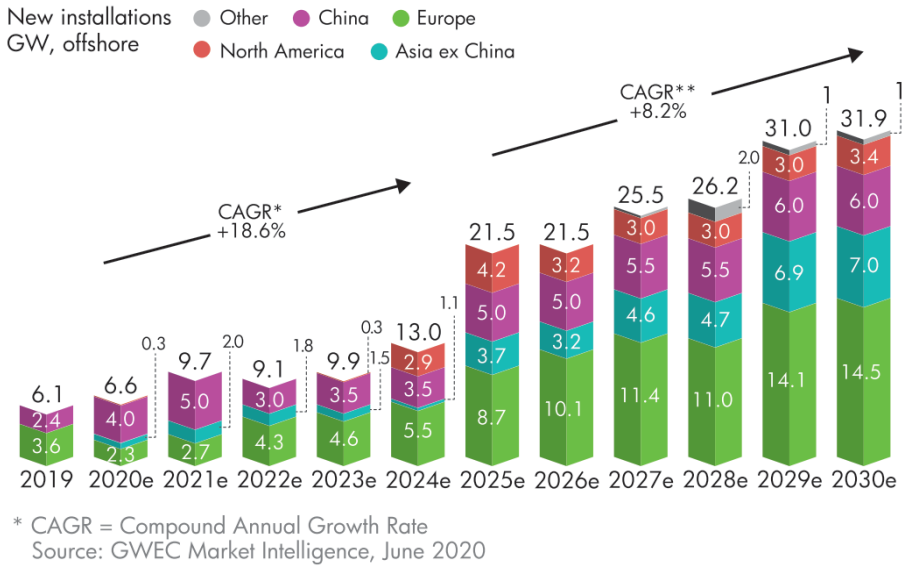

Figure 1.4: Prevision of new offshore wind installations, from [10].

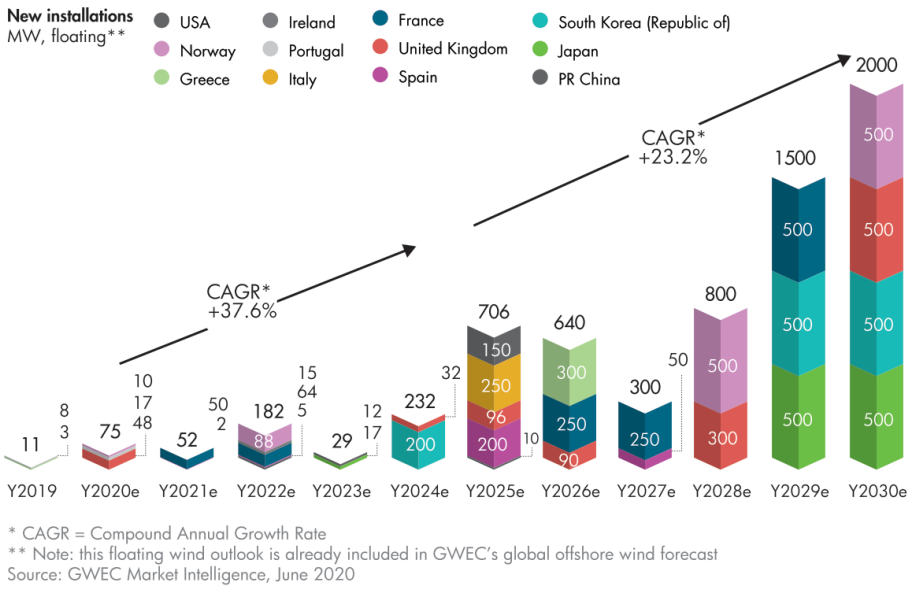

Figure 1.5: Prevision of new floating offshore wind installations, from [10].

In Portugal, *Principle Power* deployed a full-scale $2\ \mathrm{MW}$ WindFloat prototype $5\ \mathrm{km}$ off the coast of Aguçadoura in 2011. The project was successful and it was already decommissioned [11], producing over $17\ \mathrm{GWh}$ of energy, under waves up to $17\ \mathrm{m}$ tall and winds over $30\ \mathrm{m/s}$ [12]. Therefore, a pre-commercial phase project of $25.2\ \mathrm{MW}$ has been commissioned in January of 2020 by the *Windplus consortium* - the WindFloat Atlantic farm. The turbines of $8.4\ \mathrm{MW}$ are located $20\ \mathrm{km}$ off the coast of Viana do Castelo, Portugal [12].

Under this investment of green wind energy, it may occur some events of mismatch between demand and generation, associated to the characteristic of variability of the wind. When the production is high and demand is low, a possible curtailment may waste the wind resource.

Curtailment can be avoided by storing the electrical energy to be used later. Different energy storage technologies have been proposed in literature [13]:

- Mechanical energy storage: flywheel, pumped hydro, gravity, compressed air;
- Chemical energy storage: hydrogen, biofuel, biodiesel;
- Electrochemical energy storage: supercapacitor, batteries;
- Superconducting magnetic energy storage;
- Cryogenic energy storage: liquid air energy storage.

Hydrogen is the most famous chemical energy storage system [13]. Recently, the production of hydrogen from renewable energy became one of the main topics of discussion as a solution to solve some of the energy challenges of the next decades. Despite the need for some technical developments, hydrogen has a high energy density and it is storable, transportable, highly versatile and a clean energy carrier [13]. Beyond the benefit of avoiding the curtailed energy, it may be inserted in the energy economy as a new energy vector, contributing for the EU decarbonization goals [6].

Portugal responded to the decarbonization challenge, in 2016, by developing the roadmap for the Carbon Neutrality 2050 (RNC2050), presented two years later in anticipation of the draft of the National Energy and Climate Plan 2021-2030 (PNEC 2030) [14]. The initial proposals of these plans were very much based on pure electrification, which received some resistance from the gas sector and some industry. The market pointed the existence of a flaw that can be efficiently solved with hydrogen production. Therefore, the final plan proposals already included the renewable gases, namely, the hydrogen [14].

In 2020, the Portuguese government published a draft of the National Strategy for Hydrogen (EN-H_2) based on the path and discussion related to the PNEC 2030. This strategy aims to promote the gradual introduction of the hydrogen as a sustainable pillar and a more comprehensive strategy of transition to a decarbonized economy. At the same time, it pretends to provide a solid framework and a short, medium and long-term visions to all the companies and promoters of hydrogen projects. [14]

Based on the current national energy system, EN-H_2 determined a set of strategic configurations for the hydrogen value chain, including [14]:

- **POWER-TO-GAS (P2G)**: Hydrogen may be directly injected into natural gas grid or converted in synthetic methane via a methanation process;

- **POWER-TO-MOBILITY (P2M)**: Hydrogen is transported or locally produced to provide vehicle filling stations, with particular focus on heavy transportation, railway (on non-electrified lines), taxis, fleets of companies and shared mobility, and ships;

- **POWER-TO-INDUSTRY (P2I)**: To reduce the GHG emissions, the natural gas is replaced by the hydrogen in the industrial sector, namely in those that use high temperatures (eg.: steel and cement industry);

- **POWER-TO-POWER (P2P)**: Stored hydrogen obtained from the excess of renewable electricity can be reconverted again to electricity through the use of fuel cells or gas plant turbines properly adapted and converted for this purpose;

- **POWER-TO-SYNFUEL (P2FUEL)**: Production of fuels could be decarbonized, replacing them by synthetic fuels of renewable origin.

Therefore, based on the hydrogen production from renewables, namely the offshore wind that is increasing in the market, this thesis studies the feasibility of the hydrogen production applied to a case-study in Viana do Castelo, using electricity from the Windfloat Atlantic farm and assuming the Portuguese electricity market prices of 2019. In the next Section 1.2, the objectives of this work are presented.

1.2 Objectives

Within the study of the feasibility of the hydrogen production, the main objectives consist of:

- To know the floating wind technology, its main parameters for energy production and to simulate the energy production of a floating wind turbine in the presence of turbulent wind, computing the respective dynamic power curve;
- To understand the main technologies of green hydrogen production, their basic operation, advantages and drawbacks, creating scenarios to study a realistic case in the Portuguese context;
- To analyze the Portuguese electricity market, correlating the electricity prices with the respective wind production;
- To compute the hydrogen production costs, analyzing the feasibility of its production.

1.3 Thesis Outline

For a better reading of the thesis, an outline is depicted in the Fig. 1.6. Chapters are connected by arrows and the main questions that each chapter aims to answer are presented in the respective attached box.

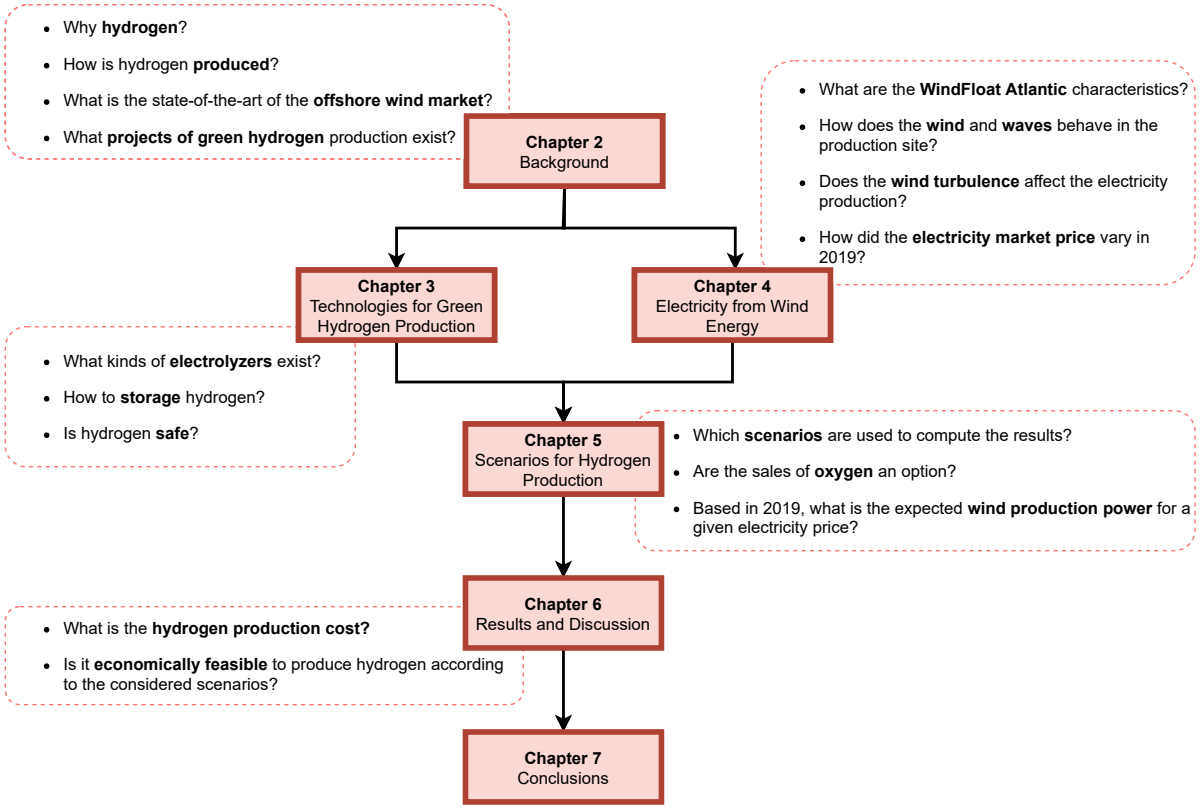

Figure 1.6: Thesis outline.

Chapter 2

Background

Hydrogen is the simplest atom and its molecule (H_2) is the most abundant in the universe. However, to generate pure hydrogen, energy must be used [15]. At standard temperature and pressure, hydrogen is a colorless, odorless and tasteless non-toxic gas. Some of its physical properties are presented in Table 2.1. The molar enthalpy of vaporization of the water, hence the difference between high and low heating values, is $44.01\ \mathrm{kJ/mol}$ [15].

Sections 2.1 and 2.2 introduce hydrogen as an energy vector and its production methods, with particular emphasis on the hydrogen produced from renewable energy. Section 2.3 describes a short state-of-art of the offshore wind energy production and some of the projects for wind-based green hydrogen.

Table 2.1: Some physical proprieties of hydrogen, from [15] and [16].

H_2 Molecular Weight	2.016
Heating Values	HHV: $142\ \mathrm{MJ/kg}$ ($39.4\ \mathrm{kWh/kg}$) LHV: $120\ \mathrm{MJ/kg}$ ($33.3\ \mathrm{kWh/kg}$)
Boiling Point @ 1 atm	$20.25\ \mathrm{K}$
Freezing Point @ 1 atm	$13.85\ \mathrm{K}$
Density, Gas @ 20°C, 1 atm	$0.08376\ \mathrm{kg/m^3}$
Density, Liquid @ B.P., 1 atm	$70.80\ \mathrm{kg/m^3}$
Flammability Limits @ 1 atm in air	LFL: $4.00\ \%$ (by Volume) UFL: $74.2\ \%$ (by Volume)
Autoignition Temperature @ 1 atm	$844.15\ \mathrm{K}$
Expansion Ratio, Liquid to Gas, B.P. to 20°C	1 to 845

2.1 Hydrogen as an Energy Vector

Hydrogen has a great potential in many energy sectors, acting not as an energy source but as a flexible energy carrier with a high heating value [15]. Seen as the key for the energy transition, allowing a faster

decarbonization of the energy sector, it can also provide synergies for the energy system (Fig. 2.1), linking different energy sectors and energy T&D networks [17]. Producing it with electricity can help solve challenges related to the integration of high levels of variable renewables into the grid, enhancing grid stability and reducing curtailment [18]. At the same time, while the renewable energy is getting lower prices, the cost of the **green hydrogen**, designated name when it comes from renewables, becomes consequently lower.

Nevertheless, when compared with the green hydrogen, hydrogen from fossil fuel-based sources is in general cheaper. For fossil fuel-based hydrogen, the designated term is **grey hydrogen**, but when combined with carbon capture, utilization and storage (CCUS), **blue hydrogen** in the correct term.

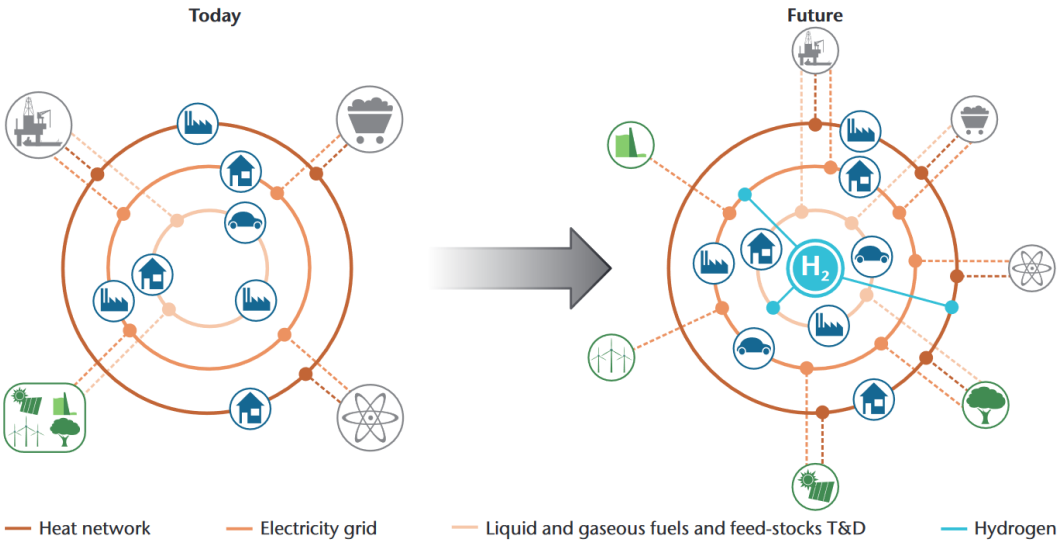

Figure 2.1: Energy system today and in the future, from [17]

Within the current and potential applications, in the transport sector, hydrogen can be used to power fuel cells electric vehicles directly or to produce or upgrade fuels made from renewable or fossil sources. In the industrial sector, it can be used in the fertilizer manufacturing, oil refining, metals refining, and the production of various plastics and chemicals. In a decarbonized energy system scenario by 2050 [14], hydrogen has a potential role as a mean of energy storage. Low-cost and intermittent electricity may be stored and then used for power generation as a value proposition in power-intensive industries and regions with high levels of curtailment and interest in zero-emission peak demand technologies. Another possibility is to mix the hydrogen into the natural gas pipeline, decreasing the fossil fuel content. [18]

To achieve high penetration of renewables, the hydrogen, as well as the batteries, could be used as technologies for energy storage, since a variety of storage scales and periods of discharge likely will be necessary to support the grid. The advantage of hydrogen is that it can be stored in large quantities for long periods over time with minimal loss, enabling to storage energy over time scales up to the season level (Fig. 2.2) [18]. A more detailed description about hydrogen storage is presented later.

Following, to better understand how hydrogen can be introduced into the market, a review about hydrogen production technologies is presented.

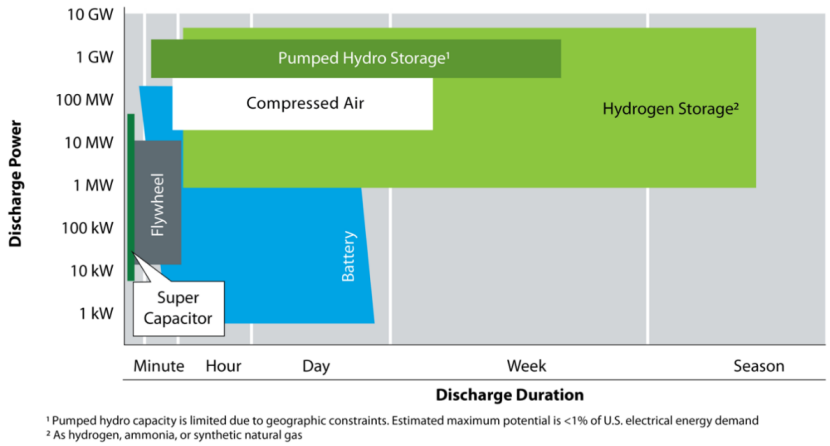

Figure 2.2: Optimal power and discharge-duration characteristics of energy storage technologies, from [18].

2.2 Hydrogen Production

Currently, the majority of hydrogen produced in Portugal comes from natural gas. About 65 thousand tons (187 ktoe) were produced in 2018 in Portugal [14]. This value fell $7,7$ % compared to the previous year (2017), as a result of a reduction in refining activity, also seen in the consumption of hydrogen. Thus, this decrease was also registered in the use of natural gas for the production of hydrogen, with a drop of 10.6 % (Fig. 2.3).

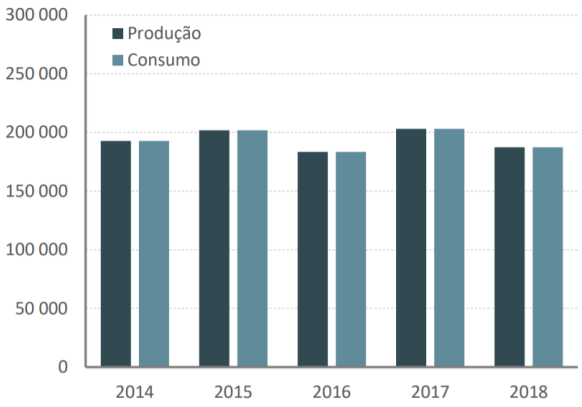

(a) Evolution of hydrogen production and consumption (toe)

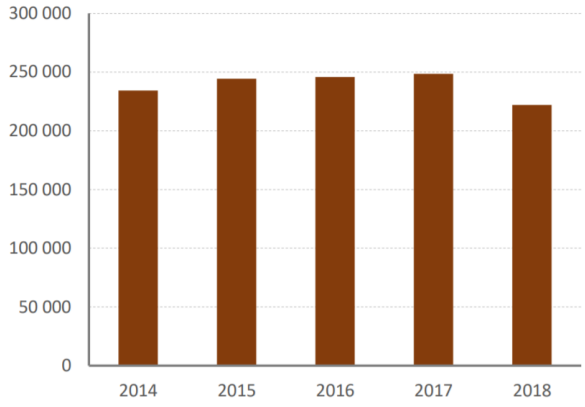

(b) Evolution of natural gas consumption for the production of hydrogen (toe)

Figure 2.3: Hydrogen production and consumption in Portugal (2014-2018), from [14].

Since one of the objectives of the energy transition is to decarbonize, the methods of hydrogen production with low carbon emissions, blue and green hydrogen, are presented then.

2.2.1 Technologies for low-carbon hydrogen production

Two primary options exist for producing hydrogen with lower carbon intensity: either via **electrolysis powered by low-carbon electricity** or **natural gas reforming and coal gasification with CCS**. Globally, less than 5 per cent of hydrogen volume comes from low-carbon sources nowadays [19].

The electrolysis consists in the separation of water molecules into hydrogen and oxygen using direct current. If the electricity comes from renewable sources, then the production is low-carbon hydrogen.

For producing low-carbon hydrogen from natural gas with CCS, either steam methane reforming (SMR), the most common process, and autothermal reforming (ATR) can be used [19].

SMR combines natural gas and pressurized steam to produce syngas, which is a blend of carbon monoxide and hydrogen [19]. Besides both products, depending on the steam-to-carbon ration, the syngas may also contain CH_4, H_2O and CO_2. This first reaction (Eq. 2.1) typically occurs with a nickel-based catalyst at high temperatures ($900 - 1200\ K$) and pressures of $5 - 25\ bar$ [15]. The heat for the endothermic reaction is usually provided via combustion of additional methane and the use of the available energy of the exhaust stream ($\Delta H_R = +206; \mathrm{MJ/kmol_{CH_4}}$) [20].

$$CH_4 + H_2O(g) \rightleftharpoons CO + 3\,H_2 \tag{2.1}$$

After the reformer (Fig. 2.4), there is a second reaction in the water-gas shift reactor, where in the presence of steam, the carbon monoxide is transformed in carbon dioxide (Eq. 2.2). Although exothermic, this reaction releases less energy that the first one ($\Delta H_R = -41\ \mathrm{MJ/kmol_{CO}}$). In the end, the hydrogen is separated obtaining a purity higher than $99\ \%$ [15].

$$CO + H_2O(g) \longrightarrow CO_2 + H_2 \tag{2.2}$$

About $60\ \%$ of the total carbon can be captured by separating the CO_2 from the hydrogen and the additional must be extracted from the exhaust gas, although more expensive, allowing for up to 90 per cent of total capture [19].

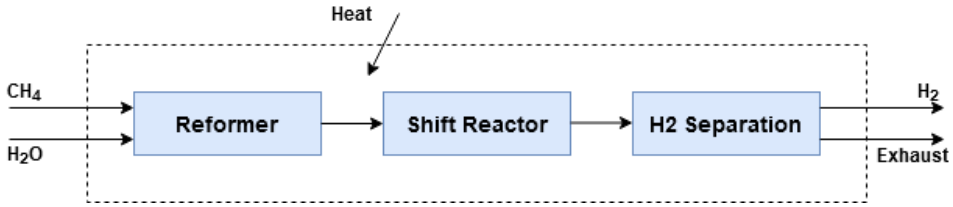

Figure 2.4: Simplified diagram of SMR without CCS system, adapted from [15].

Hydrogen might also be produced via partial oxidation reforming (POR). Oxygen and natural gas are combined to produce syngas (Eq. 2.3) with an exothermic reaction ($\Delta H_R = +319\ \mathrm{MJ/kmol_{CH_4}}$) [20].

$$CH_4 + O_2 \rightleftharpoons CO_2 + 2\,H_2 \tag{2.3}$$

ATR combines SMR and POR to produce hydrogen. The heat needed for endothermic reforming is provided in situ by methane oxidization [20]. Up to 95 per cent of CO_2 emissions can be easily captured. This technology is typically used for larger plants [19].

Coal gasification produces hydrogen by reacting coal with oxygen and steam and allows a relatively easy capture of CO_2 emissions. This technology emits four times more CO_2 per unit of hydrogen than the ATR, increasing the amount of carbon that must be transported and stored [19].

Other possibility is to produce **hydrogen from biomass resources**: either solid biomass or methane biogas. This way is limited since the production of other alternatives from biomass, such as biofuel, are more competitive [18]. One process is the biomass gasification that involves the gasification of solid biomass into a synthesis gas followed by steam reforming of the synthesis gas to hydrogen. The second way, using the methane biogas, is to produce via SMR, described before for the natural gas [18].

In the scope of this work, since one wants to produce hydrogen through offshore wind electricity, the next subsection 2.2.2 deepens the process of water electrolysis in general (its principle, thermodynamics and electrochemistry) and not the other alternatives previously presented that are based on natural gas, coal, or biomass. Subsection 2.4 focus on the costs of hydrogen production and sales. A better description of each type of electrolyzer (AE, PEM, SOEC) is given in Chapter **??**.

2.2.2 Green hydrogen

Fundamentals of water electrolysis

- **The principle**:

Water electrolysis consists in the separation of water molecules into hydrogen and oxygen using direct current. The electrolytic cell is configured by the electrodes, the diaphragm or separator and the electrolyte (Fig. 2.5).

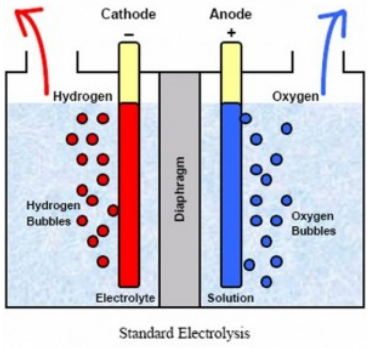

Figure 2.5: Representation of a water electrolyzer, from [21].

Current is applied to flow between the two electrodes and a multiphasic gas-liquid-solid system is generated in the electrode surfaces [22] . On the anode, that is polarized positively, the water molecules are divided in oxygen and hydrogen, and the electrons flows through the positive electrode to the negative one, producing oxygen molecules (Eq. 2.4). On the cathode, the electrons are released in the electrode to produce hydrogen molecules with the H^+ ions that flowed from the anode through the electrolyte and diaphragm (Eq. 2.5). The global reaction is in Eq. 2.6.

$$2\,H_2O \longrightarrow O_2 + 4\,H^+ + 4\,e^- \tag{2.4}$$

$$4\,H^+ + 4\,e^- \longrightarrow 2\,H_2 \tag{2.5}$$

$$H_2O \longrightarrow H_2(g) + \frac{1}{2}\,O_2 \tag{2.6}$$

Some of the electrode characteristics are the corrosion's resistance, a good electric conductivity, good catalytic proprieties and a suitable structural integrity [22]. The electrolyte should raise the ionic conductivity and should not react with the electrodes to avoid any change during the process. The diaphragm or separator should have also a high ionic conductivity and it exists to avoid the recombination between hydrogen and oxygen and the short-circuit between the electrodes, presenting a high electric resistance [22].

- **Thermodynamics**:

The electrolyzer converts electric and thermal energy into chemical energy, since it is an electrochemical device. According to the fundamentals of thermodynamics, for a given temperature and pressure, the required energy for the reaction is determined by the enthalpy variation (ΔH). Part of the energy is electric, and it corresponds to the Gibb's free energy change (ΔG). Other part is thermal energy (Q) that is a product between the process temperature (T) and the entropy change (ΔS). The electrolysis process has a positive change of enthalpy and Gibb's free energy, being an endothermic and nonspontaneous chemical reaction, respectively [22]. Eq. 2.7 presents the relation between these proprieties:

$$\Delta G = \Delta H - Q = \Delta H - T \cdot \Delta S \tag{2.7}$$

The lowest required voltage for the electrolysis is called the reversible cell voltage (V_{rev}). However, in the most commercial electrolyzers also the thermal energy ($T \cdot \Delta S$) is provided by means of electricity, where the required voltage is higher than V_{rev} [22]. In this case, the minimum energy voltage is known as the thermo-neutral voltage (V_{tn}). In an ideal process, V_{rev} should be equal to the enthalpy voltage ($V_{\Delta H}$) since all the energy required is equal the enthalpy variation. Due to the thermodynamic irreversibilities, mainly related with water vapor contained in the hydrogen and oxygen flows, the lower temperature and pressure compared with the set-point conditions of the water supplied, and the thermal losses due to convection and radiation, the energy consumption of the process increases and the V_{tn} is higher than $V_{\Delta H}$, in a real process [22]. The next two expressions 2.8 and 2.9 show how V_{rev} e $V_{\Delta H}$ can be obtained, being z the number of electron moles transferred per hydrogen mole ($z = 2$), and F the Faraday constant ($96,485\ \mathrm{C/mol}$).

$$V_{rev} = \frac{\Delta G}{z \cdot F} \tag{2.8}$$

$$V_{\Delta H} = \frac{\Delta H}{z \cdot F} \tag{2.9}$$

At standard temperature and pressure ($298.15\ \mathrm{K}$ and $1\ \mathrm{atm}$), $\Delta G^\circ = 237.21\ \mathrm{kJ/mol}$, $\Delta S^\circ = 0.1631\ \mathrm{kJ/mol\,K}$, and $\Delta H^\circ = 285.84\ \mathrm{kJ/mol}$. For an ideal process, the value for the reversible and thermo-neutral voltages at these conditions are: $V^\circ_{rev} = 1.229\ \mathrm{V}$ and $V^\circ_{tn} = 1.481\ \mathrm{V}$. [22]

Fig. 2.6 shows the evolution of the energy consumption of an ideal electrolysis process. The first, (a), as a function of the temperature at standard pressure, and the second, (b), as a function of the pressure at standard temperature.

In the graphic (a), the electric energy demanded by the electrolysis reaction ΔG decreases as temperature increases; however the thermal demand ($T \cdot \Delta S$) increases. In the liquid state the total energy

(ΔH) slightly decreases as temperature increases, but in the gaseous state it slightly increases.

In the graphic (b), the total energy (ΔH) is practically constant, since the increase of ΔG with pressure is compensated with the decrease of thermal energy ($T \cdot \Delta S$).

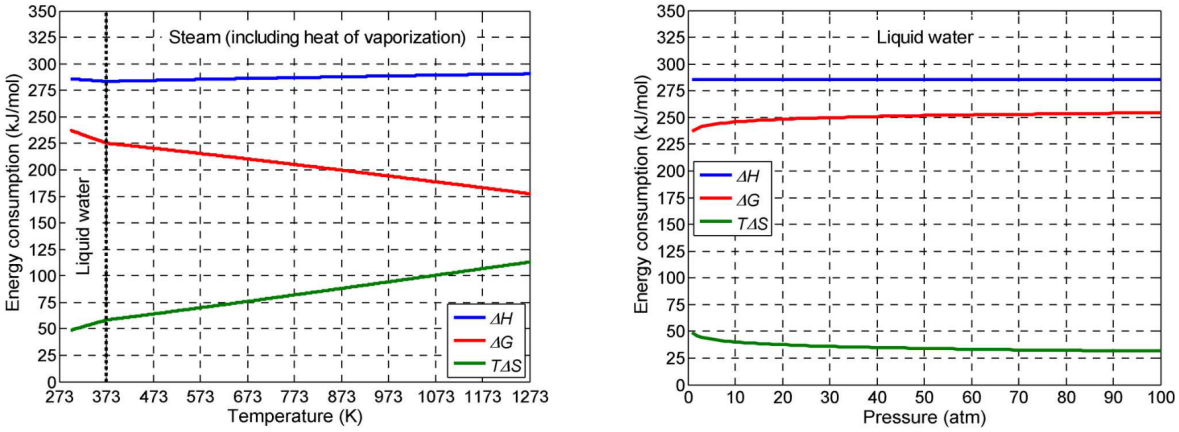

(a) Energy consumption as a function of the temperature at standard pressure (1 atm).

(b) Energy consumption as a function of the pressure at standard temperature (298.15 K).

Figure 2.6: Evolution of the energy consumption of an ideal electrolysis process, from [22].

The advantage of high temperature electrolysis ($700 - 900\,^{\circ}\mathrm{C}$), beside improved kinetics, is the possibility to use heat losses from other sources decreasing the necessary electrical energy. Furthermore, part of the heat demand corresponds to the latent heat of vaporization that is supplied by feeding water vapor, decreasing the necessary remaining heat [23].

- **Electrochemistry**:

Applying a voltage source in the electrolysis cell to produce hydrogen, the cell voltage (V_{cell}) increases and can be expressed as the sum of reversible voltages and additional overvoltages that appear in the cell (Eq. 2.10) [22]. These added voltages, typical in all electrolytic processes, represent the additional driving force required to overcome barriers such as the large activation energy for the formation of a gas at a metal surface.

$$V_{cell} = V_{rev} + \eta_{ohm} + \eta_{act} + \eta_{con} \tag{2.10}$$

The resistance of the cell elements to the electrons flow causes the ohmic losses, whose overvoltage is given by η_{ohm} and proportional to the electric current. The opposition to the ions' flow of the electrolyte also promotes of the ohmic losses [22]. Thus, the gas bubbles and the diaphragm are elements that may influence this ohmic loss [22].

The activation overvoltage, η_{act}, is due to the electrode kinetics. To transfer electric charge between the chemical species and the electrodes an energy barrier needs to be overcome. This energy barrier depends on the catalytic proprieties of the electrode and causes an overvoltage that behaves with a logarithmic tendency in respect to the electric current [22].

The last term, η_{con}, is the concentration overvoltage caused by mass transport processes and it is usually much lower than η_{ohm} and η_{act}. Transport limitations may induce a high concentration of products on the electrode interface with the electrolyte and the reduction of the reactant concentration [22].

For a given temperature, the relation between the cell voltage (V_{cell}) and current (I_{cell}) of an electrolyzer cell is given by the I-V characteristic curve. Fig. 2.7 shows two I-V characteristics curves of an alkaline electrolyzer for the operation temperatures of $25\,^{\circ}\mathrm{C}$ and $65\,^{\circ}\mathrm{C}$. The set-point for pressure is $20\ \mathrm{bar}$.

When the cell voltage in lower than the reversible voltage, V_{rev}, there is no electrolysis reaction and current is null. When the cell voltage is between V_{rev} and the thermal-neutral voltage, V_{tn}, some additional heat source needs to provide energy to the system. Finally, when the cell voltage in higher than V_{tn}, the extra power consumed by the cell becomes apparent as heat and it is the cooling system that will evacuate this energy. [22]

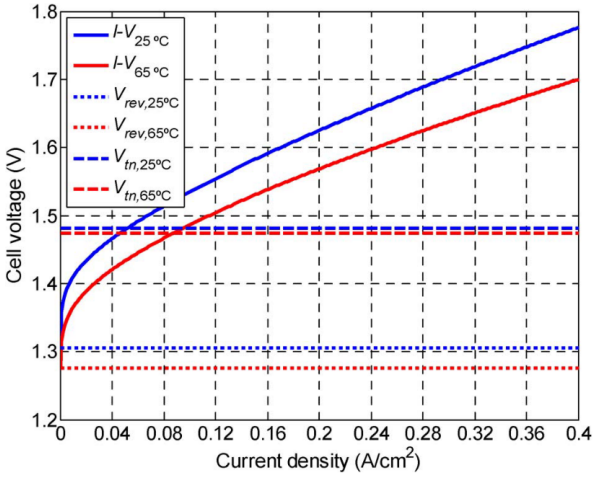

Figure 2.7: *I–V* characteristic curves of an alkaline electrolysis cell for temperatures of $25\,^{\circ}\mathrm{C}$ and $65\,^{\circ}\mathrm{C}$ at $20\ \mathrm{bar}$, from [22].

Faraday efficiency (η_F) or current efficiency can be defined as the ratio between the ideal electric charge and the real electric charge that is consumed by the electrolysis to produce a given amount of hydrogen. Lower Faraday efficiencies are mainly caused by electrical current losses and cross permeation of product gases [24]. Electrical current losses, also called parasitic currents [23], appear in the system and do not contribute for the hydrogen production. Usually this efficiency takes higher values (98 - $99.9\ \%$) when the electrolyzer operates at rated production conditions. Lower current densities and higher temperatures cause lower electric resistance and, consequently, an increase of parasitic currents. Moreover, higher temperatures and pressures facilitate the cross permeation, especially when the current densities are low [23].

The hydrogen production rate in an ideal electrolysis cell is proportional to the current, I_{cell}. Eq. 2.11 shows how the hydrogen production rate ($f_{\mathrm{H_2}}$) can be expressed in $\mathrm{Nm^3/h}$, assuming the same current for all cells and being N_{cell} the number of cells in the electrolyzer. [22]

$$f_{\mathrm{H_2}} = \eta_F \frac{N_{\mathrm{cell}} \cdot I_{\mathrm{cell}} \cdot 22.41 \cdot 3600}{z \cdot F \cdot 1000} \tag{2.11}$$

Knowing the power consumption of the electrolyzer and the hydrogen production rate, the specific

energy consumption, C_E, usually in $\mathrm{kWh/Nm^3}$, is easily obtained (Eq. 2.12).

$$\mathrm{C_E} = \frac{\int_0^{\Delta T} N_{\mathrm{cell}} \cdot I_{\mathrm{cell}} \cdot V_{\mathrm{cell}}\, dt}{\int_0^{\Delta T} f_{\mathrm{H_2}}\, dt} \tag{2.12}$$

This equation does not include other elements that consume electricity such as magnetic valves, sensors, microprocessors, electrolyte cooling systems, purification units, or losses in the electric power supply. It also does not account hydrogen losses in the electrolyzer water feeding systems, hydrogen leaks in valves and in the gas manifold. For an accurate and global C_E these elements should be in consideration.

The ratio between the energy contained in the produced hydrogen and electricity consumption can be also used as an important parameter: the electrolyzer efficiency, η_E. This parameter is given by Eq. 2.13, where the HHV of hydrogen is $3.54\ \mathrm{kWh/Nm^3}$. Instead of HHV, the electrolyzer efficiency may also be computed with the LHV of the hydrogen ($3.00\ \mathrm{kWh/Nm^3}$), if it is reused for energy production afterwards. When evaluating an overall process chain, the partial efficiencies of the steps and fuel prices are referred to the lower heating value [23].

$$\eta_E = \frac{\mathrm{HHV_{H_2}}}{C_E} \cdot 100 \tag{2.13}$$

Therefore, the decrease of the electrolyzer efficiency, or in other words, the increase of the overpotentials, may happen by **(1)** rising the current density; **(2)** decreasing the temperature and **(3)** increasing pressure [23]:

1. The first because although the hydrogen production rate is directly proportional to the current density as long as Faraday efficiency is higher than $95\ \%$ (Eq. 2.11), the consequent increase of the cell voltage is inversely proportional to the efficiency (Eqs. 2.12 and 2.13);
2. As seen in Fig. 2.7, lower temperatures cause higher cell voltages for the same current density;
3. Although not represented in Fig. 2.7, the increase of pressure induce a slightly increase of the cell voltage.

The selection of the nominal current density of an electrolyzer should be weighted between the capital costs and the operation costs. As discussed before, applying higher current densities means a increase of the hydrogen production rate and a decrease of the performance. On one hand, it corresponds to a lower specific capital cost, but on the other hand, lower performances means a increase on operation costs. Also the operation temperature strongly influence the performance, but there are more limitations related to the materials and their degradation. [23]

Water purification for electrolysis

Electrolyzers cannot be operated directly with **sea water**, **tap water** or **water treatment effluent**, since there is a maximum of $0.5\ \mathrm{ppm}$ of total dissolved solid units (TDS) allowed [25]. The water treatment includes desalination and/or purification.

For **sea water**, the desalination can be divided into electrical and thermal processes [25]:

- Reverse osmosis is the most used electrical technology;

- Multi-effect distillation and multi-stage flash distillation are the main thermal processes to produce better quality and require less post-treatment for demineralization (better for SOEC technology since it requires steam).

In the desalination process chemicals are also included to prevent scale. After the desalination, a post-treatment process is necessary. It always includes chemical treatment in a resin polishing filter containing chemicals to bind remaining ions and other dissolved solids in the desalinated water. Meier presents a simplified cost of desalination of $1.45\ €/\mathrm{m}^3$ [25].

At *Energypark Mainz* in Germany hydrogen is produced with **tap water**. The electrolyzer is the *Siemens SILYZER 200* and the electrolysis plant contains a water treatment plant to produce high purity water ($< 1\ \mu\mathrm{S/cm}$). The process of demineralization includes four stages: (1) decalcification; (2) reverse osmosis; (3) membrane degasification and (4) electro deionization. The system has a buffer tank to ensure a constant supply of water even during downtime periods or maintenance of the water treatment plant. [26]

A solution obtained by the GREENLYSIS project is to deionize water using the **wastewater effluent**, required for the electrolysis [27]. The pure water is obtained by a pre-treatment (UF and UV) and a purification system (membrane distillation powered by thermal solar energy).

The conditioning process consists of three water treatment steps [27]:

1. Ultrafiltration (UF) process: It improves water quality by decreasing the turbidity and the amount of suspended matter contained in the wastewater treatment plant effluent;

2. Ultraviolet lamp (UV) disinfection: This device is installed after the UF step and it is essential in order to limit distillation membrane biofouling;

3. Membrane distillation (MD) process: MD removes dissolved ionic species from water, and in this way, a conductivity under $1\ \mu\mathrm{S/cm}$ in order to feed the electrolysis is obtained. The optimal working temperature for this MD process has been proved to be $70\,^{\circ}\mathrm{C}$ (heated only with solar collectors).

Actually, the water does not have much impact in the hydrogen price. Knowing that the molecular mass of the water is $18\ \mathrm{g/mol}$ and the correspondent hydrogen is $2\ \mathrm{g/mol}$ (a ratio of 9), and assuming there is an efficiency on the use of the water of $90\ \%$, for each kilogram of hydrogen produced, $10\ \mathrm{kg}$ ($\sim 0.01\ \mathrm{m}^3$) of water are consumed. If the price of the water and its desalination and/or purification is 2 – $10\ €/\mathrm{m}^3$, the impact on the specific price of the hydrogen may go from 2 to 10 cents.

2.3 Hydrogen from Offshore Wind Energy

In the previews section, the water electrolysis fundamentals were described. This section depicts the state-of-the-art of wind offshore energy and some of the current projects of green hydrogen produced by renewables, and more importantly, wind energy.

2.3.1 Offshore wind energy

The wind resource depends on different aspects, such as the latitude, time of the year and day or type of surface. Actually, the wind is caused by the difference of pressures resulted by the difference of temperatures, along with the influence of the Earth's rotation and terrain.

The importance of the wind energy is based in two factor: the availability of resources and the maturity of the technology in term of cost efficiency [28]. The wind together with solar and wave energy has a clear huge availability, and regarding to many economic activities (sailing, windmill, etc) since older times, the maturity of wind energy technology is high.

Offshore wind present some advantages and disadvantages in comparison with onshore wind. One of the drawbacks is especially related with the higher costs of the permitting and engineering process, and the construction and operation phases [28]. Another disadvantage is that the wake effects provoked by the own wind turbine are very important leading to a significant impact over the lifetime of the turbines [28]. A minimum distance between wind turbines must be obeyed to reduce this problem.

At the same time, some of the main advantages of offshore wind energy become this solution attractive [28]:

- Better quality of wind resource, with higher speeds, a more uniform wind with less turbulence intensity, and consequent lower impact in the lifetime of the turbine;
- Bigger suitable free areas in the sea where offshore wind farms can be installed;
- Placed far from the populations areas, the noise emission for them is reduced and, when located far from the coast, the visual impact from the coast is also reduced;
- The lower limitations in the load to transport make possible to install bigger wind turbine units, achieving more production per installed unit.

Offshore wind substructure technology

There are two main technologies of substructures for turbines: **bottom-fixed** and **floating platforms**. The kind of used substructure is directly related with the water depth where they are located. There are three main levels of water depths:

- **Shallow water:** < 30 meters depth, where bottom-fixed foundations are used;
- **Transitional water:** 30 to 60 meters depth, where also bottom-fixed foundations are used;
- **Deep water:** > 60 meters depth, where floating platforms are used.

Between the bottom-fixed foundations, the most used substructure is the monopile (Fig. 2.8), however there are other technologies such as gravity-based, tripod, jacket and tri-pile structures. Most of the shallow water offshore projects are located in the North Sea [9].

Deep water substructures are mainly based on floating platform designs, such as TLP, semi-submersible and spar platforms (Fig. 2.8).

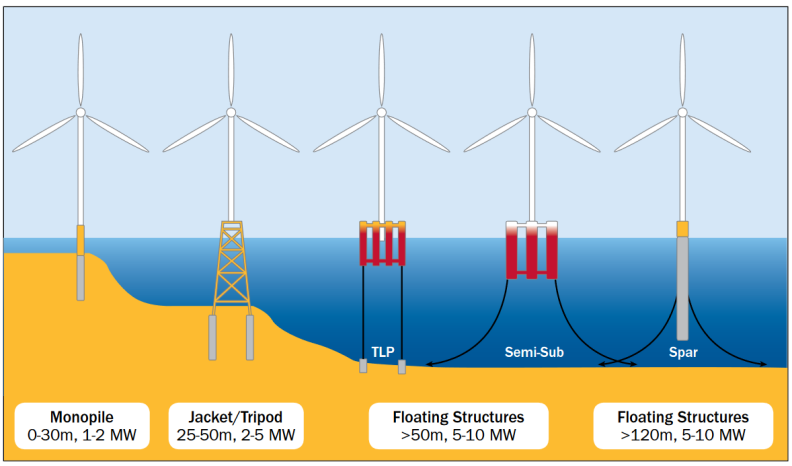

Figure 2.8: Offshore wind foundations, from [9]

Tension Leg Platform (TLP) is semi submerged and very buoyant structure. Buoyancy and stability are increased by the attached mooring lines anchored on the seabed. Spar Buoy has a very large cylindrical buoy that stabilizes the turbine using ballast on the bottom. This way, the center of gravity is much lower than the center of buoyancy. Semi-submersible combines the main principles of the previews designs since a semi-submerged structure is added with the necessary ballast to achieve stability. [9]

The emergence of floating offshore wind turbines

The industry started researching the concept of floating wind turbine (FWT) in the mid-1990s, twenty-five years after the emergence of the concept. Thus, these kind of structures are new and different designs have issued different stages of development to achieve the market [9]:

- The first test of a FWT was installed in 2008 by *Blue H technologies*. The turbine had a rated capacity of $80\ \mathrm{kW}$ and was tested during a year;
- A year later, another FWT was tested at *DONG*'s offshore wind farm at Onsevig, Denmark, within a project called Poseidon 37;
- Also in 2009, *Statoil* installed a $2.3\ \mathrm{MW}$ *Siemens* wind turbine in a floating platform, the first large scale floating system, the Hywind, in Norway;
- Later in 2011, *Principle Power* together with *EDP* and *Repsol* launched the second large scale FWT $(2\ \mathrm{MW})$, the WindFloat, a prototype near the coast of Póvoa de Varzim, Portugal. In 2012, the installation started to produce energy to the grid, and in 2016 was decommissioned;

- The first commercial floating wind farm was established by *Statoil* in 2017 in Scotland, the Hywind Scotland. Five $6\ \mathrm{MW}$ wind turbines give to the farm a production capacity of $30\ \mathrm{MW}$ [29];

- In 2020, the *Windplus* consortium developed the pre-commercial WindFloat Atlantic farm with $25.2\ \mathrm{MW}$ near Viana do Castelo, Portugal. The farm was nominated as the world's first semi-submersible floating wind farm and the first floating wind farm in continental Europe [12].

Many other projects at different stages of development, not only in Europe, but also in Japan and USA, are presented in bibliography [9], [10]. Chapter 1 exposed already the expected growth of the offshore wind market until 2030 on Figs. 1.4 and 1.5.

2.3.2 Hydrogen production using wind energy

As already stated in Chapter 1, green hydrogen production and use, beyond their near-zero carbon production route, benefit from important synergies together with the accelerated deployment of renewable energy: the increase of the power system flexibility using **curtailed electricity of variable renewables**. [30]

The transition to green hydrogen has the electrolyzer as the central technology for its deployment. In 2019, $6\ \mathrm{MW}$ was the maximum capacity achieved for a single electrolyzer, but a big number or projects and investments are ready for an upscaling effort of this technology [30]. For instance, currently, Air Liquid is working on a $20\ \mathrm{MW}$ PEM electrolyzer to produce green hydrogen using hydropower [31]. Table 2.2 summaries some of the projects for green hydrogen production in different countries.

Table 2.2: International projects for green hydrogen production in different countries. Symbol † refers to a project where the electricity comes exclusively from wind.

	PROJECTS
GERMANY [32], [33]	*Energy Park Mainz* – $6\ \mathrm{MW}$ PEM electrolyzer (2017) † **Some projects approved by the government in 2019:** *Element eins* – $100\ \mathrm{MW}$ electrolyzer † *EnergieparkBL* – $35\ \mathrm{MW}$ electrolyzer † *H2 Wyhlen* – $10\ \mathrm{MW}$ alkaline electrolyzer *HydroHub Fenne* – $17.5\ \mathrm{MW}$ PEM electrolyzer *REWest100* – $30\ \mathrm{MW}$ electrolyzer †
NETHERLANDS [32], [34]	*DJewls* - $250\ \mathrm{MW}$ electrolyzer (2025), $2\ \mathrm{GW}$ system (future) † *NortH2* – $0.8\ \mathrm{Mt_{H_2}/year}$ using 3 to $4\ \mathrm{GW}$ of wind energy (2030) †
JAPAN [32], [35], [36]	*FH2R* – $10\ \mathrm{MW}$ electrolyzer (2020) *Yamanashi Fuel Cell Valley* – $1.5\ \mathrm{MW}$ PEM electrolysis (2020)
AUSTRALIA [32], [37], [38]	*Asian Renewable Energy Hub* - $15\ \mathrm{GW}$ system (2027/28) *Neoen* – 50 MW electrolyzer (near future) *Hydrogen Utility (H2U)* – $30\ \mathrm{MW}$ electrolyzer (near future)
FRANCE [32]	*Les Hauts de France* – Five $100\ \mathrm{MW}$ electrolyzers (2021) †
UK [39]	*Gigastack* – $100\ \mathrm{MW}$ system, starting with a $5\ \mathrm{MW}$ electrolyzer (near future) †
CANADA [32], [31]	*Air Liquide* – $20\ \mathrm{MW}$ PEM electrolyzer (2020)

All these projects have a specific site for electricity production, such as the offshore wind or the PV farms, and another specific site where the hydrogen is produced, where the electrolyzer is installed. Nevertheless, the developer *Environmental Resources Management* (*ERM*) reported already the first facility of offshore wind turbines where the hydrogen is produced *in situ* (Fig. 2.9). The Dolphyn project will be installed $15\ \mathrm{km}$ off the cost of Aberdeen, Scotland. Each platform with a $10\ \mathrm{MW}$ turbine has a facility for hydrogen production and is connected by pipeline to a hydrogen buffer store on shore. Firstly, the project will start with a $2\ \mathrm{MW}$ prototype, thus with a smaller platform. [40]

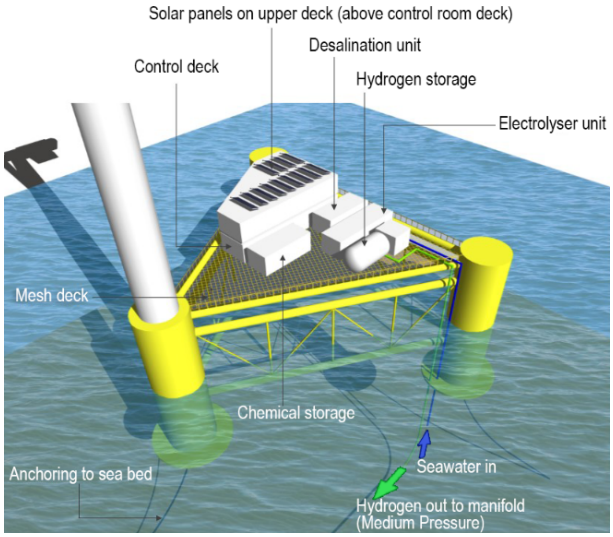

Figure 2.9: Schematic of *Dolphyn* platform - Deck details, from [40].

The power of the turbine is applied on the pump to take the seawater, desalination and electrolysis. The oxygen is vented and only the green hydrogen in piped to shore [40].

Within the preview mentioned strategy for hydrogen in Portugal, some projects have been proposed to begin a green hydrogen economy [41]:

- The biggest project for hydrogen production was proposed by *Bondalti Chemicals* to be applied in Estarreja chemical complex until 2040. Besides hydrogen, the project also aims to have green ammonia production;
- *CP - Comboios de Portugal* pretends to converse the diesel trains by hydrogen train, avoiding the need to electrify several lines;
- Replacing the coal power plant in Sines, together with other companies, *EDP* wants to build a centralized green hydrogen plant to be transported in gaseous state by ship to Northern Europe and sold in Netherlands and Germany;
- *Trustenergy*, which owns the Tapada do Outeiro natural gas power plant, in Gondomar, intends to produce hydrogen and may even promote the decarbonization of its own combustion process thought the mixture of green hydrogen in the natural gas.

Since Portugal owns good endogenous and renewable resources, projects are claimed to use not only the electricity from wind source but also others such as PV solar farms.

2.4 Green Hydrogen Production Costs

There are three main factor that mostly influence the green hydrogen price [30]:

- **LCOE**. Since the electrolysis consume electricity, the cost of it has a large influence on the hydrogen price. It only became feasible if the renewable electricity price is sufficiently low.
- **CAPEX**. If the equipment price is too high, with a limited lifetime, the hydrogen price will be high to support that cost.
- **Capacity factor** (Eq. 2.14). The bigger the hydrogen production in a fixed lifetime, the cheaper will became each unity of hydrogen.

$$\text{Capacity factor} = \frac{\text{Annual energy production}\left[\frac{\text{kWh}}{\text{year}}\right]}{\text{System rated capacity[kW]} \times 24\left[\frac{\text{hours}}{\text{day}}\right] \times 365\left[\frac{\text{days}}{\text{year}}\right]} \tag{2.14}$$

The total costs may have in account not only the production but also logistic costs such as storage and transportation. Local regulation and financial aspects should also be taken in consideration for the final delivery cost [30]. For revenues, selling the oxygen or grid balances services may be an option [15].

IRENA presents two reports [42] and [30] about green hydrogen, where some estimations for the hydrogen production costs are given.

Connecting an electrolyzer to the electricity grid with 2017 Danish electricity prices and capacity factor of $40\ \%$ (to avoid consuming fossil-based electricity), a target cost of $\text{USD}\,5$ - $6/\text{kg}$ (4.2 - 5.1 €/kg) can be achieved [42].

Assuming an electrolyzer CAPEX of $\text{USD}\,840\,/\text{kg}$ and efficiency of $65\ \%$, Fig. 2.10 shows how the LCOH change between different sources of renewable energy and some fossil fuels sources with CCS. In the scenario of "Best Case Wind", it was considered a different electrolyzer cost ($\text{USD}\,200\,/\text{kg}$). The capacity factors of the wind farms and solar PV systems were considered as 48 and $26\ \%$, respectively. [30]

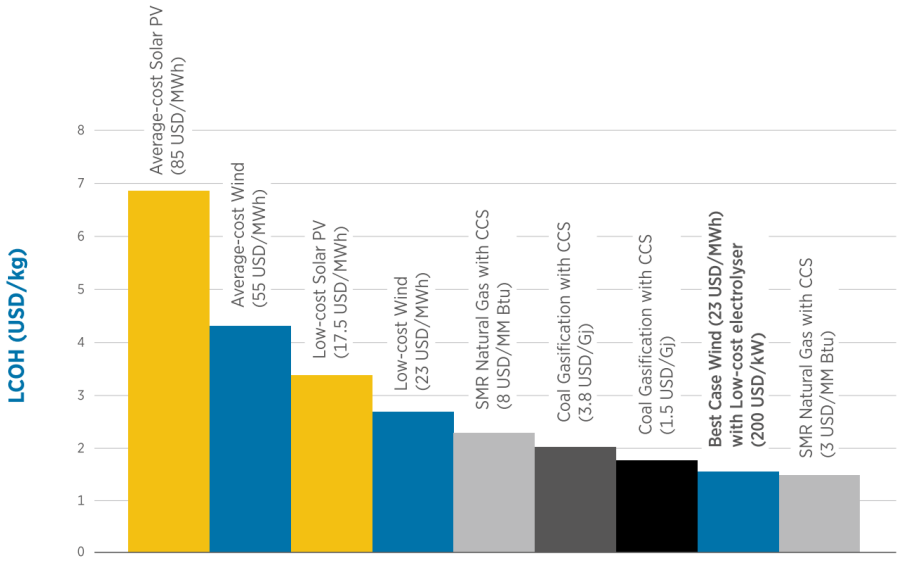

Figure 2.10: Costs of producing hydrogen from renewables and fossil fuels today, from [30]

The best green hydrogen case considers a low electrolyzer cost, which is expected to occur in 2040, and a low renewable electricity cost that is achieved already in countries such as Brazil and Saudi Arabia [30]. Although cheap renewable energy exists already, providing it during larger times to ensure higher capacity factors is more challenging. In the future, the capacity factor will take a lower weight in the hydrogen cost, since the costs of the electrolyzer and the renewable electricity prices may decrease. In addition, with the increase of the CO_2 emissions taxes, the carbon-free hydrogen may be more competitive.

The roadmap and action plan for the hydrogen in Portugal [32] also presents the projected costs of hydrogen between 2020 and 2040. A decrease of de CAPEX and electricity price, and a increase of the capacity factor and efficiency is assumed by the roadmap. Table 2.3 shows that the production cost of hydrogen may achieve a value of $1.07\ €/\mathrm{kg_{H_2}}$.

Table 2.3: LCOH with cumulative effect of the optimization of parameters, adapted from [32].

Year	**CAPEX** ($€/\mathrm{kW}$)	**Capacity factor** ($\%$)	**Electricity price** ($€/\mathrm{kWh}$)	**Efficiency of the system** ($\mathrm{kWh_{elec}/kg_{H_2}}$)	**LCOH** ($€/\mathrm{kg_{H_2}}$)
2020	861	43	0.05	54.3	4.69
2025	594	50	0.04	52.0	3.26
2030	328	55	0.03	49.5	2.12
2035	258	60	0.02	48.5	1.45
2040	189	65	0.015	47.7	1.07

Based on the value chain of the hydrogen and its configurations described already in section 1.1, the roadmap for hydrogen in Portugal also states hydrogen costs for some of those configurations [32]:

- **Power-to-Mobility:** The cost depends on the technology of production, the levels of compression and model of commercialization (if centralized, semi-centralized or decentralized). For a semi-centralized refueling station for heavy vehicles, the current final cost of hydrogen may vary from 4.2 to $9.1\ €/\mathrm{kg_{H_2}}$;
- **Power-to-Gas:** The green hydrogen could be used, together with carbon dioxide from industrial processes, for methanation increasing the renewable fraction the natural gas grid without changing the infrastructure. However, the current cost for the injection of hydrogen in natural gas grid vary from 3.5 to $7.6\ €/\mathrm{kg_{H_2}}$;
- **Power-to-Power:** Although no hydrogen costs were stated, this configuration may be feasible considering a better technology maturity index in the future (higher efficiency and lifetime, lower investments, etc), since peaks of renewable energy or dedicated production could be stored to produce electricity avoiding the use of the grid electricity.

Chapter 3

Technologies for Green Hydrogen Production

This chapter highlights the differences between electrolyzer types, presents a brief description of hydrogen storage options and ends with an appointment on hydrogen safety.

3.1 Electrolyzers

Electrolyzers can have different designs and materials, and those characteristics give them the different strengths and weaknesses. There are three most common ways to compile the two electrodes and the electrolyte (Fig. 3.1) [43]:

- **Gap-cell.** The two porous electrodes are submerged in the electrolyte with a separator between them to avoid recombination of the products. This is the simplest design but not as efficient. The gap should be large enough for the freely evolving of the produced gases, but as small as possible to reduce the ohmic losses.
- **Zero gap cell.** This type of cell is an improvement of the previous one, removing the gap between the electrodes and the separator to reduce the ohmic losses. Alkaline electrolyzers use this kind of design today.
- **Solid polymer electrolyte (SPE) cell.** The separator is a thin ion-conducting polymeric film that conducts the electric charge and no additional electrolyte is necessary. The membrane is coated with catalytic layers on both sides. The current collectors, fitted with flow channels, are pressed onto each side. These characteristics give a more complicated construction but a more theoretically efficient cell. The PEM and SOEC electrolyzers use this design.

Currently there are three main types of electrolyzer technology: **alkaline** (AE), **proton exchange membrane** (PEM) and **solid oxide** (SOEC) electrolyzers.

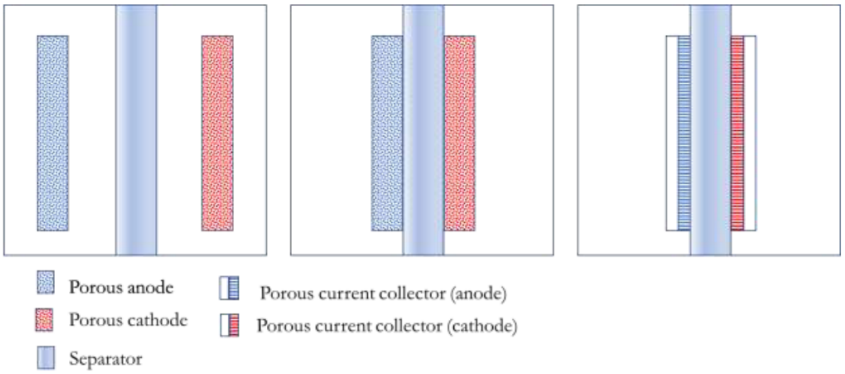

Figure 3.1: Various basic cell types, a) gap-cell b) zero gap cell c) SPE cell (solid polymer electrolyte), from [43].

3.1.1 Alkaline electrolyzers

Since 1902 more than 400 units of alkaline electrolyzers were in operation, and that's why it is a mature technology. AE electrolyzers have better durability and relatively low costs since cheap and abundant materials are used in manufacturing [15], [44]. Their lifetime can reach values up to 30 years and efficiencies up to 80 % [45].

AE electrolyzer cell consists of two electrodes separated by a gas-tight diaphragm (Fig. 3.2). The electrolyte is usually a highly concentrated aqueous solution of KOH (20-30 wt.%) to maximize its ionic conductivity, but also solutions of NaOH and NaCl can be used [22].

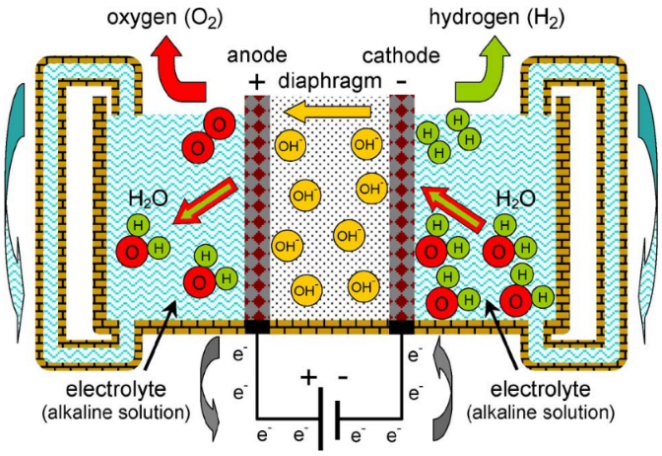

Figure 3.2: Scheme of the working principle of an alkaline electrolysis cell, from [22].

In the cathode the hydrogen is released, and water is reduced according to Eq. 3.1 yielding hydroxide anions. With an electric field established by the external power source, these hydroxide anions circulate across the diaphragm to the anode. There, these anions recombine to produce oxygen liberating electrons to close the electric circuit (Eq. 3.2).

$$2\,H_2O(l) + 2\,e^- \longrightarrow H_2(g) + 2\,OH^-(aq) \tag{3.1}$$

$$2\,OH^-(aq) \longrightarrow \frac{1}{2}\,O_2(g) + 2\,e^- \tag{3.2}$$

The purity levels of products H_2 and O_2 can be 99.9 vol.% and 99.7 vol.%, respectively [15].

The anode and cathode materials in these systems are typically made with nickel and steel [44]. The electrodes may have a large surface area, with many perforations, to have a higher contact with the electrolyte, in order to facilitate gas bubbling [22].

A convective system is also present as shown in Fig. 3.2 enabling the recirculation of the electrolyte and consequent homogenization of the concentration of the chemical species and an easier heat transfer for the refrigeration system. This recirculation happens due to the internal gradients of temperature and the liquid conveyed by the released gases. [22]

3.1.2 Proton exchange membrane (PEM) electrolyzers

Developed by the first time in the 1960's by General Electric, PEM electrolyzers are more expensive than alkaline electrolyzers, and they have a less mature technology since they are recent in the market [15]. However, they have a compact design, work under higher current densities, they have a rapid system response and a good performance on partial load [22].

The electrolyte is a gas-tight thin polymeric membrane between the electrodes ($\approx$ 20 - 300 μm in thickness), usually Nafion® or Fumapem® (Fig. 3.3), responsible for providing high proton conductivity, low gas crossover, compact system design and high-pressure operation [46]. It has a cross-linked structure and strongly acid character due to the presence of functional groups of the sulfonic acid ($-SO_3H$) type. These functional groups are responsible for the proton (H^+) exchange mechanism through the membrane [22].

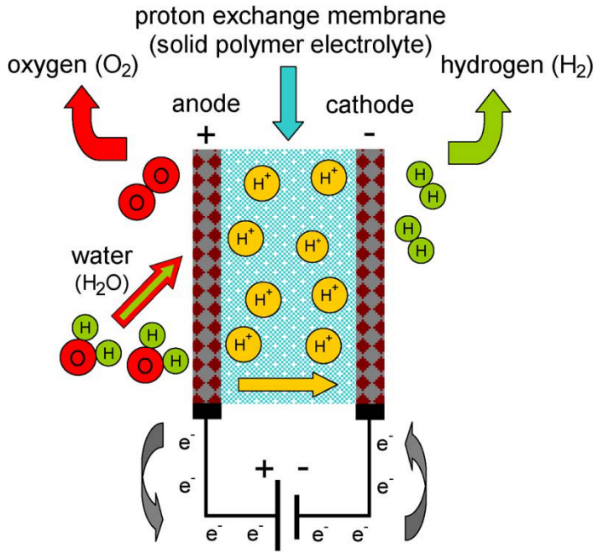

Figure 3.3: Scheme of the working principle of a PEM electrolysis cell, from [22].

In the anode, water is oxidized producing oxygen, electrons and protons (Eq. 3.3). The protons cross the membrane, and, by reduction, hydrogen is released in the cathode (Eq. 3.4).

$$H_2O(l) \longrightarrow \frac{1}{2}O_2(g) + 2\,H^+(aq) + 2\,e^- \tag{3.3}$$

$$2\,H^+(aq) + 2\,e^- \longrightarrow H_2(g) \tag{3.4}$$

Electrodes are typically made by noble metals such as platinum and iridium [22]. The membrane electrode assembly (MEA) - the polymeric membrane plus the two electrode layers - are pressed between the current collectors and bipolar plates usually made by titanium (Fig. 3.4) [47]. These materials are the main reason for the higher costs of this technology (1000-$1500\,€/\mathrm{kW}$) [15].

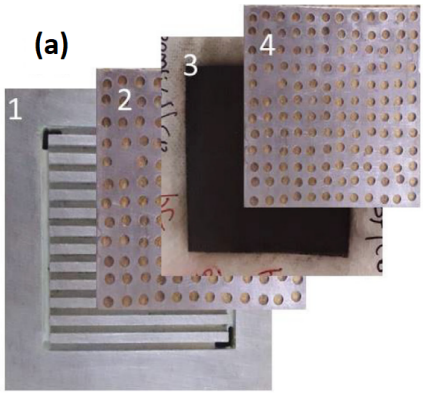

(a) Cell components; 1-Bipolar plate, 2-Anode current collector, 3-MEA, 4-Cathode current collector.

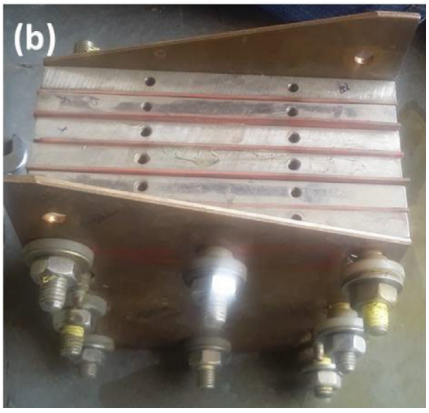

(b) PEM cell stack.

Figure 3.4: PEM water electrolysis cell assembly, from [47].

Porous current collectors must be resistive to corrosion to the acidic environment, good electrical conductors and give mechanical strength to the membrane. Current collectors have a significant role on the overall cell mechanism and efficiency, since they allow the electric current to flow between the electrodes and end-plates, and act as gas diffusion layers of the products [47].

Within a stack of PEM cells, except for the initial and final ones, the end-plates are bipolar plates because they have two polarities, positive and negative, with respect to the two cells they belongs to; hence, the cells are connected in series and the voltage source are applied on the stack terminals. Bipolar plates have also a important role in the evacuation of the products and offer a conductive route for the electrons and the heat [22], [15].

Due to compactness and structural proprieties, hydrogen can be released at higher pressures and oxygen at atmospheric pressures (avoiding hazard issues of high-pressure oxygen). Moreover, there are low risks of flammable mixtures due to very low gaseous permeability of polymeric membranes [22].

There is another promising technology under development named as anion exchange membrane electrolyzer (AEM) [45]. It has a similar structure as the PEM cell but transports anions OH^- instead of protons H^+. The evaluated catalysts, based on nickel or cobalt, do not use noble metals. The membrane may use benzyltriethylamine as the functional group, for example [48].

3.1.3 Solid oxid electrolyzers (SOEC)

This type of electrolyzer is an advanced concept enabling steam electrolysis at high temperatures (600 – $900\,^\circ\mathrm{C}$), and consequently, higher efficiencies. The high temperatures increase the probability of collision between elements, facilitating the electro-chemical reactions, and therefore, there are fewer

losses, increasing efficiency. This technology is not yet commercialized, being under development to overcome some challenges related to the high temperatures. [22]

The electrolyte is a solid ceramic membrane, and typically a gas-tight thin film of yttria (Y_2O_3)-stabilized zirconia (ZrO_2) (YSZ), with good ionic conductivity at the prevailing high operating temperatures (Fig. 3.5). The cathode is a cermet, usually consisting of nickel and YSZ and the anode is commonly a composite of YSZ and perovskites such as lanthanum manganites ($LaMnO_3$), ferrites ($LaFeO_3$) or cobaltites ($LaCoO_3$) partially substituted with strontium in order to promote structural and electronic defects that increase the electrocatalytic activity. [22]

At $1000\,^{\circ}\mathrm{C}$, $40.1\ \%$ of the required energy to produce hydrogen can be supplied as heat, while at $25\,^{\circ}\mathrm{C}$, only $16.9\ \%$ is required. The thermo-neutral voltage (V_{tn}) at $1000\,^{\circ}\mathrm{C}$ in comparison with the temperature of $25\,^{\circ}\mathrm{C}$ just increase from 1.48 to $1.52\ \mathrm{V}$, while the reversible cell voltage (V_{rev}) decrease from 1.23 to $0.91\ \mathrm{V}$. Thus, this technology is attractive when a high-temperature heat source is available (nuclear energy sector, geothermal energy) [22]. Overvoltages concentration are also high due to diffusional transport limitations of steam.

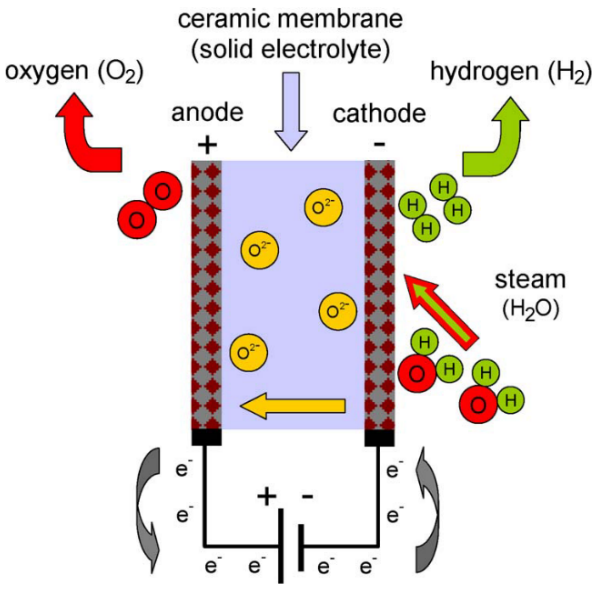

Figure 3.5: Scheme of the working principle of a SOEC electrolysis cell, from [22].

$$H_2O(g) + 2\,e^- \longrightarrow 2\,H^+(g) + O^{2-} \tag{3.5}$$

$$O^{2-} \longrightarrow \frac{1}{2}\,O_2 + 2\,e^- \tag{3.6}$$

Steam is fed to the cathode and hydrogen is released by water reduction (Eq. 3.5). The oxide anions cross the solid electrolyte forming gaseous oxygen in the anode and releasing electrons to the circuit (Eq. 3.6).

The reactions evolve the electrodes in contact with the vapor, being necessary to maximize the interfacial area between the electrodes and the gaseous chemical species with a porous character electrode [22].

3.1.4 Technology comparison

A summary table 3.1 is presented below. The most important parameters about operation, flexibility, capacity and durability of each technology are stated.

Table 3.1: Important parameters of the main water electrolysis technologies, from [49], [43], [50].

	Alkaline	**PEM**	**SOEC**
Ions electrolyte	OH^-	H^+	O_2^-
Current density (A/cm^2)	<0.45	>1.0	0.3 – 1.0
Cell voltage (V)	1.8 – 2.4	1.8 – 2.2	0.3 – 1.0
Temperature $(°C)$	60 – 80	50 – 80	700 – 1000
Pressure (bar)	<30	<80	1
Electrical efficiency[a] $(\%, HHV)$	60 – 80	80	100
Lower partial load range [% of nominal load (NL)]	10 – 40	0 – 10	–
Overload (% of NL)	<150	<200	–
Cold start up time (min)	15	5 – 10	>60
Warm start up time (min)	1 – 5	<0.2	–
Cell area (m^2)	<4	<0.13	<0.06
H_2 purity $(\%)$	99.8	99.999	–
Stack lifetime (kh)	60 – 90	30 – 90	10 – 30
System lifetime $(year)$	20 – 30	10 – 20	–
Efficiency degradation (% per year)	2 – 3	3 – 5	–

[a] At conditions (i $[A/cm^2]$, U_{cell} $[V]$, $T[°C]$): AE $(0.2–0.5, 2.0, 80)$, PEM $(1.0, 1.8, 65)$ and SOEC $(3.6, 1.48, 950)$ [50]

Although AE technology is the most mature and cheapest (with non noble catalysts), PEM electrolyzers are predicted to become the most prominent technology in the close future since they present better flexibility, good compactness (low cell area) and higher theoretical efficiency. SOEC technology promises the better efficiencies since a source of heat is provided, however the technology is still in the R&D stage and poses uncertainties for investments [43].

The potential for future cost reduction is more evident in PEM and SOEC electrolyzers (Fig. 3.6).

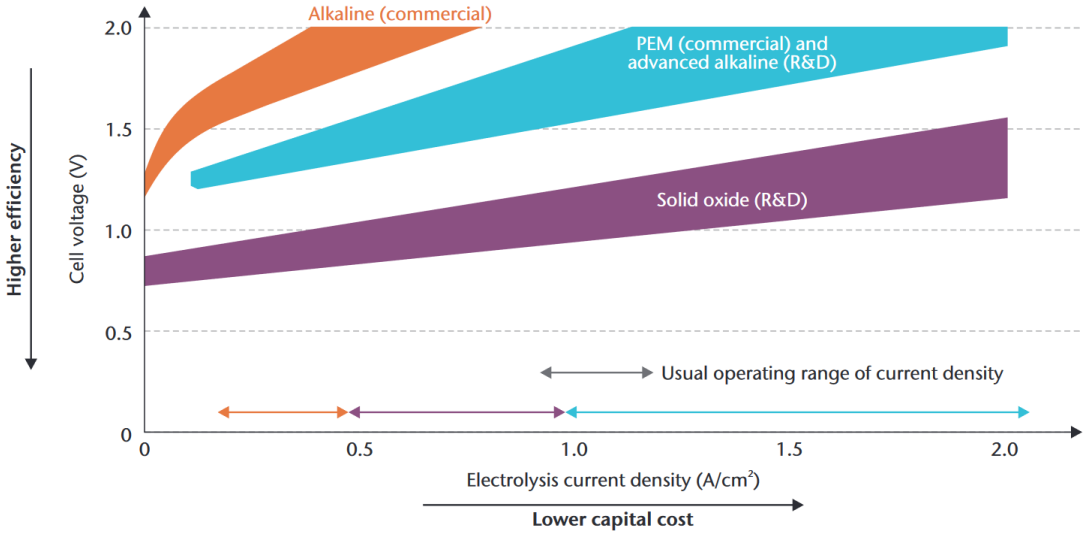

Figure 3.6: Representation of development potential of the different electrolyzers types, from [17].

PEM electrolyzers have both the highest current densities and operational range; thus, the requirements for lower specific capital costs and good operational flexibility at the same time. Working at lower cell voltages, SOEC technology presents the higher potential for further efficiency reductions [17].

The benefit of high currents in PEM technology brings also higher cell voltages and the consequent drawback of higher operational costs [43]. R&D is required for future technology improvements to increase the current densities and decrease the cell voltages, for instance, by using more efficient catalysts, thinner solid polymer membrane, less resistive cells, and appropriate cell design [51].

Based on the advantages and drawbacks, Table 3.2 qualitatively depicts the performance of each technology for an easier comparison.

Table 3.2: Pro/ con comparison between different electrolysis technologies, from [43].

	Alkaline	**PEM**	**SOEC**
Electrolysis efficiency	−	+	++
Ease of thermal management	+	++	−
Quick start-up	+	++	−
Overload capacity	+	++	++
Low duty capacity	+	++	++
Auxiliaries consumption	+	++	+
Hydrogen purity at stack outlet	+	++	+
Technology maturity	++	+	−
Reliability	++	+	−
Degradation due to intermittency	+	+	+
System capital cost	++	+	−

3.2 Storage

Hydrogen has a low energy density ($9.9\ \mathrm{MJ/Nm^3},\ \mathrm{LHV}$) and a consequent necessity of large tank vessels. To avoid so large tanks, there is three main solutions: high storage pressure, low storage temperature, or using a material that attracts large amount of hydrogen molecules.

Hydrogen storage technologies can be classified in two main types: physical-based and material-based. Compressed gas storage, cold/cryo compressed and liquid storage are the three foremost physical-based technologies. Material-based technologies comprehends chemical sorption (ammonia, metal hydrides, formic acid, etc) and physical sorption (carbon materials, zeolites, metal organic framework, etc) [52].

Several compressor technologies exist in the market: mechanical and non-mechanical compressors. The first group of compressors, the mechanical compressors, includes reciprocating, diaphragm, linear and liquid compressors. All of them work by mechanical compression of hydrogen confined in a closed volume. The most used is the reciprocating compressor since it ensures good performances for high-pressure applications. Diaphragm compressors are used when low flows are required. Linear compressors have been used for aerospace applications and cooling electronics. Finally, ionic liquids hydrogen compressors appeared as a promising solution for automotive applications since it allows to

compress hydrogen to values up to $1000\ \mathrm{bar}$ with a simple system [53]. The green hydrogen's project *Park Mainz* of $6\ \mathrm{MW}$ utilizes an ionic compressor for the compression necessities [26].

The second group of non-mechanical hydrogen compressors comprehends cryogenic, metal hydride, electrochemical and adsorption compressors. The first works by pressurizing liquid hydrogen and storing in cryo-compression systems. Metal hydride ensures both safe hydrogen storage and compression and requires heat exchange. Electrochemical compressors achieved the highest efficiencies of compression, based on the use of selective polymeric membranes. Adsorption compressors are controlled by heat transfer and consists in the hydrogen adsorption in a solid bed made of a porous material with high surface area [53].

Compressed gaseous H_2 is usually stored between 200 and $300\ \mathrm{bar}$ [54]. However, at least $700\ \mathrm{bar}$ have already been used for automotive vessels. The volume per vessel is limited by the high pressures [55]. Up to 13% of the hydrogen energy content is affected negatively by pressurizing [56]. Materials, such as steel, aluminium or carbon fiber reinforced by polymer composite, determine the pressure resistance and possible dimensions. Thus, there are four main types of vessels for gaseous hydrogen (Fig. 3.7) [52], [54]:

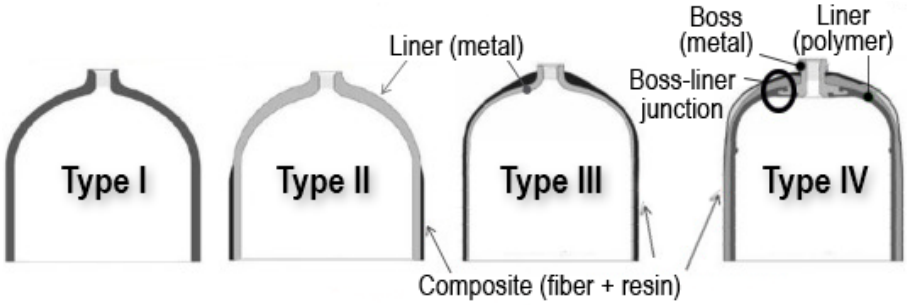

Figure 3.7: Schematic representation of the four pressure vessels types, adapted from [54].

- **Type I**: Fully metallic pressure vessels. These are the cheaper and heavier tanks. Usually they are mode from aluminum or steel and contain pressures up to $50\ \mathrm{MPa}$;
- **Type II**: Steel pressure vessel with glass fiber composite overwrap. More expensive than Type I by $50\ \%$ and less heavy by 30 - $40\ \%$. The structural load is distributed by the steel and the composite material;
- **Type III**: Full composite wrap with metal liner. The cost is twice the cost of Type II, but the weight is roughly half of it. The structural load is mainly carried by the composite (carbon fiber composite) and the liner (aluminum) serves for sealing purposes, withstanding pressures until $45\ \mathrm{MPa}$ without problems;
- **Type IV**: Fully composite. The structural loads are carried by carbon fiber or carbon-glass composites. It has not a metal liner for sealing purposes, instead, a composite liner is used, commonly a polymer like High Density Polyethylene, HDPE. It is the lightest pressure vessel, more expensive, but withstanding pressures up to $100\ \mathrm{MPa}$.

Type III and Type IV have grown to a dominant position in vehicular applications [57]. Another vessel, Type V, that is fully composite and linerless, is under development since their operational pressure is yet too low for hydrogen applications [52].

Liquefied hydrogen is costly due to the very low necessary temperatures ($-250\,^{\circ}\mathrm{C}$) and maintenance of such temperatures. Up to $40\ \%$ of energy content can be lost in the process. Therefore, this process is preferred for large-scale storage and for truck delivery and intercontinental hydrogen shipping [52]. There's a possibility of cryo-compressed H_2 storage when hydrogen in compressed and cooled at about $-233\,^{\circ}\mathrm{C}$. *BMW Group* has already started validation of this kind of hydrogen storage for vehicles with high energy requirements [54]. Fig. 3.8 presents the relation of hydrogen density versus pressure and temperature. For liquid hydrogen density values of $70\ \mathrm{g/L}$ are obtained. Cryo-compressed hydrogen can be stored at $80\ \mathrm{g/L}$. For compressed gaseous hydrogen, depending on pressure, it can be stored at values up to $50\ \mathrm{g/L}$ ($1000\ \mathrm{bar}$).

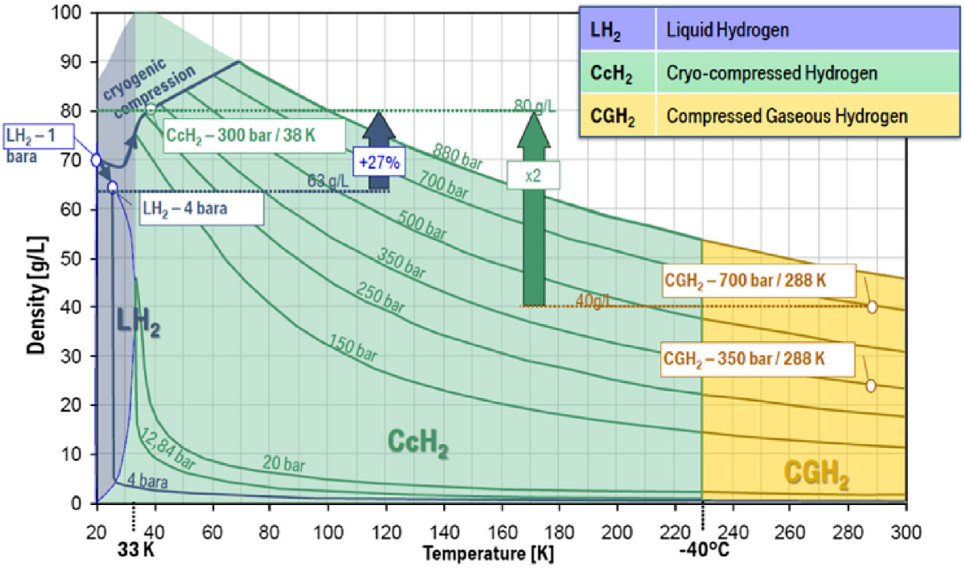

Figure 3.8: Hydrogen density versus pressure and temperature, from [54].

Material-based storage are still in development stage and needs more time to prove itself as a viable long-term solution. Chemical sorption consists in to split hydrogen molecules in atoms and to integrate them with the chemical structure of the material [52]. Compared with compressed and liquefied hydrogen, chemisorbed hydrogen has a shorter mean distance between hydrogen atoms, increasing the energy density [57]. Physical sorption consists in the use of a porous storage systems as a mean to achieve high capacity and reliable storage units. The hydrogen is physically attached to the adsorbent via Van der Waals interactions and is limited to a monolayer of hydrogen [57]. Table 3.3 presents the maximum reported storage capacity for different materials, and a more detailed description of these material-based methods is given in [52], [56].

The most established H_2 storage system is the physical storage in the form of pressurized hydrogen gas [56]. To make storage systems competitive with other types of fuel, some guidelines are needed to

Table 3.3: Max. storage capacities reported for a number of different material-based H_2 storage methods, from [52].

	Material-based storage method	Max. storage capacity [%wt]
Chemical	Ammonia Borane	19.4
	Metal Hydrides	12.6
	Alanates	9.3
	Formic Acid	4.4
	Carbohydrate	14.8
	Liquid Organic Hydrogen Carriers	7.2
Physical	Carbon Materials	8
	Zeolites	9.2
	Glass Capillary Arrays	10
	Glass Microspheres	14

be considered: high energy density by mass and volume; acceptable levels of security; low energy consumption; long service lifetime; good mechanical and vibration resistance; appropriate thermodynamics and acceptable cost.

The best option for large scale pressurized hydrogen storage is the use of salt caverns, whose typical volume is about $700,000\ \mathrm{m}^3$ and pressure of $20\ \mathrm{MPa}$ [52]. Salt is inert and it would not react with hydrogen. Other option is to use the depleted natural gas reservoirs or natural aquifer formations, but the hydrogen reaction with micro-organisms and minerals need to be studied [52].

Transportation addresses the same storage challenges, representing an added cost to the final H_2 price [56]. It can occur by sea, road, rail and also through a pipeline system. However, transport vessels could be avoided producing hydrogen at the place where it is consumed, if the electric grid is robust and resilient enough to ”transport” that energy. Most common distribution systems are:

- Compressed gaseous hydrogen through pipelines;
- Compressed gaseous hydrogen by road on trailer mounted vessel;
- Liquid hydrogen by road, sea or rail also on trailer mounted vessel.

A brief qualitative overview of the three main technologies for hydrogen delivery are presented in Table 3.4 [17]. Nevertheless, transportation of hydrogen is not explored in this thesis.

Table 3.4: Qualitative overview of hydrogen T&D technologies for H_2 delivery in the transport sector, from [17].

	Capacity	Transport distance	Energy loss	Fixed costs	Variable costs	Deployment phase
Gaseous tube trailers	Low	Low	Low	Low	High	Near term
Liquefied truck trailers	Medium	High	High	Medium	Medium	Medium to long term
Hydrogen pipelines	High	High	Low	High	Low	Medium to long term

3.3 Safety

There is a collective unconscious that classifies hydrogen as dangerous due to some failures that happened in the past, such as the fire of the Hindenburg airship in 1937. As all the other fuels (gasoline, diesel, natural gas, etc), hydrogen is certainly not without risk and should be handled in accordance with its specifications [48]. Between the main characteristics, some of them related to safety are underlined below [58], [48]:

- Hydrogen can diffuse through no appropriate materials. Only a few materials are suitable for use with H_2 to decrease the probability of leakage. Also the number of connections shall be minimized (eg. welded and screwed connections).
- Diffusion may cause 'hydrogen embrittlement' in some materials, leading to negative changes on their proprieties.
- When released, hydrogen rises and disperses quickly (at a speed of almost $20\ \mathrm{m/s}$) because it is fourteen time lighter than air. The risk of explosion or asphyxiation is therefore reduced. However, in closed rooms there is a risk of an accumulation at the top if there is no sensors and ventilation system. Furthermore, if the hydrogen leakage is from a small orifice, shockwaves may cause overheating and ignition.
- Human senses can not detect hydrogen because it is odorless, colorless and tasteless. Unlike natural gas, adding odorants is not a solution since there is no odorant light enough to disperse with the same rate of hydrogen.
- The hydrogen delivery installations shall be chosen such that escaped hydrogen is blown in a safe direction.
- A mixture of hydrogen gas and air can be ignited along a very wide volume fraction interval: 4 to $75\ \%$ (flammability range). A very little energy to ignite is required ($20\ \mu\mathrm{J}$, compared to $290\ \mu\mathrm{J}$ for natural gas). Constructions shall use materials that conduct electricity well, avoiding static charges accumulation;
- The self-ignition temperature is high ($585\,^{\circ}\mathrm{C}$).
- Hydrogen fire cannot be easily detected by people since it is colorless and has hardly any heat radiation. Special thermal imaging cameras and/or UV measurement could be used to detect flame.
- Hydrogen is non-toxic and non-poisonous. It is a gas under normal conditions and does not contribute to atmospheric or water pollution.

If the guidelines of hydrogen safety are taken in consideration, and users understand its behavior, hydrogen can be used as safely as other common fuels [58]. Therefore, companies that handle with hydrogen systems, such as *NASA*, have a set of guidelines for safety operation.

One of the guidelines shall be the personnel training. Personnel handling hydrogen must become familiar with physical, chemical and specific hazardous proprieties. Also the personnel involved in equipment design and operation planning must be trained to carefully adhere the safety standards. Operator certifications, hazard communication programs and annual reviews of the operations should be applied [59].

The use of inherent safety features and controls are also very important. Adequate ventilation, prevention of leakage and elimination of potential ignition sources are some examples. To minimize risks and control failures, some barriers or safeguards should be provided. Safety systems should be installed to detect and counteract or control the possible hazards effects, such as vessel failures or ignitions. A safety interface must be maintained so at least some failures occur before hazardous events that could lead to personal injury or loss of life. Warning systems and flow controls should be installed to detect abnormal conditions [59].

Effective public education will be essential to the widespread social acceptance of hydrogen technologies, for instance, with continued information campaigns and technology-related training programs. It is critical an early education of all relevant stakeholders, including ambulance and fire service personnel. For instance, the results of FCEV crash tests should be shared through information campaigns [17].

It's also noticeable that in many countries for decades, such us USA in 1950's or Britain in 1970, 'city gas' was used for heating and cooking. This gas consisted mainly of hydrogen (up to $60\ \%$), methane (up to $55\ \%$) and CO (up to $10\ \%$) [48].

Chapter 4

Electricity from Wind Energy

Chapter 4 is divided in three main parts. Sections 4.2 and 4.1 describe the WindFloat Atlantic characteristics and the resources at farm's location. Section 4.3 analyzes the influence of wind turbulence in the turbine's energy production. Finally, Section 4.4 reviews the correlation of the wholesale electricity market prices with wind electricity production.

4.1 WindFloat Atlantic

As stated in Chapter 1, after the successful $2\ \mathrm{MW}$ WindFloat offshore prototype installed in Aguçadoura, the pre-commercial phase of $25.2\ \mathrm{MW}$ was installed off the coast of Viana do Castelo in 2020. Table 4.1 presents the main characteristics of the farm.

Table 4.1: Main characteristics of the WindFloat Atlantic, from [60].

	WindFloat Atlantic
Developer	*WindPlus*
Turbines	3 x V164-8.4 MW turbines from *MHI Vestas*
Blade tip height	190 meters
Foundation	WindFloat (floating, semi-submersible)
Foundation technology supplier	*Principle Power, Inc.*
Project Capacity	25.2 MW
Location	Viana do Castelo, Portugal
Distance From Shore	20 km
Sea Depth	100 meters
Nominal Voltage	66 kV

WindFloat platform is a floating semi-submersible and triangular foundation laid by MiniFloat^{TM} and patented in 2003 by the offshore engineering consulting company *MI&T* (*Marine Innovation & Technology*). The patent was acquired by the company *Principle Power*, a member of the WindPlus consortium [61].

A turbine from any manufacturer can be installed without having to make changes on the turbine

or the platform and it is sustained by one of the columns of the platform (Fig. 4.1). Water ballast in the other two columns and the stabilization plates at the base of the columns ensure to the platform static and dynamic stability, respectively. Moreover, the platform and turbine are entirely constructed and assembled on land, which leads to a simplified installation process that may occur in any site with depth greater than 40 meters [62].

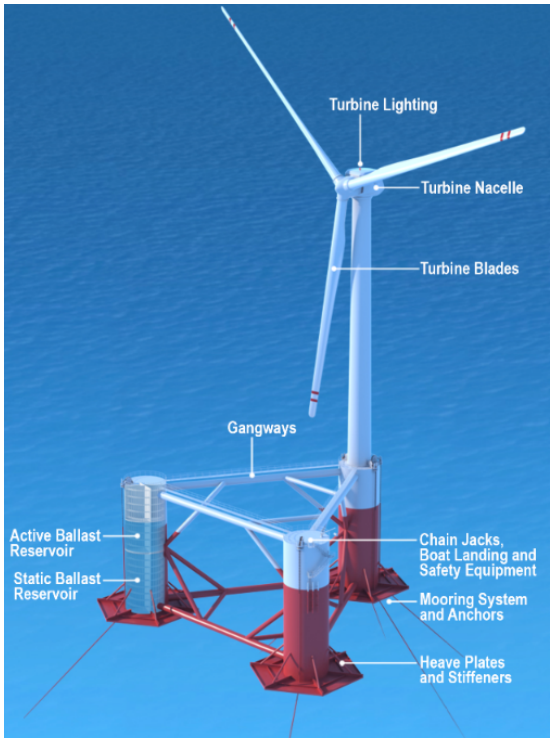

Figure 4.1: Scheme of the WindFloat platform, from [63].

4.2 Wind Resource and Waves

Portugal has a good offshore wind resource that can be explored, mainly in the north of the country. Fig. 4.2 represents the average of wind speed in the western part of Europe, according to the Global Wind Atlas (GWA) [64]. GWA is a web-based application to help policymakers, planners and investors identify high-wind areas for wind power generation. It was developed by the Technical University of Denmark (*DTU Wind Energy*) and the *World Bank Group* (consisting of *The World Bank* and the *International Finance Corporation*, or *IFC*). The methodology of the GWA is based in a downscaling process, starting with a large-scale wind climate data (20 - 200 km), then a medium scale modelling (1 - 20 km) considering medium resolution topography, and ending with a micro-scale modelling (0.1 - 1 km) where high resolution topography is used. The large-scale dataset is the ERA5 from the *European Centre for Medium-Range Weather Forecasts* (*ECMWF*) and the considered period was 2008-2017. A more detailed description of methods and datasets used are given in [64].

For the analysis of the energy production behavior, it is necessary to take into account the external conditions of the site of production: wind and ocean.

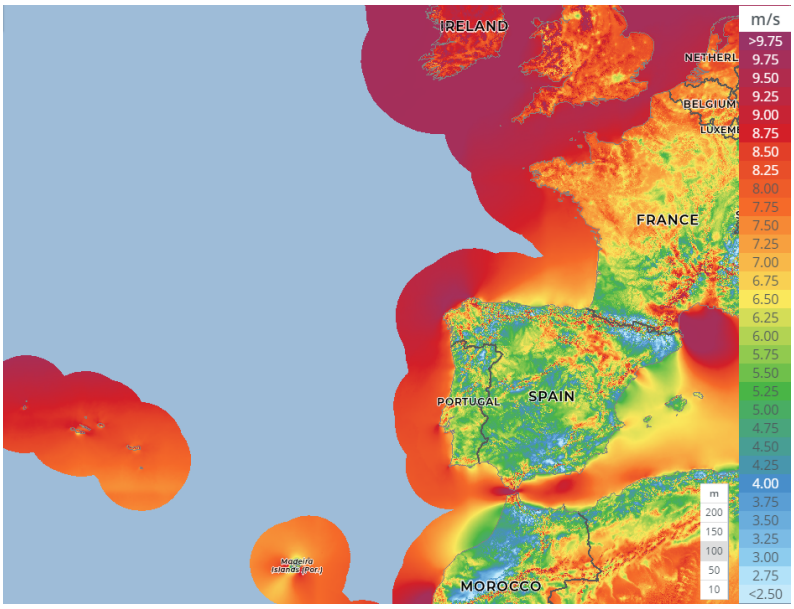

Figure 4.2: Average wind speed map of Western Europe at 100 meters high, according to Global Wind Atlas [64].

The wind varies in time and space, due to it's turbulent character. It can be divided in the three components: longitudinal u_w, transversal v_w and vertical w_w. The main wind component is u_w and can be given by the sum of the average wind speed $\overline{u}_w$ with the component that describes the variation of velocity u'_w (Eq. 4.1).

$$u_w = \overline{u}_w + u'_w \tag{4.1}$$

When the data of average wind speed is not given for rotor's height, it is necessary to adjust the value for the right level. For that, the Power Law (Eq. 4.2) is used, where z is the rotor's level, z_{ref} is the measure data's level, and a the exponent coefficient that depends on the surface roughness.

$$\overline{u}_w(z) = \overline{u}_w(z_{ref}) \left(\frac{z}{z_{ref}} \right)^a \tag{4.2}$$

To define the turbulence u'_w in offshore conditions, unless site-specific full-scale models are available, one of the main models is the Kaimal spectral model, according to IEC 61400-1 and IEC 61400-3 standards [65]. Although frequently used for offshore conditions, Kaimal spectral model was developed in a flat and homogeneous onshore site, representing the atmospheric turbulence [65].

The significant wave height, H_s, is the average of the highest third of the recorded waves, in a given time interval, while the peak period, T_p is the value of the period corresponding to the maximum of the wave energy spectrum.

An important aspect for the analysis is that the significant wave height is dependent of the wind velocity, $\overline{u}_w$. This relation is defined by the long-term joint-probability distribution and it enables to define the expected value of the significant wave height conditioned on the mean hub-height wind speed, $E[H_s|V_{hub}]$.

The energy spectrum of the waves may be defined by the Pierson-Moskowitz (P-M) spectrum or

the JONSWAP spectrum. The first model is the most generally accepted to describe fully-developed wind-driven wave systems. The second model shows that the wave system may not have the time fully developed, leading to a higher peak and a higher frequency peak [8]. The concept of fully-developed wave system is related with the energy transfer between the wind and the sea, considering that a state of equilibrium is reached when the wave energy remains constant [8]. P-M spectrum is, after all, a particular case of the JONSWAP spectrum, since when the peak shape parameter equals unity, JONSWAP spectrum formulation is reduced down to the P-M spectrum formulation [66].

4.2.1 Wind at farm's location

WindFloat Atlantic farm is located $20\ \mathrm{km}$ off the coast of Viana do Castelo. According to the GWA [64], the site's average wind speed ($\overline{u}_w$) at 100 meters height is $8.37\ \mathrm{m/s}$. A more detailed average wind speed data (hourly vs. monthly) and a frequency rose of the wind speed direction in the site are given in Fig. 4.3. The wind speed index is a factor to be multiplied by $\overline{u}_w$ at the site.

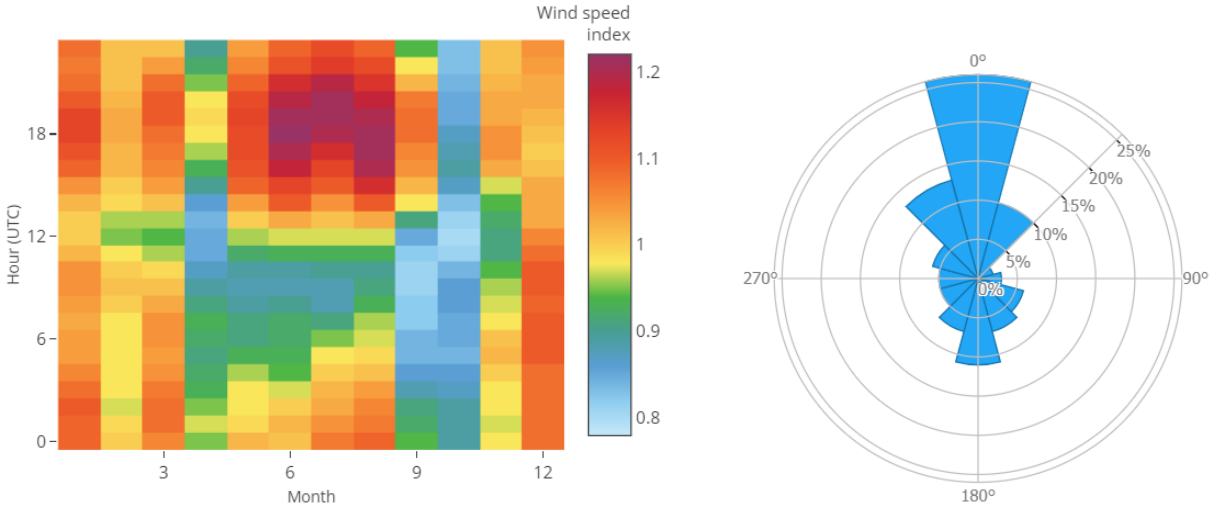

(a) Hourly vs. monthly (cross table).

(b) Wind frequency rose (%).

Figure 4.3: Average wind speed and frequency wind direction at WindFloat Atlantic location, from [64].

From Fig. 4.3, yearly, $\overline{u}_w$ vary from 6.70 to $10.04\ \mathrm{m/s}$ (0.8 to 1.2 wind speed indexes). Seasonally, the highest $\overline{u}_w$ is achieved on Summer afternoons but Winter months present the tendency for higher $\overline{u}_w$ throughout the day. Autumn is the season with lower $\overline{u}_w$ values. Daily, there is a tendency for the highest $\overline{u}_w$ in the afternoon, around 18 p.m., and the lowest $\overline{u}_w$ in the morning, around 9 a.m.. From the wind rose map, a more frequent wind from the North can be noted ($26\ \%$).

4.2.2 Waves at farm's location

To get the relation between waves and wind, data from the coast of Viana do Castelo (2015 – 2019) were obtained from WindGURU [67]. WindGURU is a service specialized in forecasting weather. Different forecast models are provided by the platform and mentioned in [67]. Wind velocities are given for one meter height, and therefore, the power law equation (Eq. 4.1) was used to get the correspondent velocity

at hub height (100 m). An exponent a of 0.11 applied in offshore conditions was considered [68].

Fig. 4.4 shows the correlation between the wind velocity at hub height (U_{hub}) and the significant wave height (H_s). A probability for higher wave heights when there are higher wind velocities can be verified from the graph.

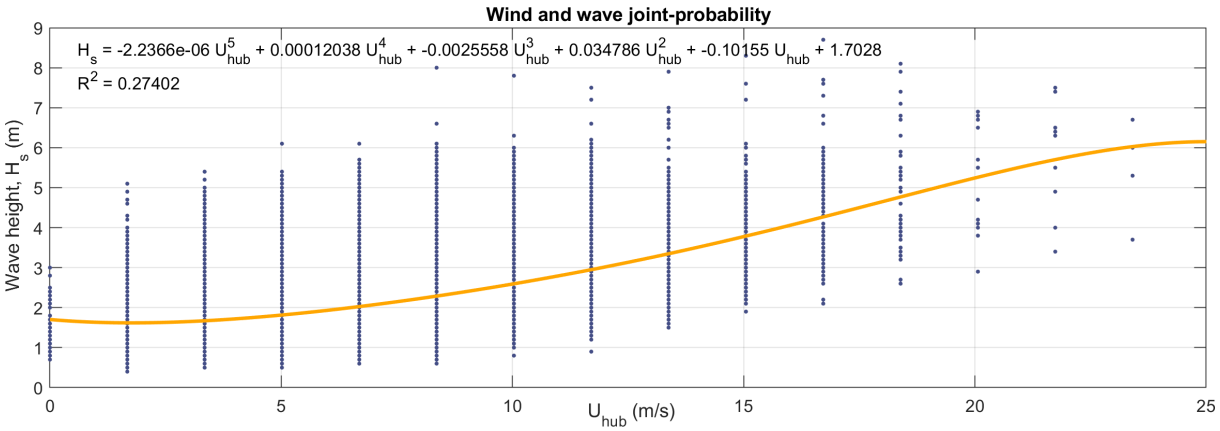

Figure 4.4: Wind and wave joint-probability and respective trend line (fit with *Matlab*).

Based on the dataset from WindGURU (2015-2019), no correlation between the wind velocity at hub height (U_{hub}) and peak wave period (T_p) was obtained. Therefore, a histogram was built to verify what is the most frequent peak wave periods (Fig. 4.5). A period about 11 seconds was the most often.

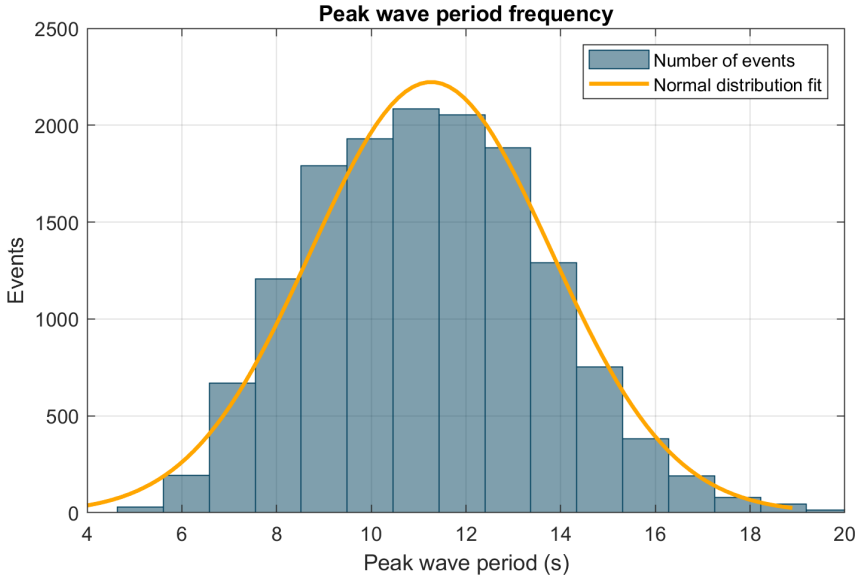

Figure 4.5: Peak wave period frequency and respective normal distribution line.

4.3 Dynamic Power Curve

This section presents the influence of the wind turbulence on the energy production. Using an aero-hydro-servo-elastic numerical tool and a turbulent wind file (Subsection 4.3.1), a dynamic power curve is computed and compared to the static power curve of the chosen turbine model (Subsection 4.3.2).

4.3.1 Numerical tool: FAST

FAST is a time-domain numerical method developed by NREL to analyze fixed and floating horizontal-axis wind turbines. It's a fully coupled aero-hydro-servo-elastic tool that have been verified and validated along its development [69]. It's a complex coupling between codes, so called modules, that permits the user to analyze the dynamics of different types of structures with two or three blades horizontal-axis wind turbines, among much other different factors such as the type of control, mooring system configurations and the sea-state or wind conditions.

In Fig. 4.6 is represented the working diagram of the openFAST, that is the last and open-source version resulted from FAST 8, where is possible to understand the relation between the different main modules.

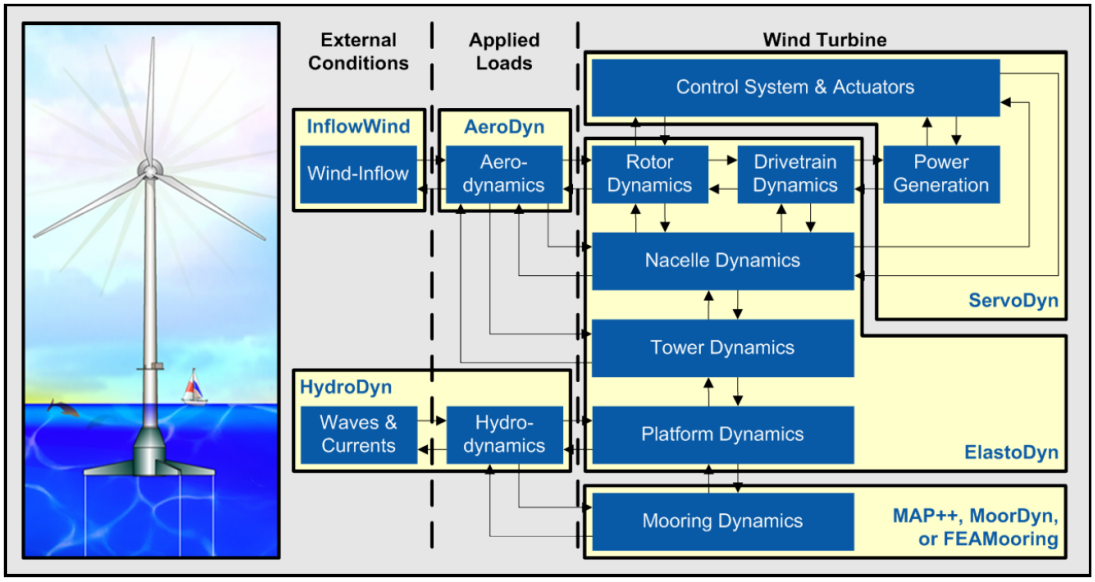

Figure 4.6: The program setup of FAST 8, from [70].

A brief description of each one is presented to better understand the different modules [69] [71]:

- **InflowWind** is the module that processes the wind-inflow velocities, unperturbed by the turbine, on the desired positions. For simple wind models as steady wind, it can model the wind without an exterior file. For complex wind files, with turbulence models, this module reads data files as binary TurbSim full-field (FF), binary Bladed-style FF or HAWT formatted binary FF.

- **AeroDyn** is the responsible for the aerodynamics. Wind and structural motions are the necessary information for the module to compute the aerodynamic loads on the blades and tower, and it is divided into four sub-modules: airfoil aerodynamics; blade rotor wake/induction; tower influence on the wind local to the blade nodes, and tower drag. Some features aren't yet included as the nacelle, hub and tail-vane wind influence and loading, aeroacoustics, or wake and array effects between turbines in a wind plant. The methodology used is based on the BEM theory with Glauert's empirical correction with Buhl's modification, and in the BEM solution, Prandtl tip-loss, Prandtl hub-losses, and Pitt and Peters skewed-wake are all 3D optional corrections.

- **HydroDyn** is the module to compute the hydrodynamics loads for both bottom-fixed and floating substructures. The primary input file defines the substructure geometry, hydrodynamic coefficients, incident wave kinematics and current, ballasting and marine growth, and other auxiliary parameters. The waves can be regular (periodic) or irregular (stochastic) and long-crested or short-crested, and they are treated using the linear Airy or first- plus second-order wave theory. The potential-flow theory is used when the substructures are large relatively to the typical wavelength, and the frequency-domain panel code WAMIT is needed to supply the hydrodynamic coefficients. When the substructures are small in diameter relative to the typical wavelength, the strip-theory may be used including Morison's equation for the distributed fluid-inertia, added mass and viscous-drag components. Some substructures and sea conditions may need potential-flow theory with the viscous-drag component of the strip-theory solution.

- **ElastoDyn** is a structural-dynamic model for the tower, platform, nacelle, drivetrain and rotor, and it is considered the "glue code" (interface) of FAST. Aero and hydrodynamic loads, controller commands and substructure reactions are the inputs to compute the displacements, velocities, accelerations and reaction loads (outputs). The model comprises 22 DOFs for a turbine with three blades and combines a multi-body and a modal system. The latter one is used for the blades and tower, assuming Bernoulli-Euler beams under bending, which implies there's no shear deformation nor axial or torsional deformation. Moreover, an isotropic material without mass or elastic offsets, and small tower and beam deflections are assumed. For the platform, rotational DOFs have a constraint of small-angle assumption.

- **ServoDyn** is the module of control and electric drive, where the main features are the blade-pitch, generator-torque and nacelle yaw controls. The conventional active controller method is the variable blade-pitch-to-feather. This controller was designed to optimize the energy production with generator-torque controller, maintaining the optimal TSR constant before to achieve the rated wind speed. When rated wind velocity is surpassed, the blade-pitch controller is the responsible for a constant energy generation, maintaining the rotor speed constant.

- **MoorDyn** acts with a lumped-mass mooring line discretized model and accounts with internal axial stiffness and damping forces, weight and buoyancy forces, hydrodynamic forces from Morison's equation, vertical spring-damper forces resulted from the contact with the seabed and wave kinematics interactions with the mooring lines. It supports line interconnections, clump weights and floaters and different line proprieties (length, diameter, density and Young's modulus). Also, the model accepts three kind of node for the ends of the mooring lines: fixed nodes for anchors (never move), vessel nodes for the fairlead connections (move under the control of an outside program) and connect nodes for different mooring lines attached (not fixed in space).

Another software, **TurbSim**, is used to create space-time wind series needed for the FAST simulations with turbulent wind. TurbSim is based on statistical models and creates turbulent wind time series in the three spatial dimensions [72].

4.3.2 Aero-hydro-servo-elastic simulation

The influence of turbulence on the wind turbine power production is analyzed by computing a dynamic power curve. 'Dynamic' because wind is considered turbulent instead of uniform. For each turbulent wind file, the simulated mean power production and respective standard deviation are plotted. A set of 14 simulations were performed. Each performance corresponds to a different mean wind speed and the expected significant wave height (Tab. 4.2), based on the wind and wave relation described in Fig. 4.4.

Table 4.2: Simulation specifications: average wind speed $[\mathrm{m/s}]$ and significant wave height $[\mathrm{m}]$.

$\overline{U}_{hub}$	3	5	7	9	10	11	12	13	15	17	19	21	23	25
H_s	1.63	1.74	1.93	2.16	2.30	2.44	2.60	2.76	3.13	3.55	4.03	4.57	5.16	5.77

The turbulence intensity, assumed as a characteristic value for offshore conditions, and the wave period were maintained constant. Current effect was neglected. Table 4.3 indicates other significant parameters assumed for the simulation.

Table 4.3: Other wind and wave parameters applied in the simulation.

Parameters	
Wind	
Turbulence model	Kaimal spectral model
IEC standard	61400-3 (Offshore wind turbine)
Turbulence intensity	10% [73]
Wind profile type	Power Law
Waves	
Wave kinematics model	JONSWAP/Pierson-Moskowitz spectrum (irregular)
Peak period	11 seconds (most frequent in Fig. 4.5)

Power law exponent was set as 'default' in accord to IEC 61400-3. Wave kinematics model may be the JONSWAP or Pierson-Moskowitz spectrum model depending on the peak shape parameter. Based on the peak wave period and significant wave height, peak shape parameter is computed and may vary from 1 to 5 [66]. The chosen model for simulation (turbine and platform) is now presented.

Model for simulation

With the deployment of the offshore wind market, new and bigger wind turbines have been designed and modelled for higher productions. The construction and assembly close to the coast make it easier to produce wind turbines with higher capacities, since the size is not a constraint to move the platform and turbine to the production site.

There is no freely available input files for the simulation of the WindFloat Atlantic semi-submersible platform and $8.4\ \mathrm{MW}$ turbine, neither a definition of all their characteristics to create new input files. Due to that, based on the emergence of larger wind turbines, the chosen model was the IEA Wind $15\ \mathrm{MW}$ offshore reference wind turbine together with UMaine VolturnUS-S reference platform (semi-submersible type). OpenFast input files to run the simulation are free and available online on [74] and [75].

The characteristics of the turbine and platform are well defined and can be consulted in [76] and [74]. The system was designed for a water depth of $200\ \mathrm{m}$ and the mooring system consists in three-line chain catenary. Tables 4.4 and 4.5 present the main key parameters of the $15\ \mathrm{MW}$ turbine and semi-submersible platform. Fig. 4.7 depicts the system and its coordinates.

Table 4.4: Key Parameters for the IEA Wind $15\ \mathrm{MW}$ Turbine, from [76].

Wind turbine parameters	
Power rating [MW]	15
Rotor orientation	Upwind
Number of blades	3
Cut-in wind speed [$\mathrm{m/s}$]	3
Rated wind speed [$\mathrm{m/s}$]	10.59
Cut-out wind speed [$\mathrm{m/s}$]	25
Design tip-speed ratio	9.0
Minimum rotor speed [rpm]	5.0
Maximum rotor speed [rpm]	7.56
Rotor diameter [m]	240
Airfoil series	FFA-W3-370
Hub height [m]	150
Drivetrain	Direct drive
Shaft tilt angle [deg]	6
Rotor nacelle assembly mass [t]	1,017

Table 4.5: Semisubmersible Platform Properties, from [74].

Platform parameters	
Hull Displacement [m^3]	20,206
Hull Steel Mass [t]	3,914
Tower Interface Mass [t]	100
Ballast Mass (Fixed/Fluid) [t]	2,540/11,300
Draft [m]	20
Vertical Center of Gravity from SWL [m]	-14.94
Vertical Center of Buoyancy from SWL [m]	-13.63
Roll Inertia about Center of Gravity [$\mathrm{kg\,m^2}$]	1.251E+10
Pitch Inertia about Center of Gravity [$\mathrm{kg\,m^2}$]	1.251E+10
Yaw Inertia about Center of Gravity [$\mathrm{kg\,m^2}$]	2.367E+10

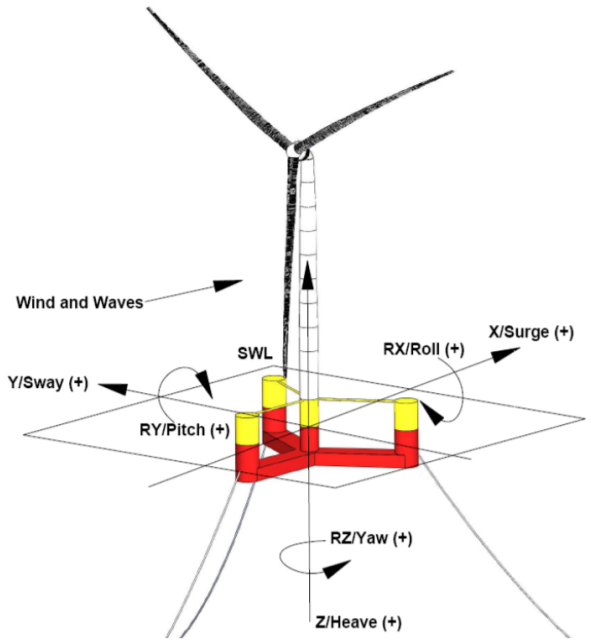

Figure 4.7: Floating offshore wind turbine reference coordinate system, from [74].

Simulation results

After the creation of the turbulent wind files, each simulation is run for 10 minutes. The first 45 seconds of energy production were removed from the results due to the transient initial stage. As an example of simulation, Fig. 4.8 depicts the results for the case when $\overline{U}_{hub}$ is $9\ \mathrm{m/s}$, a situation close to the WindFloat Atlantic average wind speed ($8.37\ \mathrm{m/s}$).

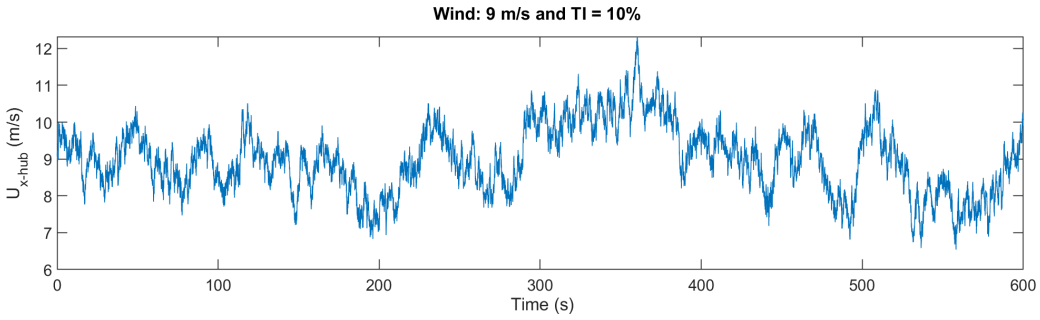

(a) Wind speed variation in the x direction (aligned with the turbine's rotor).

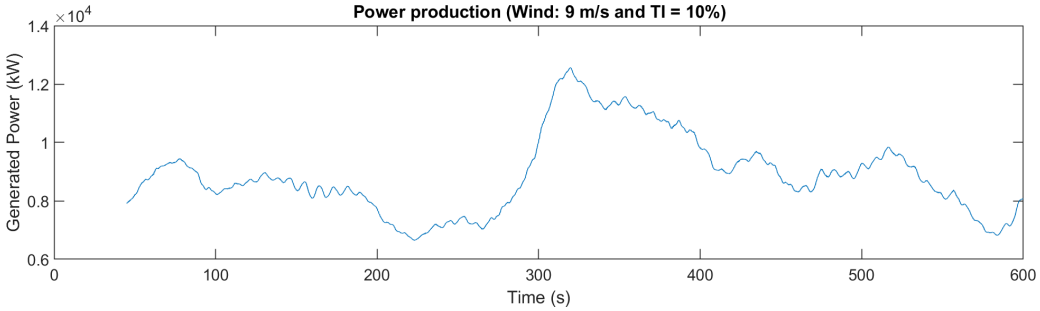

(b) Generated power (initial transient phase is removed).

Figure 4.8: Ten-minute simulation results in the case of $\overline{U}_{hub} = 9\ \mathrm{m/s}$.

Computing the average and standard deviation for all cases, a dynamic power curve is plotted in Fig. 4.9. The theoretical power curve given in [76] is also depicted for comparison.

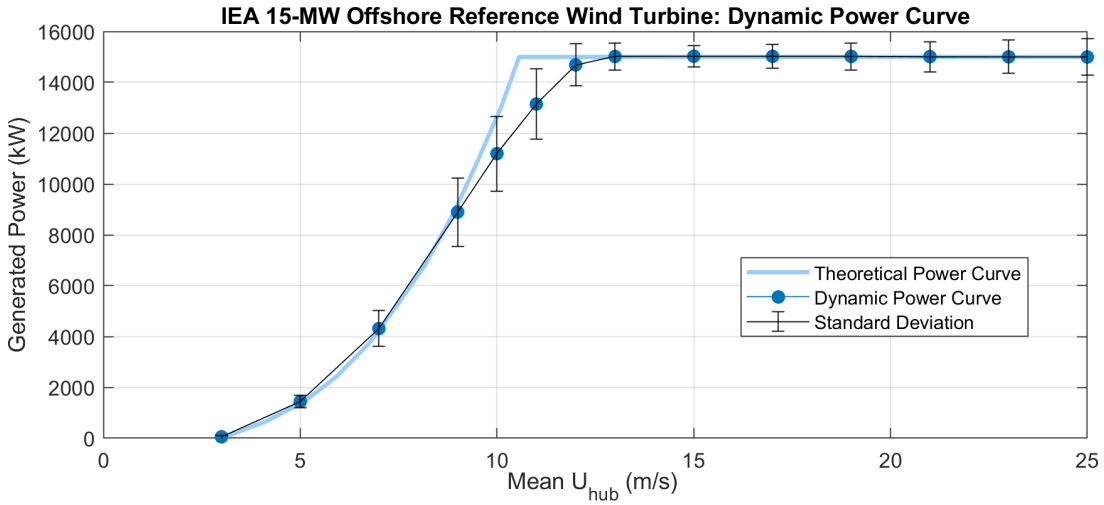

Figure 4.9: Comparison between the turbine's theoretical power curve and the simulated dynamic power curve ($\mathrm{TI} = 10\ \%$ for all cases).

Observing the previous Fig. 4.9, theoretical and dynamic curves are almost coincident. The exception happens in the transition to the rated production (between 9 and $13\ \mathrm{m/s}$). Wind turbine's power curves are obtained from mean values of a set of measurements, and that is the reason for the typical smooth shape they present around the rated wind speed [77]. In fact, the theoretical power curve given in [76] is not a measured curve, but a system of three stages:

1. For wind speeds below the cut-in wind speed and above the cut-out wind speed, there is no generated power;

2. Between the cut-in wind speed and rated wind speed, the power production presents a non-linear relationship with the wind speed (varies with the power of 3);

3. From rated wind speed until the cut-out wind speed, the power generation is constant at its rated value.

The non-linear relation of the stage 2) is roughly represented by a cubic expression. Typically, the cubic power curve ($P(u_w)$) is given by the Eq. 4.3, where ρ is the air density, A the rotor area, C_p the power coefficient and u_w the wind velocity.

$$P(u_w) = \frac{1}{2}\rho A C_p u_w^3 \tag{4.3}$$

As an approximation, C_p is roughly assumed as the maximum value of the effective power coefficient, $C_{p,max}$ [77].

Standard deviations are higher around the rated wind speed, because the wind speed fluctuations caused by turbulence inevitably create the same behaviour on the generated power. With the increase of the wind speed and consequent distancing from the rated speed, the standard deviations decrease a lot and are mainly result of the controller delay.

4.4 Electricity Market

Last part of this chapter is to understand how wind energy in correlated with wholesale electricity market prices. One of the main factors for the hydrogen production costs is the electricity price. Next subsections present a description how the wholesale electricity market works in Iberian Peninsula and an analysis to understand how the electricity price is related with renewable production, namely the wind.

4.4.1 MIBEL market

Iberian Electricity Market – MIBEL is the result of a cooperation between the Portuguese and Spanish Governments with the aim of promoting the integration of both countries' electrical system [78]. It is a free market where each consumer can freely choose the electricity supplier. Fig. 4.10 shows a representative scheme of the energy offer and its intersection with hypothetical demand curves. In effect, this intersection of curves is the operating base of the complex algorithm Euphemia [79], responsible for maximizing the welfare of the consumers and producers.

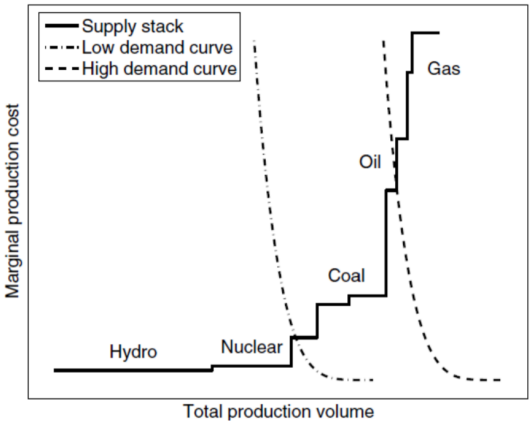

Figure 4.10: Scheme of the energy offer and its intersection with hypothetical demand curves, from [80]. Supply curve is organized in increasing order of marginal production costs. The demand curves represent the needs of electricity purchasers, and at what price they are willing to purchase it.

In the lower parts of the supply curves are the renewable offers due to the low cost of opportunity, except hydro production with reservoir that has a higher cost of opportunity in order on the expected price at another time.

Usually, Portugal and Spain are in the same market, however at the moments that the interconnections between both countries exceed their capacity, the market splitting occurs, and consequently different electricity prices.

Electricity prices are widely influenced by three characteristics of the market: randomness, volatility and seasonality [80]. In the context of this competitive economic environment, different models to preview the electricity price have been developed, because it is beneficial to predict the future electricity prices for better strategies and profits of producers and for financial benefit of those who buy it.

To combine all the variables, the developed models to predict the electricity price are complex and different methods have been used, such as multi agent models (game theoretic, simulation), fundamental models (structural), quantitative models (stochastic), statistical models or even artificial intelligence-based models. Detailed information about these models is available in [80].

Also, in the Chapter 4 of [80], the author depicted a statistical analysis of some variables with the electricity price of the years 2012 and 2013. Some of the main conclusions are presented herein:

1. Volatile nature of the electricity price is a direct consequence of the incapacity to storage electricity;
2. When the consumption is high, just a small increase may increase the electricity price a lot (see Fig 4.10);
3. Seasonal and meteorological factors are the most important ones for the electricity price preview;
4. Electricity price is higher during week comparing with weekends due to the higher consumption;
5. Minimum price is achieved during night and there are two peaks, the first when people wake up and go to work and the latter when people return home after work;
6. Seasonal price difference can be also expressed by temperature, and the prices are higher for temperatures lower than $5\,^{\circ}\mathrm{C}$, due to heating, or higher than $20\,^{\circ}\mathrm{C}$, due to cooling;

7. Wind is considered the most important preponderant factor in the MIBEL market due to the high wind production;

8. Dry months tend to create higher electricity prices.

4.4.2 Analysis of the electricity price of 2019

Though, the aim of this thesis is not to design a complex model to preview the electricity price, but some data about 2019's electricity market prices, production and consumption in Portugal were obtained for a statistical analysis:

- *REN* [81], the concession that holds the national electricity transmission grid, provides data about electricity production and consumption in Portugal along the day. For demand, consumption, hydro pumping and exportation were given data. For supply, the special regime generation (wind, solar, co-generation, wastes and small hydro [< 10 MW]), hydro, non-renewable, such as coal and natural gas, and importation were the available data.

- On the *OMIE*'s website [82], the entity that manage the Iberian Peninsula's day-ahead and intraday electricity markets, it's possible to obtain the hourly electricity prices of the MIBEL daily market in Portugal.

From now on, for an easier writing, every time that renewable production is mentioned means special regime generation and all hydro production.

Definition of the cases of study

Consumption is one of the most significant factors of the electricity price due to the high amounts of energy needed to ensure all consumption demand. Fig. 4.11 shows the variation of the electricity price and consumption in January of 2019 and their relation can be easily observed.

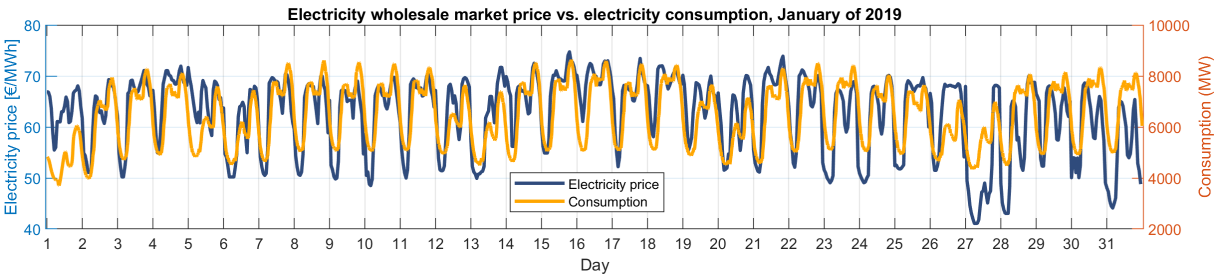

Figure 4.11: Consumption vs. electricity price – January, 2019.

In a first approach, this market analysis was done for the nights – **Case 1**. Nights are the time when the electricity is in general cheaper since there is lower electricity consumption (see Fig. 4.12). The interval from 3 to 8 a.m. ($\mathrm{C1}_{5h}$) comprehends the five hours of the day with lower electricity prices, on

average (Eq. 4.4). $h_{\min}$ denotes for the hour where the yearly average electricity price ($\overline{p}_{\text{elec}}$) is lower.

$$\begin{cases} h_{\min} = \min\left[\overline{p}_{\text{elec}}(h)\right], h \in \{1, \ldots, 9, 10\} \\ \text{C1}_{5h} = [h_{\min} - 2, h_{\min} + 2] \end{cases} \tag{4.4}$$

In a second approach, the analysis was done for the local minimum of consumption that happens during the afternoon (about 4 hours in Winter) – **Case 2** (see Fig. 4.12). The considered interval (C2_{4h}) was from 3 to 7 p.m. (Eq. 4.5).

$$\begin{cases} h_{\min} = \min\left[\overline{p}_{\text{elec}}(h)\right], h \in \{12, \ldots, 21, 22\} \\ \text{C2}_{4h} = [h_{\min} - 2, h_{\min} + 1] \end{cases} \tag{4.5}$$

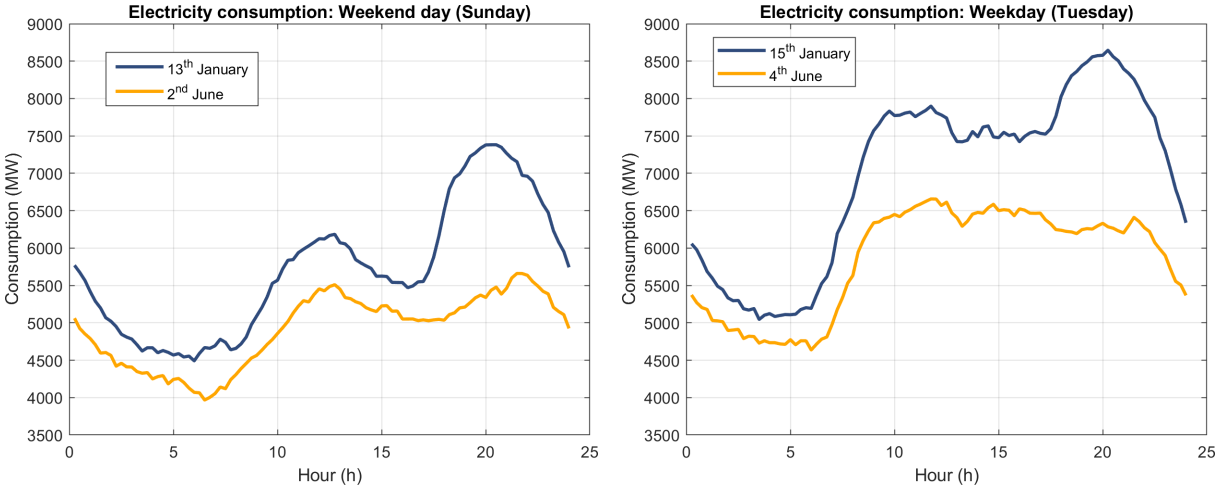

(a) Sunday (b) Tuesday

Figure 4.12: Typical electricity consumption curves in January and June of 2019.

Therefore, an average of the electricity prices was done for each interval of hours, for all days of the year. Daily average electricity price in Case 1 ($p_{\text{elec}\,[\text{C1}_{5\text{h}}]}$) is computed with Eq. 4.6, where i is the hour of the day and p_{elec} the market electricity price.

$$p_{\text{elec}\,[\text{C1}_{5\text{h}}]} = \frac{\sum_{i=3}^{7} p_{\text{elec}_i}}{5} \tag{4.6}$$

Eq. 4.7 shows the formula for the Case 2 daily average electricity prices ($p_{\text{elec}\,[\text{C2}_{4\text{h}}]}$).

$$p_{\text{elec}\,[\text{C2}_{4\text{h}}]} = \frac{\sum_{i=15}^{18} p_{\text{elec}_i}}{4} \tag{4.7}$$

Then, the five lower and the five higher averages of each month were taken and associated to the respective renewable and non-renewable production. Due to practical reasons, the production data is not an average for that intervals, but the values at 5 a.m. or 5 p.m. ($h_{\min}$) for Cases 1 and 2, respectively. Thus, each case has 10 data points for each month, 120 for the whole year. All the following analysis takes only these points into consideration.

Case 1: Nights (3 – 8 a.m.)

During nights, the mean electricity consumption is around 5000 MW in the winter semester, and 4500 MW in the summer semester. A weighted calculation has been made to take consideration the difference between week and weekend consumption.

The relation between the electricity price and the ratio of renewable production under all energy demand (consumption, hydro pumping and exportation) is depicted on Figs. 4.13 and 4.14 for 2019 and its semesters, respectively.

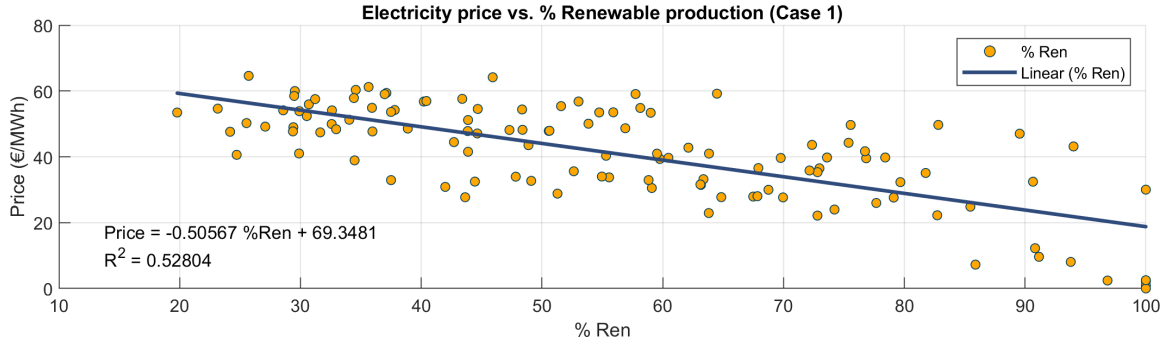

Figure 4.13: Electricity price vs. percentage of renewable production in 2019 (Case 1).

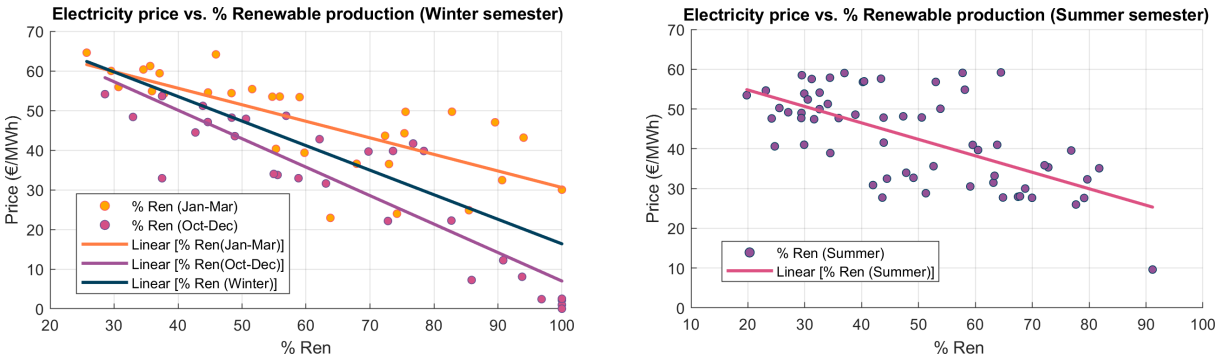

(a) Winter semester: Jan - Mar; Oct - Dec.

(b) Summer semester: Apr - Sep.

Figure 4.14: Electricity price vs. percentage of renewable production separated by semesters (Case 1).

Table 4.6 shows the different linear correlations by year, semester and seasons. January, February and March months of 2019 had below average precipitation – dry months, and October, November and December had above average precipitation – humid months [83].

Winter, namely humid months, presents a tendency for higher slopes, and consequently, the electricity prices became more unstable than Summer or dry months. If there is no renewable production (0 % Ren), the electricity price reaches the higher values, but for 100 % renewable production the lowest price values are obtained.

The correlation of wind production with renewable production at night is necessary to enable the establishment of wind scenarios. Fig. 4.15 shows that relation for a given hydro production, i.e, for a given season and precipitation conditions. During night, at 5 a.m., solar production does not exist yet, and the renewable production almost only depends on wind and hydro power. Biomass, co-generation and small hydro power plants at night are roughly constant (about 700-1000 MW in total).

Table 4.6: Linear correlations between the percentage of renewables ($\%$ Ren) with the electricity price (€/MWh) for Case 1. Winter semester comprehends Jan, Feb, Mar, Oct, Nov and Dec and Summer semester the remaining months. Seasons correspond to the meteorological divisions.

2019: Case 1	X-**Domain** [%]	Y-**Domain** [€/MWh]	**Slope** [(€/MWh)/%]	Y-**Intercept** [€/MWh]	**Coefficient of determination** R^2
Year	[20,100]	[19,59]	-0.506	69.35	0.528
Winter Semester	[26,100]	[16,62]	-0.619	78.31	0.618
Winter Semester (Jan – Mar)	[29,100]	[7,58]	-0.718	78.81	0.792
Winter Semester (Oct – Dec)	[26,100]	[31,61]	-0.418	72.34	0.543
Summer Semester	[20,91]	[25,55]	-0.414	63.06	0.419
Winter	[26,100]	[17,67]	-0.677	84.70	0.674
Spring	[29,100]	[20,62]	-0.580	78.40	0.549
Summer	[20,77]	[31,52]	-0.370	59.04	0.477
Autumn	[29,94]	[14,53]	-0.604	70.93	0.689

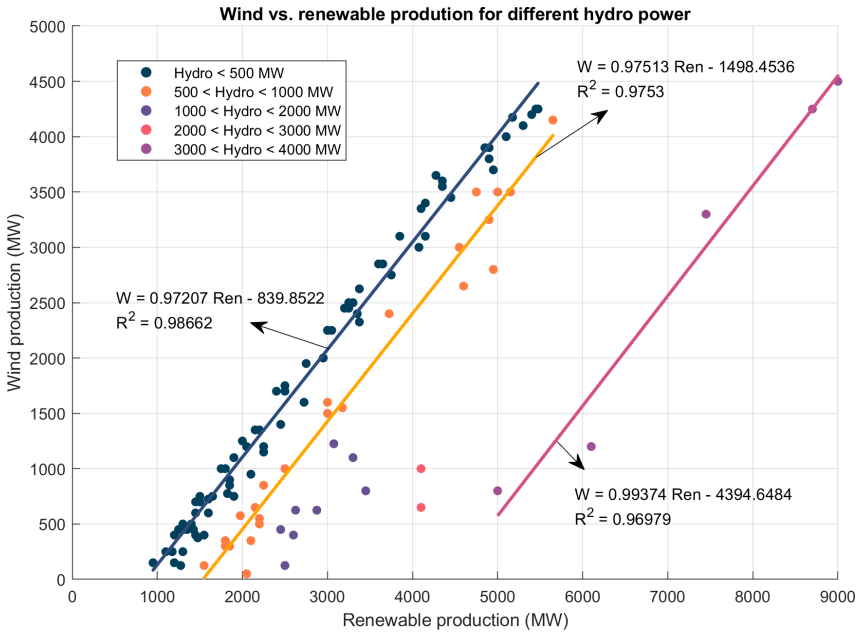

Figure 4.15: Wind vs. renewable production for different hydro power (Case 1).

At 5 a.m., on Winter, the average of hydro production on the dry months (January and February) was 390 MW while in December the average reached the value of 2280 MW. On Spring, Summer and Autumn the produced average was respectively 571 MW, 127 MW and 249 MW.

Exportation and importation do not have a significant impact on the electricity price and there is no correlation as seen in Fig. 4.16 a). Only in a scenario of very high renewable production, and consequently very low price (< 20 €/MWh), there was a tendency to export the excess of energy, while in a scenario of lower renewable production, and higher price (> 20 €/MWh), there was a bigger tendency to import electricity, for sure cheaper than the non-renewable produced in Portugal. Fig. 4.16 b) shows that in a scenario of importation at night there is a tendency for lower hydro power.

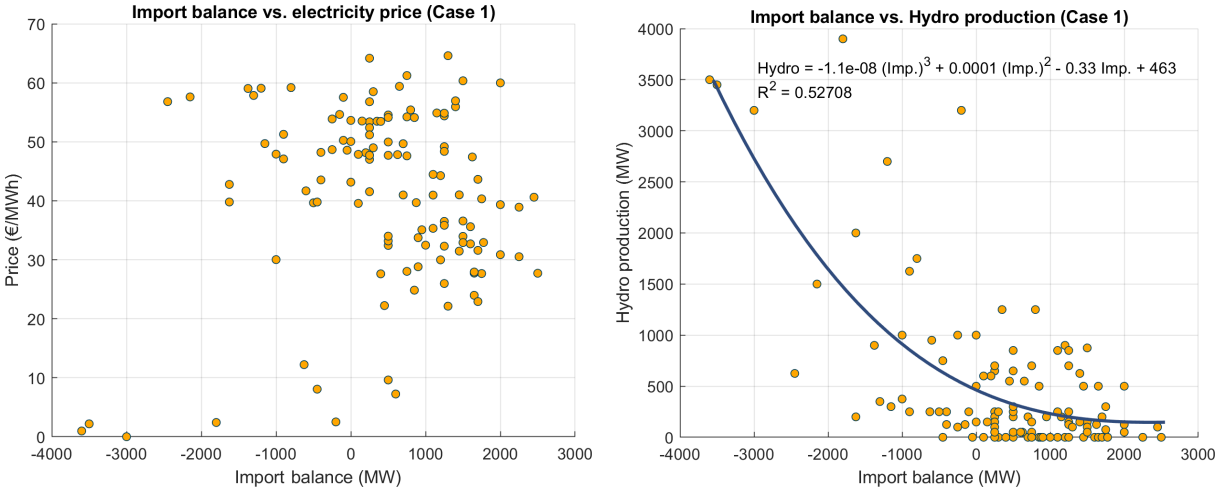

(a) Relation with electricity price.

(b) Relation with hydro production.

Figure 4.16: Import balance analysis (Case 1).

Hydro pumping is a possible way of "storing" cheap electricity to be sold afterwards. Thus, the relation between hydro pumping and wind production is shown on Fig. 4.17. An heteroscedastic behaviour is shown on the scatter chart. Therefore, high wind production caused not only the highest hydro pumping demand, closer to $2\ \mathrm{GW}$, but also values close to $0\ \mathrm{GW}$.

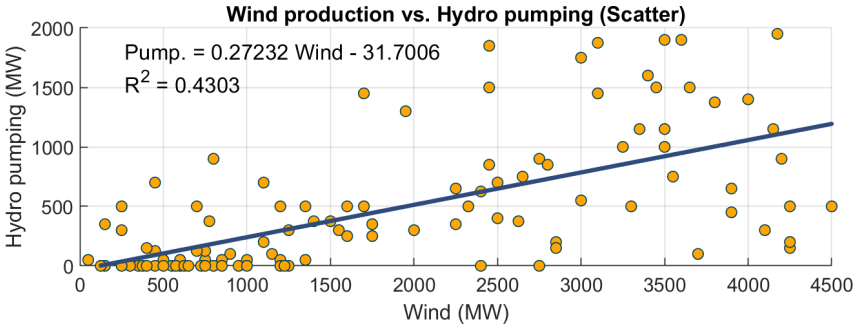

(a) Scatter graph

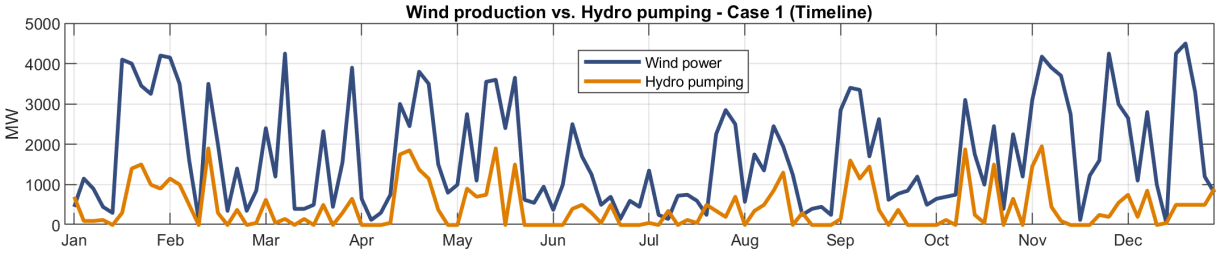

(b) Timeline plot.

Figure 4.17: Wind production power vs. hydro pumping power (Case 1).

Case 2: Afternoons (3 – 7 p.m.)

During afternoons, the mean electricity consumption is around $6500\ \mathrm{MW}$ in the Winter semester, and $6000\ \mathrm{MW}$ in the Summer semester.

As in the previous case, Figs. 4.18 and 4.19, and Table 4.7 depict the linear correlations of the

wholesale market electricity price with percentage of renewable production during the afternoon period of this Case 2. In general, coefficients of determination (R^2) are substantially lower than in the Case 1. That may occur due to a more dynamic electricity market during afternoon comparing with nights, such as solar energy power or more unexpected consumption events.

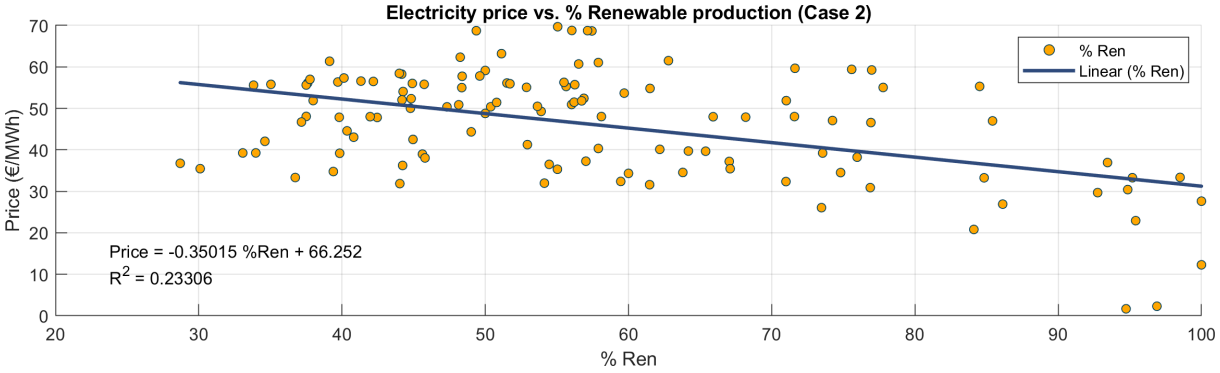

Figure 4.18: Electricity price vs. percentage of renewable production in 2019 (Case 2).

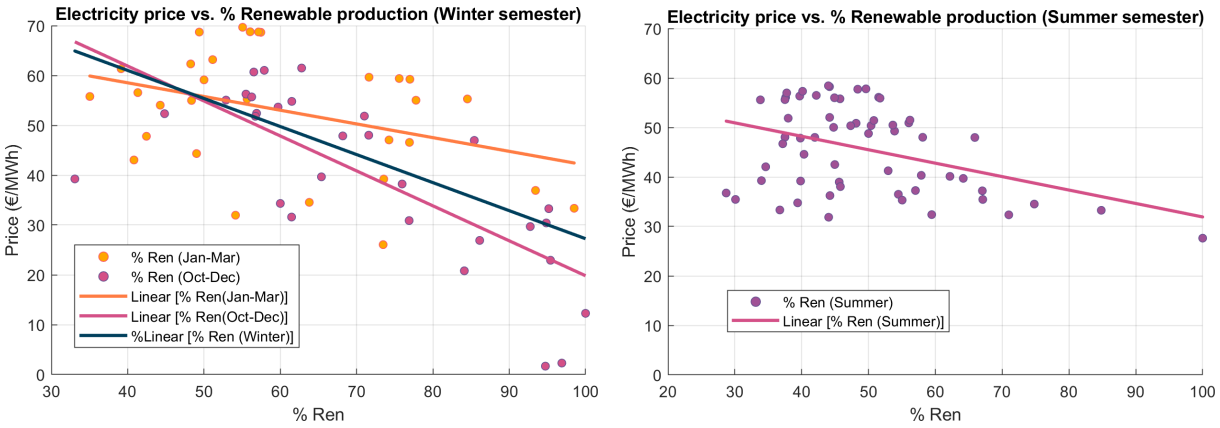

(a) Winter semester: Jan - Mar; Oct - Dec.

(b) Summer semester: Apr - Sep.

Figure 4.19: Electricity price vs. percentage of renewable production separated by semesters (Case 2).

To correlate the wind production power to the renewable's, unlike to what was done before, Fig. 4.20 presents one graphic for the winter (a) and another for the summer semester (b). For Case 2, the separation was necessary to take in account the solar power. Solar power was $0 - 200$ MW in the Winter semester months and $200 - 400$ MW in the Summer semester, and that facilitated the division of the data.

Analyzing the import balance power, once again there is no evident relation between it and the electricity price (Fig. 4.21 (a)). However, the relation between importation/exportation and hydro power in much more evident, even when compared with Case 1 (Fig. 4.21 (b)). Assuming a scenario where the import balance is null, based on this dataset of 120 points, it is reasonable to assume that hydro production will take low values (< 1000 MW).

The relation between hydro pumping and wind production is shown on Fig. 4.22. Comparing with Case 1, less energy dedicated to hydro pumping during these afternoon periods can be noted. Even so, during dry months, especially late Spring and Summer, there were significant events of hydro pumping.

Table 4.7: Linear correlations between the percentage of renewables ($\%$ Ren) with the electricity price (€/MWh) for Case 2. Winter semester comprehends Jan, Feb, Mar, Oct, Nov and Dec and Summer semester the remaining months. Seasons correspond to the meteorological divisions.

2019: Case 2	X**-Domain** [%]	Y**-Domain** [€/MWh]	**Slope** [(€/MWh)/%]	Y**-Intercept** [€/MWh]	**Coefficient of determination** R^2
Year	[28,100]	[30,56]	-0.350	66.25	0.233
Winter Semester	[32,100]	[20,65]	-0.563	83.53	0.403
Winter Semester (Jan – Mar)	[35,99]	[42,60]	-0.275	69.53	0.142
Winter Semester (Oct – Dec)	[32,100]	[20,68]	-0.701	89.94	0.554
Summer Semester	[28,100]	[30,51]	-0.272	59.09	0.1613
Winter	[39,100]	[24,71]	-0.784	102.58	0.538
Spring	[33,100]	[44,50]	-0.418	67.85	0.415
Summer	[29,68]	[28,55]	-0.141	53.56	0.045
Autumn	[30,95]	[34,51]	-0.262	59.28	0.148

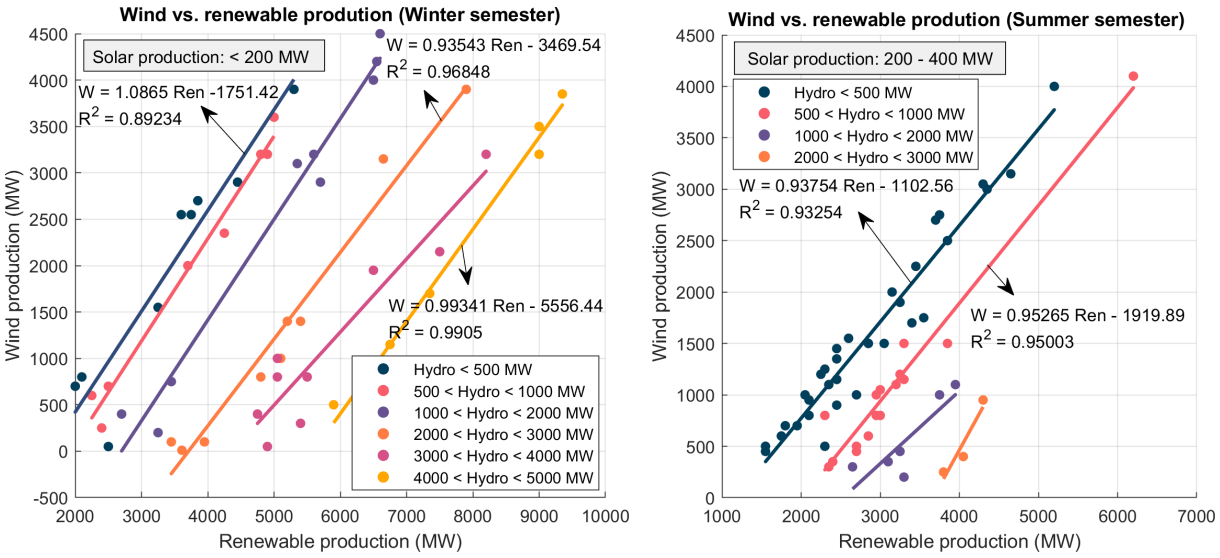

(a) Winter semester.

(b) Summer semester.

Figure 4.20: Wind vs. renewable production for different hydro power (Case 2).

Summing up, some ideas may be taken in consideration:

1. Consumption is lower during night and may decrease during afternoons between lunch and dinner time, and therefore these are the chosen intervals for hydrogen production;

2. Summer and dry months of Winter correlation curves (Elec. price vs. $\%$ Ren) have a lower slope, and consequently, the lowest electricity prices of the year are hardly achieved on those times;

3. An expected value for wind production is easily obtained knowing the renewable production, the hydro power and the time of the year (for solar power);

4. Importation and exportation do not have a direct impact on electricity price, but present some

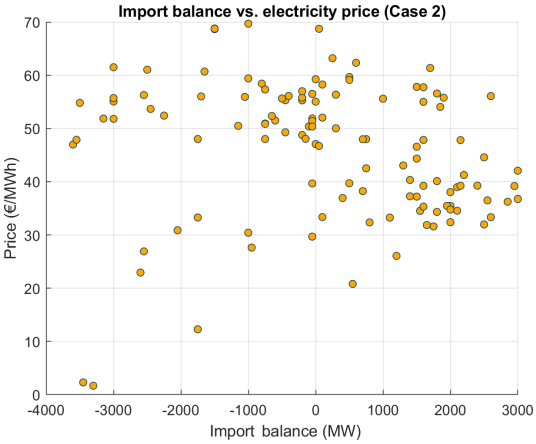

(a) Relation with electricity price.

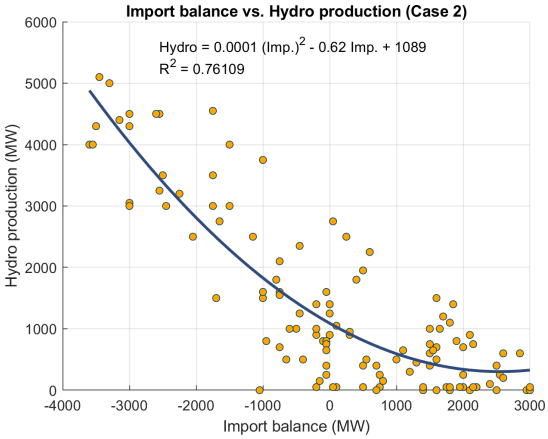

(b) Relation with hydro production.

Figure 4.21: Import balance analysis (Case 2).

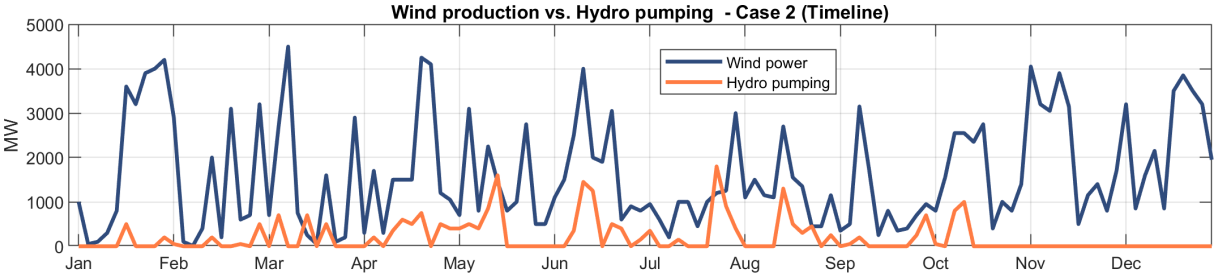

Figure 4.22: Wind production vs. hydro pumping power in 2019 (Case 2).

relation with hydro power. Thus, no import balance and low hydro power are considered in the scenarios;

5. When high wind production happens, hydro pumping may occur from 0 to 2 GW, since it depends on the reservoir capacity and cost of opportunity, *i.e.* pumping during night may or not be advantageous depending on the electricity price at the moment of pumping and the expected valorization afterwards.

Correlation data considering both semesters (Winter and Summer) is utilized in Section 5.2 to execute the reverse engineer of estimating the likely wind production at each electricity price in both periods of the day. Hydrogen production cost is then computed considering the number of events of each electricity price in 2019.

Chapter 5

Scenarios for Hydrogen Production

After knowing the current technologies for hydrogen production, the electricity production from an offshore wind turbine, and the relation between the electricity market and wind energy, a definition of the scenarios for hydrogen production is described on Chapter 5. Section 5.1 depicts the two main considered scenarios. Section 5.2 describes the considered cases of study to be applied on both scenarios.

5.1 Hydrogen Production Plant

PEM technology, although more expensive than alkaline electrolyzers, presents better adaptation to the wind variability with faster responses and better performances at partial load. Moreover, hydrogen is produced with higher degree of purity (without extra equipment for purification) and higher current densities. Thus, Scenarios 1 and 2 consider the PEM technology. Fig. 5.1 depicts a basic layout for a PEM electrolysis system.

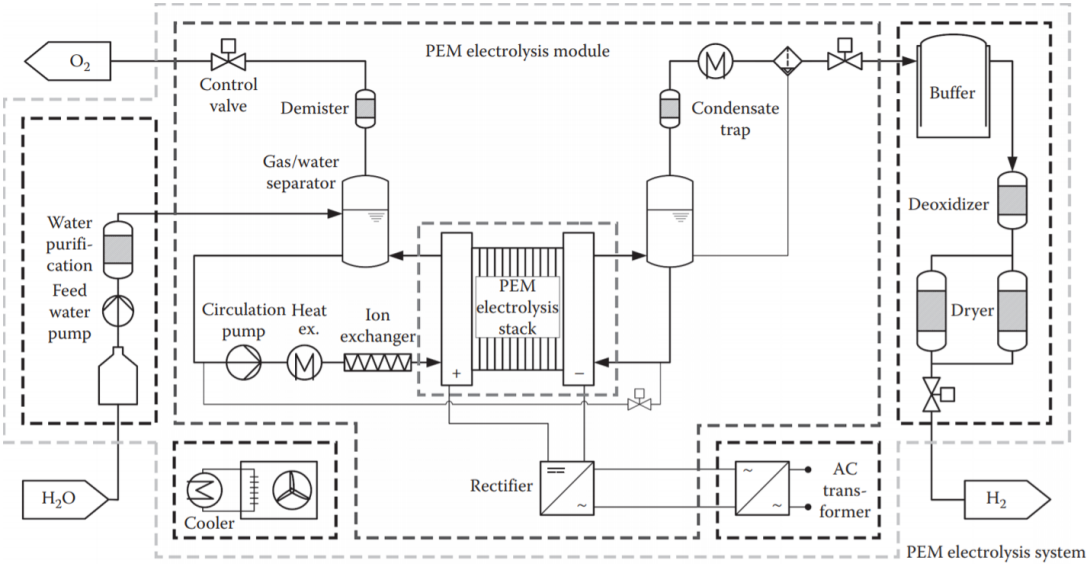

Figure 5.1: General layout of a PEM electrolysis system consisting of the PEM stack and module with power electronics and the EL subsystems for water purification, gas drying, and fine purification and cooling unit, from [51].

The chemical reactions in which water is decomposed with DC current happens in the PEM stack itself. However, PEM system comprises all necessary peripheral components to operate the stack properly at the desired operating conditions (pressure and temperature) [51]:

- The rectifier converts the incoming AC power into a regulated DC current.
- Cathode $(+)$ side is where water is supplied, pumped to ensure stack cooling and filtrated by an ion exchanger to trap heavy metals from the balance of plant (BoP) and stack corrosion.
- From the gas/water separator, water temperature and aerosol content in the oxygen may be adjusted with heat exchangers and baffles; Oxygen then flows through demisters (retaining fine droplets of liquid water) and a control valve that regulates the pressure.
- In the anode $(-)$ side, where the water level shall also be controlled for the circulation loop, a condensate trap and a buffer for hydrogen storage shall be installed to guarantee higher hydrogen purity and a constant hydrogen flow, respectively.
- As an option, for better hydrogen purity, a deoxidizer and dryer should be installed after the buffer: the first stage recombines remaining oxygen with hydrogen producing water, and second stage dries the hydrogen to remove the moisture.

5.1.1 Scenario 1: Stand-alone case-study

First scenario is called 'stand-alone case-study', a near-term scenario where the green H_2 economy is not fully-developed (no pipelines for H_2 distribution, nor any underground large-scale storage system, and lower H_2 demand). Fig. 5.2 presents the diagram of Scenario 1 for hydrogen production in Viana do Castelo using the electricity from the 25 MW WindFloat Atlantic offshore farm.

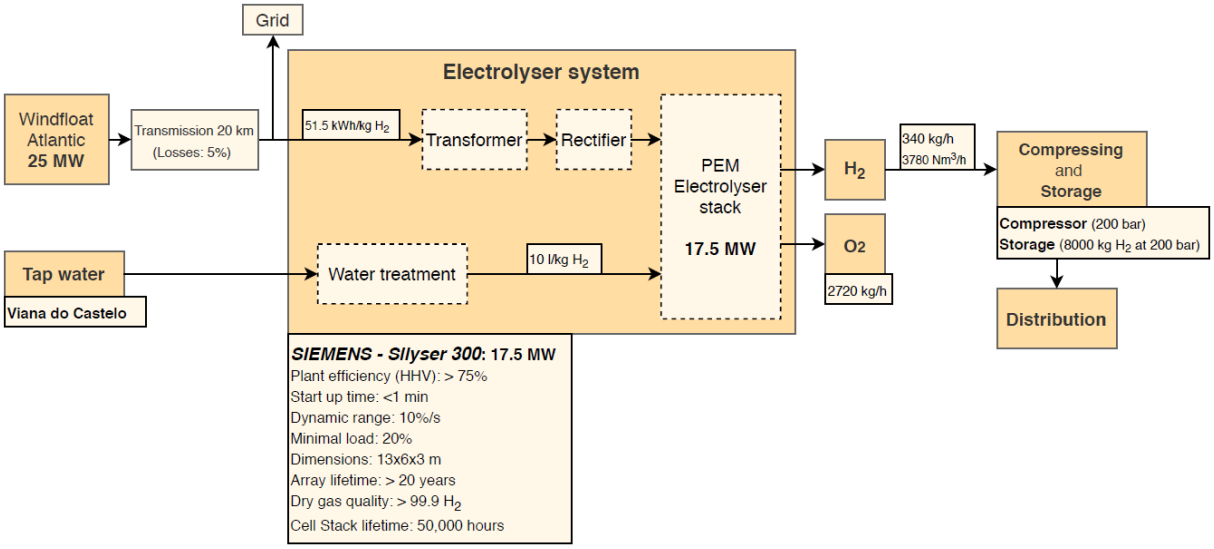

Figure 5.2: Scenario 1 outline.

Starting from the left side, there is the transmission of the electricity to the grid or the electrolyzer system depending on the electricity cost. For the transmission losses $(5\ \%)$, a high-voltage alternating

current (HVAC) transmission system was considered, since it is the most commonly used technology for not too long distances [84].

The water for electrolysis was assumed to be the tap water, since it is easier to treat for the necessary purity requirements. Theoretically, to produce 1 kg of hydrogen, 9 liters of water are needed, and the considered electrolyzer uses 10 liters of treated water (10 % of loss) [85]. There is also the possibility to use water from the sea or from the wastewater effluent, but as they have a lower purity, more energy and equipments are needed to make it with the necessary requirements for the electrolyzer. The cost per cubic meter of tap water is 1.9901€ for industrial use in Viana do Castelo [86].

A *Siemens* PEM electrolyzer [85] was chosen because they have been used in different projects of green hydrogen production in Germany and Austria [87]. Most of the current projects with *Siemens* electrolyzers utilize the Silyzer 200 of 2 MW. Nevertheless, *Siemens* presented already the next generation, the Silyzer 300 with the maximum capacity of 17.5 MW per full module array. A pilot project with Silyzer 300 is already implanted in Austria – *H2Future* [87]. Since the WindFloat Atlantic farm has a capacity of 25 MW, the Silyzer 300 with 17.5 MW was considered for this Scenario 1. Some of its main characteristics are shown in Fig. 5.2, from [85] and [88]. The stated efficiency of 75 % has in consideration not only the PEM stack (about 77 % efficiency) but also the rectifier, transformer, transformer cooling and gas cooling [89]. Fig. 5.3 is a representation of the module array of Silyzer 300.

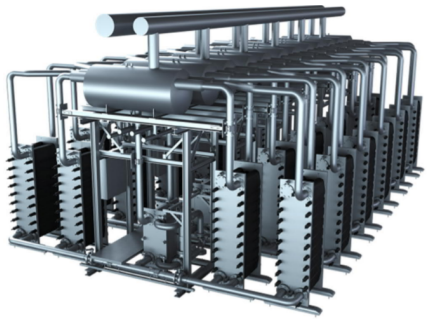

Figure 5.3: *Silyzer 300* - Module array (24 modules), from [87].

Capital and operation costs for this specific electrolyzer are not available, and the assumed values were taken from bibliography for the same kind of electrolyzers. Roadmap for Flanders [90] presents some cost assumptions for PEM electrolyzers in MW scale and multi-MW scale. The values were in accordance with other sources, such as [55], [91] and [43]. Therefore, for further analysis, the costs were assumed to linearly decrease from the MW scale (1 MW) until the multi-MW scale (10 MW) according to the plant size, and constant from there on (Fig. 5.4).

OPEX, in its broad sense, stands for all the operational costs and they are assumed as fixed or variable costs, such as the water expenses, the energy cost of the stack and peripheral equipments, and regular maintenance. On Fig. 5.4 and from now on, the tap water, stack energy consumption and stack replacement costs are not included in the electrolyzer OPEX, that is now regarded as a fixed operational cost.

Beyond the water and electricity consumed by the electrolyzer stack, the stack replacement is the third assumed variable operational cost. By taking the stack replacement cost as half of the capital

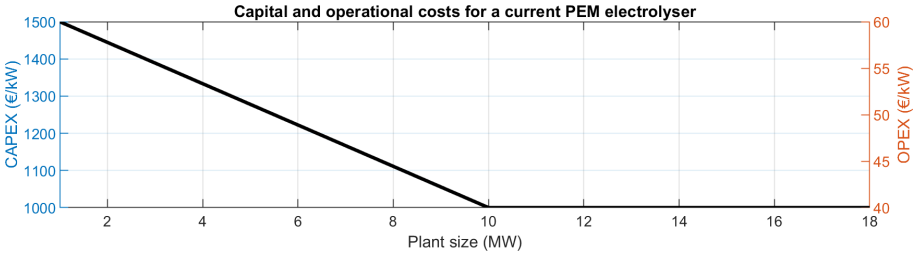

Figure 5.4: Assumed capital and operational costs for a current PEM electrolyzer. These OPEX values do not include the stack energy expenditure, water and stack replacement.

cost [90], and knowing that stack lifetime is $50,000$ hours, a linear cost as a function of the number of operating hours was assumed by computing the cost per operating hour.

As output of the electrolysis there are the hydrogen and oxygen. For the oxygen, it may be released in the air or stored to be sold. The last possibility is explored in Subsection 5.1.3. For the hydrogen, since there is a rated production of $340\ \mathrm{kg/h}$ and there is no hydrogen grid system for injection, the plant needs to have capacity to store a fixed quantity of hydrogen to inject in the natural gas grid and to supply hydrogen carriers. For Scenario 1, it is assumed that there is a regular demand and the plant needs to have the capacity to store 24 hours of rated hydrogen production $(8,160\ \mathrm{kg})$. At normal conditions, this quantity of hydrogen would take a volume of $90,767.5\ \mathrm{m^3}$, so compressing or liquefying is necessary.

Storing the hydrogen as compressed gas at 200 or $500\ \mathrm{bar}$ would require a storage volume of $523,1$ or $247,3\ \mathrm{m^3}$, respectively. For stationary applications, tanks of type I (Section 3.2) are the best option since they have the best cost performance and the weight of the tank is not a significant decision factor. However, the usual storing pressure of type I is $200\ \mathrm{bar}$ [54]. For higher pressures, type II tanks may be chosen but they are more expensive than type I. For this scenario, a specific cost of compressed hydrogen storage was obtained from the roadmap for Flanders $(225\ €/\mathrm{kg})$ [90].

To compress the hydrogen from $p_{\text{in}} = 30\ \mathrm{bar}$ (typical operational pressure for PEM technology) to $p_{\text{out}} = 200\ \mathrm{bar}$, the necessary compressed power $P(\mathrm{kW})$ is computed using Eq. 5.1 from [91]:

$$P = Q \times \frac{ZTR}{M_{H_2} \times \eta_{comp}} \times \frac{N\gamma}{\gamma - 1} \times \left[\left(\frac{p_{\text{out}}}{p_{\text{in}}} \right)^{\frac{\gamma-1}{N\gamma}} - 1 \right] = 314.60\ \mathrm{kW} \tag{5.1}$$

Where Q is the flow rate in $\mathrm{kg/s}$, Z the compressibility factor (set at 1 as an approximation), T the temperature at the inlet (set at $278\ \mathrm{K}$), R the ideal gas constant $(8.314\ \mathrm{J/K\,mol})$, M_{H_2} the hydrogen molecular mass, η_{comp} the compressor efficiency (set at $75\ \%$), N the number of compressor stages and γ the isentropic coefficient (1.4). Then, knowing the compressor power, the capital costs are computed using Eq. 5.2 adapted from [91]:

$$\mathrm{CAPEX\ compressor}(€) = 0.84 \times 15,000 \times \left(\frac{P(\mathrm{kW})}{10\ \mathrm{kW}} \right)^{0.9} \tag{5.2}$$

Operational costs are assumed to be $0.5\ \%$ of the CAPEX for the storage tanks and $3\ \%$ for the compressor [90]. Lifetime of both equipments are assumed as 20 years, equal to the electrolyzer system.

The hydrogen liquefaction is the process that requires more energy since it needs to achieve very

low temperatures. However, with liquid hydrogen the storage volume would be $116.6\ \mathrm{m}^3$. The cryogenic vessel is normally vacuum insulated and composed of an inner pressure vessel and an external protective jacket. This solution would require a hydrogen liquefier and since it is a more expensive process, the compression storage described above has been assumed instead.

Balance of plant (BoP) and other capital costs are considered as $5\ \%$ of the electrolyzer system CAPEX. Table 5.1 presents the capital and operation costs assumed for the Scenario 1.

Table 5.1: Capital and operational costs for Scenario 1.

Equipment	Costs
Electrolyzer system	
CAPEX [€]	$17,500,000$
OPEX [€/year]	$700,000$
Specific stack consumption [kWh/kg]	51.5
Stack replacement [€/h]	175
Tap water [€/m^3]	1.9901
H_2 Compressor	
CAPEX [€]	$280,769$
OPEX [€/year]	$8,423$
Specific consumption [kWh/kg]	0.93
H_2 Storage	
CAPEX [€]	$1,836,000$
OPEX [€/year]	$9,180$
BoP and others	
CAPEX [€]	$875,000$

5.1.2 Scenario 2: Integrated case-study

After phase 1 with a $2\ \mathrm{MW}$ prototype (WindFloat) and the current pre-commercial phase 2 of $25.2\ \mathrm{MW}$ (WindFloat Atlantic), the construction of a commercial $150\ \mathrm{MW}$ offshore wind farm is planned (phase 3) [92]. Based on that commercial phase offshore wind scenario, Scenario 2 is presented as a long-term solution for hydrogen production, when the H_2 economy is more established and pipeline grid systems exist for H_2 distribution. Thus, it is called 'integrated case-study'. Fig. 5.5 presents the diagram of Scenario 2.

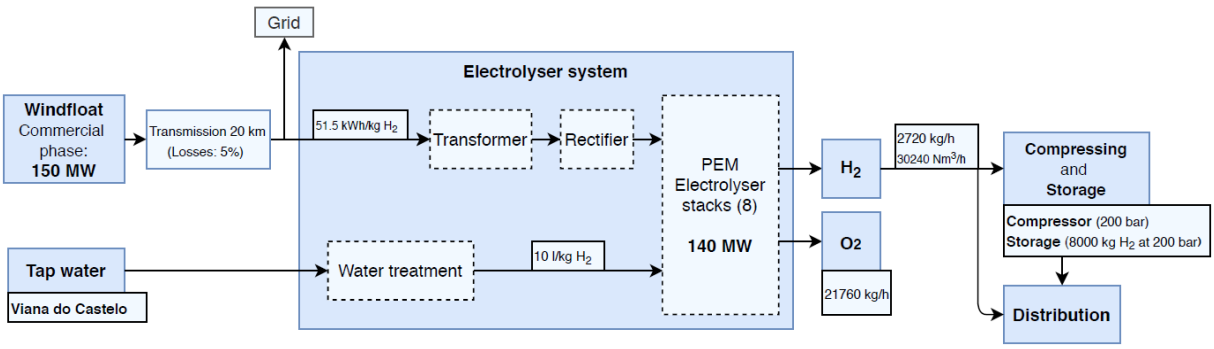

Figure 5.5: Scenario 2 outline.

A system of eight Silyzer 300 electrolyzers of 17.5 MW (140 MW) is assumed. This scenario makes sense if there is a developed hydrogen economy with a hydrogen distribution grid where it can be injected to be stored in salt caves or to be directly used by the industry, for instance. For that reason, after its production, this scenario considers that the hydrogen is directly distributed for the pipelines and partially stored in tanks. Comparing with Scenario 1, the capacity of hydrogen compression increases linearly with its nominal flow rate production, but the costs of storage capacity in stationary tanks is maintained constant, since there are the national or regional pipelines for distribution.

As a long-term scenario, the capital and operational costs of the electrolyzer may be lower than a short-term scenario, due to the emergence of an economy of scale with new and more efficient forms of production. Therefore, Fig. 5.6 shows the adopted costs for a long-term project, taken from [90].

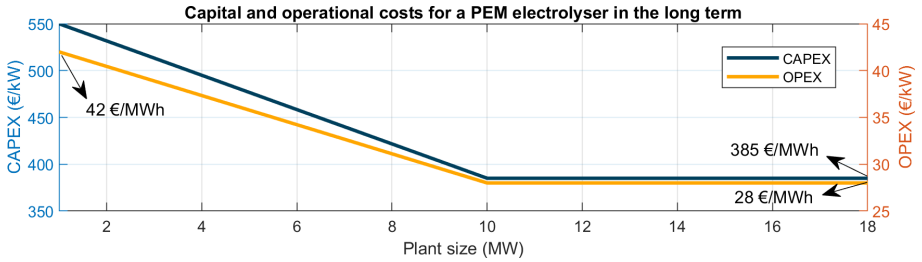

Figure 5.6: Assumed capital and operational costs for a PEM electrolyzer in the long term (2050).

Specific costs related with the compressor and storage are the same as Scenario 1. Table 5.2 presents the assumed capital and operation costs for the Scenario 2.

Table 5.2: Capital and operational costs for Scenario 2.

Equipment	**Costs**
Electrolyzer system	
CAPEX [€]	$53,900,000$
OPEX [€/year]	$3,920,000$
Specific stack consumption [kWh/kg]	51.5
Stack replacement [€/h]	539
Tap water [€/m^3]	1.9901
H_2 Compressor	
CAPEX [€]	$1,824,439$
OPEX [€/year]	$54,733$
Specific consumption [kWh/kg]	0.93
H_2 Storage	
CAPEX [€]	$1,836,000$
OPEX [€/year]	$9,180$
BoP and others	
CAPEX [€]	$3,012,772$

5.1.3 Oxygen selling option

Although the main goal is to produce hydrogen, oxygen is also produced in large quantities and could be sold as well, improving the overall economics of the plant [91]. For each kg (or m^3) of hydrogen, $8\ \mathrm{kg}$ (or $0.5\ \mathrm{m}^3$) of oxygen are produced. Oxygen has the largest global industrial gas market share ($26\ \%$) [15]. However, potential of selling all the oxygen is considered low, unless the location of the plant is favorable to use it on site, in local industry for instance [91]. Nevertheless, the scenario of oxygen capture is considered and some assumptions are taken to be applied on Scenarios 1 and 2.

Liquefaction and storage tanks for liquid oxygen were assumed due to the high production rates and possibility to sell it as liquid state and high purity not only for industry but also for medical applications. The criteria for the storage capacity is the same as hydrogen: possibility to storage 24 hours of rated production ($65,28\ \mathrm{kg}_{\mathrm{O_2}} \approx 57\ \mathrm{m}^3$ of liquid O_2) for Scenario 1; and the same capacity of storage vessels in Scenario 2 assuming also that exists a pipeline for distribution of gaseous oxygen for local industry. Liquefaction capacity is also the same in both scenarios. Table 5.3 presents therefore the capital and operational costs of the equipments and respective references.

Table 5.3: Capital and operational costs for oxygen capture in both scenarios.

Equipment for O_2	Costs	Observations
O_2 Liquefaction		
CAPEX [€]	$2,187,500$	$0.125\ \mathrm{M€/MW}_{\mathrm{electrolyzer}}$, from [93]
OPEX [€/year]	$18,000$	$3\ \%$ of CAPEX
Specific consumption [$\mathrm{kWh/ton}_{\mathrm{O_2}}$]	520	From [93]
Liquid O_2 storage		
CAPEX [€]	$600,000$	2 tanks of $30\ \mathrm{m}^3$ from [94]
OPEX [€/year]	$65,625$	$3\ \%$ of CAPEX

Selling price of oxygen vary in literature and depends on form (gaseous/liquid) and end-use application. The price per ton was claimed to be from $24.5\ €/\mathrm{ton}$ in [90] to values of $250\ €/\mathrm{ton}$ for medical use in Finland (liquid oxygen). Considered value for the oxygen cost is $100\ €/\mathrm{ton}$, reported by [95] for industrial use.

5.2 WindFloat Atlantic over the year 2019

Calculation of the cost of hydrogen for each of the scenarios takes into account the year 2019. Therefore, the electricity costs for all periods of the night (3 - 8 a.m.) and the afternoon (3 - 7 p.m.) in Portugal have been compiled. Fig. 5.7 is the result of this data collection.

As described in Section 4.4, there is a relation between renewable/wind production and electricity prices, and some correlations were taken for night and afternoon periods. Based on that correlations and on the data of Fig. 5.7 , an attempt has been made to go in the reverse engineer of estimating the probable wind production from electricity prices. Thus, following assumptions were made:

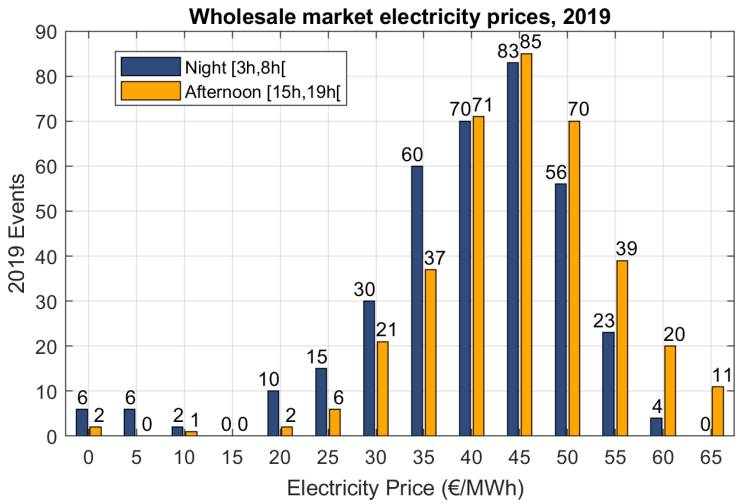

Figure 5.7: Wholesale market electricity prices in 2019, Portugal.

- A.1. – The wind production is uniform throughout the country, *i.e.* all the wind farms are assumed to produce at the same rate of capacity;
- A.2. – Months in the Winter have normal levels of precipitation (dry Winter months are ignored);
- A.3. – Wind energy is dedicated to produce H_2, thus there is no hydro pumping for reservoirs;
- A.4. – No importations or exportation of electricity are considered, and therefore the hydro production is assumed to be low (< 500 MW) – Figs. 4.16 and 4.21.

The procedure to determine the most likely wind production is then introduced: first, from the correlations between electricity price and percentage of renewables, $p_{\text{elec}} = f_1(\%\,\text{Ren})$ (Tabs. 4.6 and 4.7), the percentage of renewable production for each electricity price is taken for winter (humid months – A.2.) and summer semesters, $\%\,\text{Ren} = f_1^{-1}(p_{\text{elec}})$; then, that percentage is multiplied by the electricity consumption power, $e_{\text{cons.}}$ (according with the day period and semester); after obtaining the renewable production ($P_{\text{Ren}}[\text{MW}]$), assuming low hydro production – A.4., from Figs. 4.15 and 4.20 the expected wind production power is obtained, $P_{\text{wind}} = f_2(P_{\text{Ren}})$; each wind production power is divided by the maximum value of wind production ($P_{\text{wind}_{\text{MAX}}} \approx 4500$ MW) to obtain the wind farm's rate of capacity – $R_w[\%]$ (Eq. 5.3) – for each price of electricity (A.1).

$$R_w[\%] = \frac{P_{\text{wind}}}{P_{\text{wind}_{\text{MAX}}}} = \frac{f_2\left(P_{\text{Ren}}\right)}{P_{\text{wind}_{\text{MAX}}}} = \frac{f_2\left(\%\text{Ren} \times e_{\text{cons.}}\right)}{P_{\text{wind}_{\text{MAX}}}} = \frac{f_2\left(f_1^{-1}(p_{\text{elec}}) \times e_{\text{cons.}}\right)}{P_{\text{wind}_{\text{MAX}}}} \tag{5.3}$$

The case study of 2019 is divided in two main cases: **Case A** in which production is assumed to occur only during night and **Case B** during nights and afternoons (both on the considered interval of hours). Results for the expected wind power for hydrogen production are following presented.

5.2.1 Case A: Nights

In Case A, where the hydrogen is only produced during night, the lowest electricity price ($p_{elec} = 0$ €/MWh) is corresponded to a maximum wind farm's rate of capacity (R_w) of 89 %. In Scenarios

1 and 2, this percentage means a wind production power of 22.5 and 134.0 MW, respectively. After removing the transmission losses and the power for hydrogen compressor, the available power to produce hydrogen (P_{H_2}) is 17.5 (max.) and 140 MW for each of the scenarios. The application of this approach to all electricity prices is shown in Table 5.4. Silyzer 300 has a minimum load of 20 % for each module array, thus a minimum power of 3.5 MW is necessary.

Table 5.4: Case A: available power for hydrogen production (R_w) for each electricity price (p_{elec}). W. S. and S. S. stand for Winter and Summer semesters.

			Scenario 1: 17.5 MW (25.2 MW)				**Scenario 2: 140 MW (150 MW)**			
p_{elec}	R_w [%]		Wind Power [MW]			P_{H_2}	Wind Power [MW]			P_{H_2}
[€/MWh]	W. S.	S. S.	W. S.	S. S.	Avg.	[MW]	W. S.	S. S.	Avg.	[MW]
0	89%		22.5		22.5	**17.5**	134.0		134.0	**125.0**
5	89%		22.5		22.5	**17.5**	134.0		134.0	**125.0**
10	85%		21.4		21.4	**17.5**	127.3		127.3	**118.7**
15	77%		19.5		19.5	**17.5**	116.0		116.0	**108.2**
20	70%		17.6		17.6	**16.4**	104.7		104.7	**97.7**
25	62%	71%	15.7	17.8	16.8	**15.6**	93.4	106.1	99.8	**93.1**
30	55%	59%	13.8	14.9	14.3	**13.4**	82.1	88.5	85.3	**79.6**
35	47%	47%	11.9	11.9	11.9	**11.1**	70.9	70.8	70.9	**66.1**
40	40%	35%	10.0	8.9	9.5	**8.8**	59.6	53.2	56.4	**52.6**
45	32%	24%	8.1	6.0	7.0	**6.6**	48.3	35.6	42.0	**39.1**
50	25%	12%	6.2	3.0	4.6	**4.3**	37.0	18.0	27.5	**25.7**
55	17%	0%	4.3	0.1	2.2	**0.0**	25.7	0.4	13.1	**12.2**
60	10%	0%	2.4	0.0	1.2	**0.0**	14.4	0.0	7.2	**6.7**
65	2%	0%	0.5	0.0	1.2	**0.0**	3.2	0.0	1.6	**0.0**

5.2.2 Case B: Nights and afternoons

Case B assumes that hydrogen is produced not only in the afternoon but also at night. The following analysis in Tab. 5.5 shows the expected wind power for hydrogen production for each electricity price during the afternoon period.

To better visualize the relationship between wind farm production and hydrogen production, *i.e.* the influence of the maximum and minimum loads of the electrolyzer, the transmission losses and the power used in compression, Fig. 5.8 depicts the results presented in the previous tables.

Table 5.5: Case B (only afternoon period): available power for hydrogen production (R_w) for each electricity price (p_{elec}). W. S. and S. S. stand for Winter and Summer semesters.

			Scenario 1: 17.5 MW (25.2 MW)				**Scenario 2: 140 MW (150 MW)**			
p_{elec}	R_w [%]		Wind Power [MW]			P_{H_2}	Wind Power [MW]			P_{H_2}
[€/MWh]	W. S.	S. S.	W. S.	S. S.	Avg.	[MW]	W. S.	S. S.	Avg.	[MW]
0	100%		25.2		25.2	**17.50**	150.0		150.0	**140.0**
5	100%		25.2		25.2	**17.50**	150.0		150.0	**140.0**
10	100%		25.2		25.2	**17.50**	150.0		150.0	**140.0**
15	100%		25.2		25.2	**17.50**	150.0		150.0	**140.0**
20	100%		25.2		25.2	**17.50**	150.0		150.0	**140.0**
25	100%		25.2		25.2	**17.50**	150.0		150.0	**140.0**
30	89%	100%	22.5	25.2	23.9	**17.50**	133.7	150.0	142.2	**132.7**
35	78%	87%	19.6	21.8	20.7	**17.50**	116.6	129.8	123.2	**114.9**
40	66%	63%	16.7	16.0	16.4	**15.26**	99.6	95.2	97.4	**90.9**
45	55%	40%	13.9	10.2	12.0	**11.22**	82.5	60.6	71.6	**66.8**
50	44%	17%	11.0	4.4	7.7	**7.17**	65.4	26.1	45.8	**42.7**
55	32%	0%	8.1	0.0	4.1	**3.79**	48.4	0.0	24.2	**22.6**
60	21%	0%	5.3	0.0	2.6	**0.00**	31.3	0.0	15.7	**14.6**
65	9%	0%	2.4	0.0	1.2	**0.00**	14.2	0.0	7.1	**6.7**

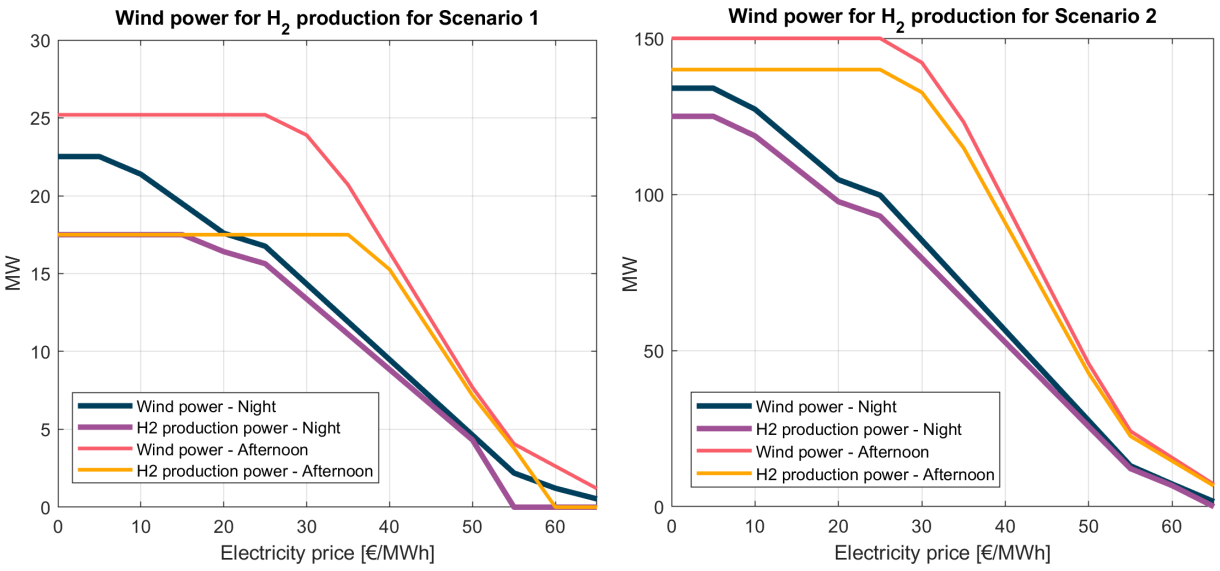

(a) Scenario 1: 17.5 MW from the 25.2 MW farm.

(b) Scenario 2: 140 MW from the 150 MW farm.

Figure 5.8: Wind power from the wind farm and its usage for the hydrogen production.

Chapter 6

Results and Discussion

The calculation of the cost of hydrogen is presented in this chapter. Section 6.1 starts the chapter with a preliminary cost analysis, where Cases A and B are not taken into account, *i.e.* an analysis which is independent of the year. Section 6.2 presents a cost analysis for Scenario 1 and 2, and Cases A and B. In Section 6.3, some economic parameters are applied on the results for a better feasibility study. Finally, in Section 6.4 a discussion of the results is given.

6.1 The Cost of Hydrogen Production

As a first approach, the cost of H_2 is calculated having in consideration the scenarios (different sizes and costs of the plant), the price of electricity and the number of operating hours. The possibility of storage and selling O_2 is also considered. The formula for the specific cost of H_2 without O_2 sales ($c_{\mathrm{H_2}}$) is presented below in Eq. 6.1:

$$c_{\mathrm{H_2}} = e_{\mathrm{Silyser}} \cdot \left(p_{elec} + \frac{\mathrm{CAPEX_{H_2}} + \mathrm{OPEX_{H_2}}}{P \cdot h} + \frac{\dot{C}_{\mathrm{stack}}}{P} \right) + e_{\mathrm{comp}} \cdot p_{elec} + \left[v_{\mathrm{H_2O}} \cdot c_{\mathrm{H_2O}} \right]_{\mathrm{water}} \tag{6.1}$$

Where e_{Silyser} stands for the specific electrolyzer energy consumption [$\mathrm{kWh/kg_{H_2}}$]; p_{elec} the electricity cost [€/kWh]; $\mathrm{CAPEX_{H_2}}$ the electrolyzer system, compressor and H_2 tanks CAPEX [€/year]; $\mathrm{OPEX_{H_2}}$ their respective OPEX [€/year]; P the production load [kW]; h the annual of operating hours [h]; $\dot{C}_{\mathrm{stack}}$ the stack replacement cost per operating hour [€/h]; $v_{\mathrm{H_2O}}$ the volume of water consumption per kg of produced H_2 [$\mathrm{m^3}$]; $c_{\mathrm{H_2O}}$ the water cost [€/$\mathrm{m^3}$] and e_{comp} the specific compressor energy consumption [$\mathrm{kWh/kg_{H_2}}$]. Efficiency is considered constant independently the load, *i.e.* e_{Silyser} is always the same.

When selling the produced oxygen, the capital and operating costs of the O_2 liquefier and tanks [€/year] ($C_{\mathrm{CAPEX_{O_2}}}$ and $C_{\mathrm{OPEX_{O_2}}}$), the liquefier consumption [$\mathrm{kWh/kg_{O_2}}$] (e_{liq}) and the O_2 selling price [€/$\mathrm{kg_{O_2}}$] ($p_{\mathrm{O_2}}$) must be considered. Eq. 6.2 shows the formula for the specific H_2 cost considering liquid O_2 storage and sales ($c_{\mathrm{H_2/O_2}}$):

$$c_{\mathrm{H_2/O_2}} = c_{\mathrm{H_2}} + c_{\mathrm{O_2}} = c_{\mathrm{H_2}} + \left[e_{\mathrm{Silyser}} \cdot \frac{\mathrm{CAPEX_{O_2}} + \mathrm{OPEX_{O_2}}}{P \cdot h} + 8 \cdot e_{\mathrm{liq}} \cdot p_{elec} - 8 \cdot p_{\mathrm{O_2}} \right]_{\mathrm{oxygen}} \tag{6.2}$$

Where c_{O_2} is the impact of oxygen on the cost of hydrogen [€/kg_{H_2}] and '8' the ratio value between O_2 and H_2 mass production.

6.1.1 Scenario 1

Applying the formulas 6.1 and 6.2 to the Scenario 1 and considering the costs given in Tables 5.1 and 5.3, and a constant H_2 production load of 17.5 MW, the following graphs in Fig. 6.1 with specific H_2 costs are obtained. Results obtained with and without both CAPEX and oxygen sales are shown.

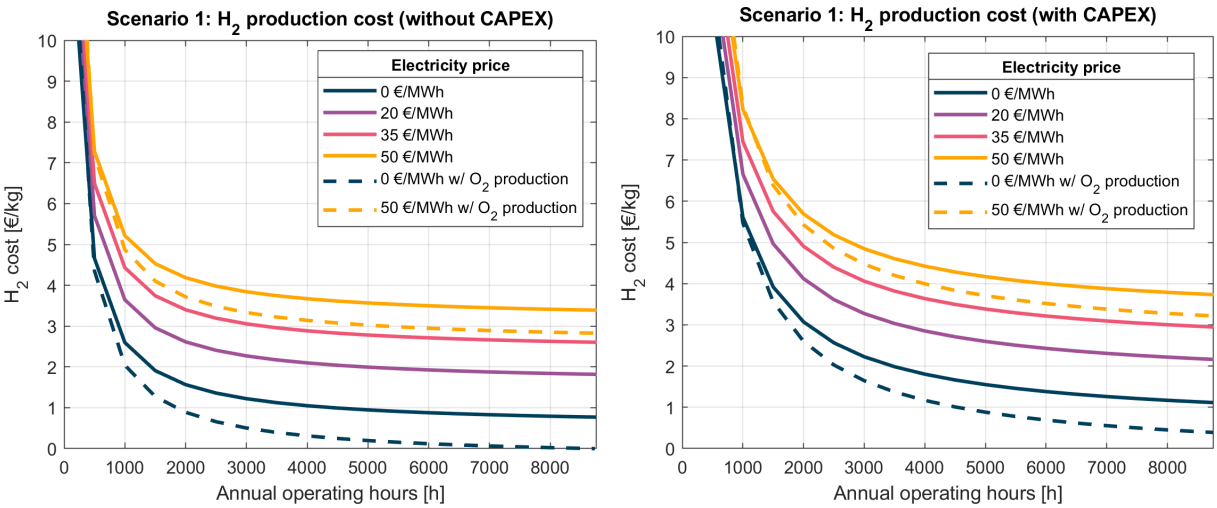

(a) Without CAPEX. (b) With CAPEX.

Figure 6.1: H_2 production cost for different number of operating hours, electricity price and either O_2 production or not for Scenario 1. Production at maximum load (17.5 MW) for all the electricity prices.

Without CAPEX, assuming an 100 % capacity factor, the H_2 costs vary from 0 €/kg ($p_{elec} = 0$ €/MWh with O_2 production) to 3.39 €/kg ($p_{elec} = 50$ €/MWh without O_2 production). With CAPEX, this variation is from 0.39 to 3.73 €/kg.

Fixing the electricity price at 35 €/MWh, a reasonable electricity price average for the upcoming years, the hydrogen production cost would achieve the value of 4 €/kg with a capacity factor of 15 % (≈ 1300 hours at full load) without considering CAPEX. To obtain the same hydrogen cost considering CAPEX, a capacity factor of 34 % (≈ 3000 hours at full load) is required.

6.1.2 Scenario 2

The same procedure was applied for Scenario 2, but now considering the costs on Tables 5.2 and 5.3, and a constant production load of 140 MW. H_2 specific costs are depicted in Fig. 6.2.

Without CAPEX, assuming an 100 % capacity factor, the H_2 costs vary from -0.34 €/kg ($p_{elec} = 0$ €/MWh with O_2 production) to 3.08 €/kg ($p_{elec} = 50$ €/MWh without O_2 production). With CAPEX, this variation is from -0.28 to 3.20 €/kg.

Fixing the electricity price at 35 €/MWh, the hydrogen production cost would achieve the value of 4 €/kg with a capacity factor of 12 % (≈ 1050 hours at full load) without considering CAPEX. To obtain

the same hydrogen cost considering CAPEX, a capacity factor of $20\ \%$ ($\approx$ 1750 hours at full load) is required.

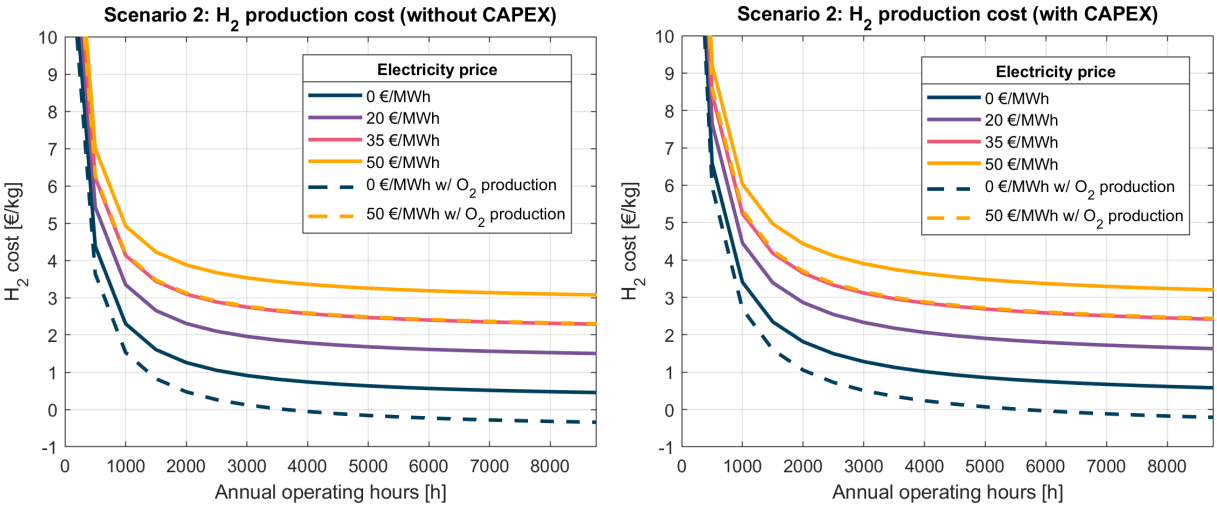

(a) Without CAPEX.

(b) With CAPEX.

Figure 6.2: H_2 production cost for different number of operating hours, electricity price and either O_2 production or not for Scenario 2. Production at maximum load ($140\ \mathrm{MW}$) for all the electricity prices.

6.2 Case Study: WindFloat Atlantic over the year 2019

Considering now the Cases A and B, *i.e.* the influence of the number of events of each electricity price (Fig. 5.7) and their correspondent likely wind production power and hydrogen production power (Fig. 5.8) during nights and afternoon, some graphs with costs, quantity of produced hydrogen, specific H_2 cost and profits are presented.

Specifications and costs for each scenario and case have been described in Chapter 5. Each analysis (Scenario/Case: 1A, 1B, 2A and 2B) was done considering a **cumulative production** starting at the lowest electricity price and finishing at the highest electricity price where hydrogen is still produced. For instance, the data at "$0\ €/\mathrm{MWh}$" means that hydrogen was produced only when the electricity cost was $0\ €/\mathrm{MWh}$, however the data at "$20\ €/\mathrm{MWh}$" was computed assuming a production in all events where the electricity price were from 0 to $20\ €/\mathrm{MWh}$.

Costs and specific hydrogen costs consider the CAPEX of the electrolyzer system, compressor and storage tanks, but not the oxygen storage equipments (liquefier and tanks) neither its sales. For the profits, three different curves are represented:

- Sale of **hydrogen**. Oxygen is vented to the environment;
- Sale of **hydrogen** and **oxygen**. Oxygen equipment (CAPEX and OPEX) is considered;
- Sale of **all electricity** to the grid, with no H_2 or O_2 production.

H_2 selling price (p_{H_2}) may vary from 4 to $8\ €/\mathrm{kg}$ [32], [96]. It is assumed a H_2 price of $8\ €/\mathrm{kg}$ for all the calculations. O_2 selling price (p_{O_2}) is $0.1\ €/\mathrm{kg}$ (Section 5.1.3). Eq. 6.3 is the formula to calculate de

profits:

$$\text{Profit} = (p_{\text{H}_2} - c_{\text{H}_2}) \cdot Q_{\text{H}_2} + [(8 \cdot p_{\text{O}_2} - c_{\text{O}_2}) \cdot Q_{\text{H}_2}]_{\text{oxygen}} \tag{6.3}$$

Where Q_{H_2} is the quantity of produced H_2 [kg]. c_{O_2} [€/kg_{H_2}] is defined in Eq. 6.2.

6.2.1 Scenario 1

Case A

First calculation for Scenario 1 and Case A is depicted on Fig. 6.3. The cheapest H_2 production cost (8.47 €/kg) is achieved in the case of all nights production, *i.e.* when electricity cost from 0 to 50 €/MWh. As the H_2 selling price is 8 €/kg, there is no profit in this scenario. Even adding O_2 storage and sales, there is still no profit. It is worth noting that H_2 production cost does not vary when produced from 10 to 15 €/MWh due to the null number of events with 15 €/MWh of electricity price in 2019.

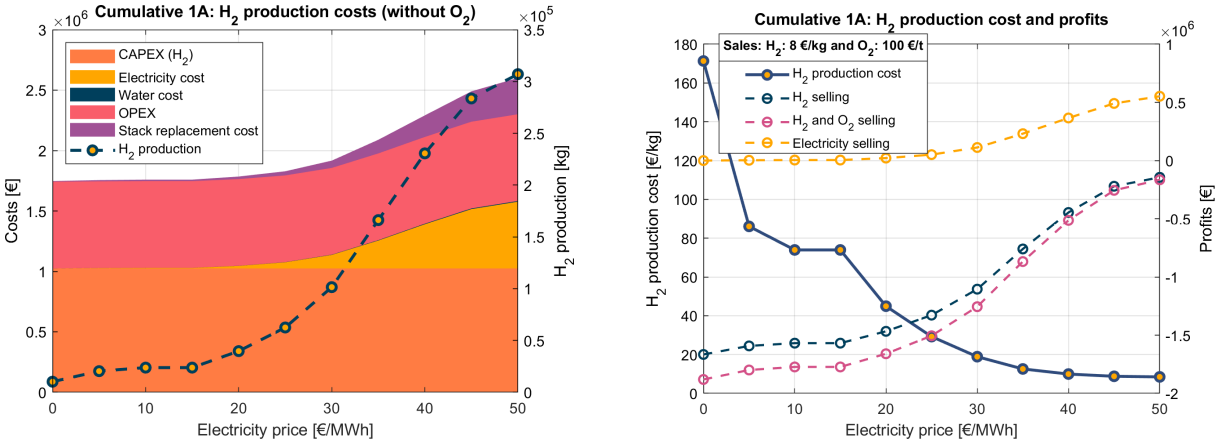

(a) Cumulated production costs (€) and quantity of produced H_2 (kg).

(b) H_2 specific cost and profits by selling H_2, H_2 and O_2 or electricity to the grid.

Figure 6.3: H_2 production analysis for Scenario 1 and Case A.

Case B

Hydrogen is also produced during afternoons, Case B, in Fig. 6.4.

Although with more expensive electricity events comparing with nights (Fig. 5.7), the H_2 production cost reaches the minimum value of 5.71 €/kg when produced up to 50 €/MWh of electricity price, and 5.74 €/kg when up to 55 €/MWh.

There are profits in H_2 sales when hydrogen is at least produced up to ≈ 37 €/MWh of electricity price, including O_2 sales or not. Both situations are advantageous over the sale of electricity when produced at least up to ≈ 42.5 or 41 €/MWh of electricity price, respectively. Finally, producing it in all days (up to 55 €/MWh) the highest profits are achieved, but with a difference of 170 thousand euros favoring the sale of oxygen as well.

For this particular case (1B), an extract of the spreadsheet is given in Appendix A, where the methodology followed in this Section 6.2 is presented.

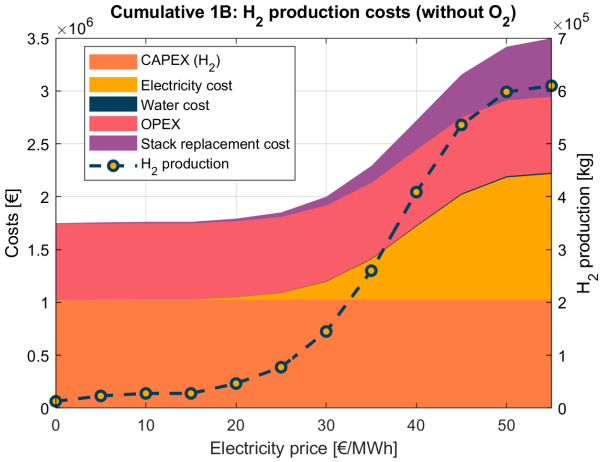

(a) Cumulated production costs (€) and quantity of produced H_2 (kg).

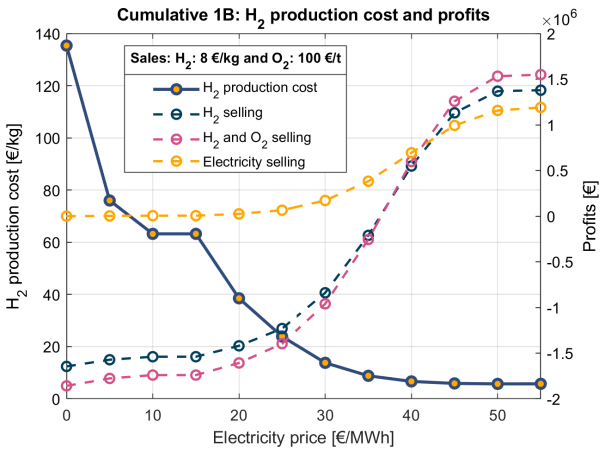

(b) H_2 specific cost and profits by selling H_2, H_2 and O_2 or electricity to the grid.

Figure 6.4: H_2 production analysis for Scenario 1 and Case B.

6.2.2 Scenario 2

Scenario 2 has three main differences when compared to Scenario 1 (Chapter 5): the size of the electrolyzer system and wind farm ($17.5/25.2$ MW vs. $140/150$ MW); the capital and operational costs of the electrolyzer; and the strategy for hydrogen storage. The first considers a storage capacity for 24 hours of rated production and the second a pipeline system for distribution (maintaining the same storage capacity of Scenario 1). As an intermediate step between both scenarios, Appendix B shows the results for a scenario similar to Scenario 2 but still with CAPEX and OPEX values of Scenario 1.

Case A

Calculations for Scenario 2 and Case A are depicted in Fig. 6.5. Unlike Scenario 1, producing only at

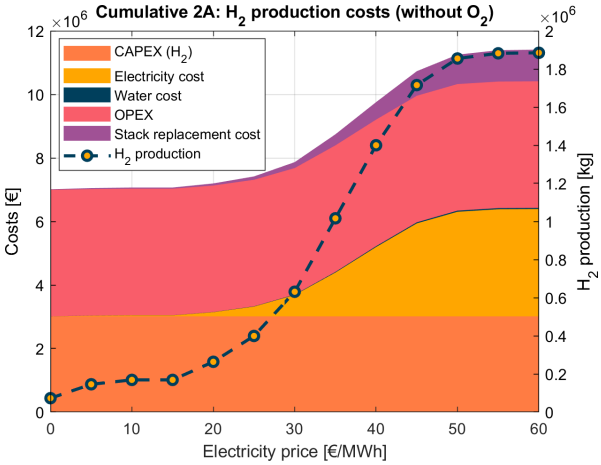

(a) Cumulated production costs (€) and quantity of produced H_2 (kg).

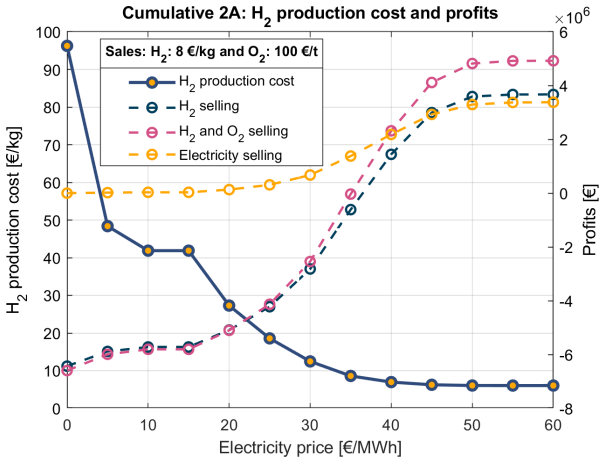

(b) H_2 specific cost and profits by selling H_2, H_2 and O_2 or electricity to the grid.

Figure 6.5: H_2 production analysis for Scenario 2 and Case A.

night is profitable and H_2 production cost reaches the minimum value of 6.05 €/kg. Profits are obtained when hydrogen is produced at least up to about 35 and 36.5 €/MWh electricity prices, selling both H_2

and O_2, or just H_2, respectively. However, to be more advantageous than selling all electricity to the grid, hydrogen must be produced at least up to ≈ 45 €/MWh of electricity price, or ≈ 40 €/MWh if oxygen is sold. Better profits are achieved selling also the oxygen, but now reaching a difference of 1.25 million euros, compared to selling hydrogen only.

Case B

Scenario 2 and Case B, represented in Fig. 6.6, is where the lowest H_2 production costs and highest profits are achieved. H_2 production cost reaches the minimum of 4.25 €/kg when producing it for all electricity prices up to 60 €/MWh. Producing hydrogen gives profit when produced up to about 30 €/MWh electricity prices. Nevertheless, to compensate for producing hydrogen instead of selling electricity alone, hydrogen must be produced at least up to ≈ 31 or 33 €/MWh electricity prices, with or without oxygen sales, respectively. About 2.76 million euros is the difference between including oxygen sales or not, if producing hydrogen in all electricity price events.

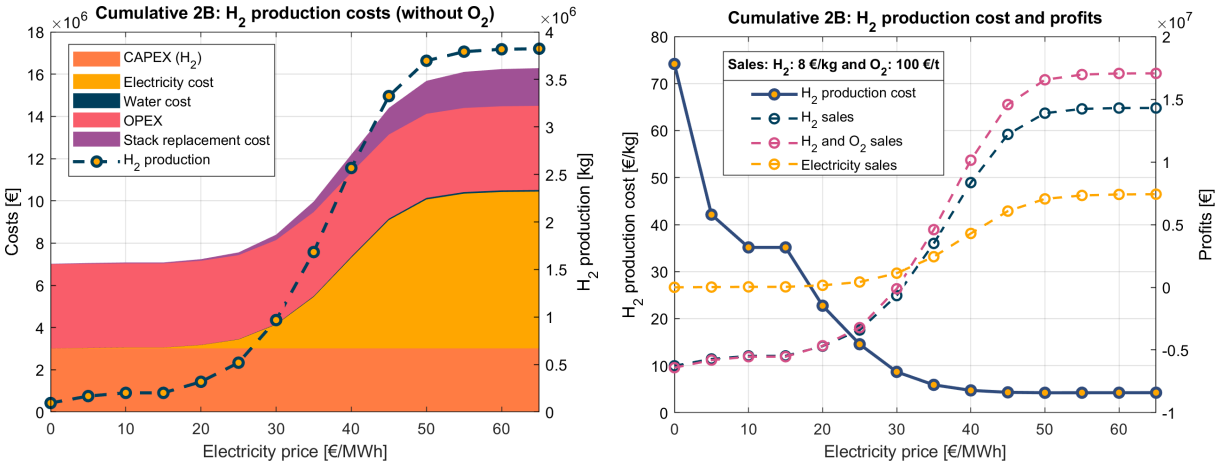

(a) Cumulated production costs (€) and quantity of produced H_2 (kg).

(b) H_2 specific cost and profits by selling H_2, H_2 and O_2 or electricity to the grid.

Figure 6.6: H_2 production analysis for Scenario 2 and Case B.

6.2.3 Plant power ratio

After the previous results, the best rated capacity for electrolyzers was investigated, taking in account the size of the wind farm and the year 2019. For that, different plant power ratios (PPR) were analyzed (Eq. 6.4).

$$\mathrm{PPR}[\%] = \frac{\text{Rated electrolyzer plant's load capacity}}{\text{Wind farm's load capacity}} \times 100 \tag{6.4}$$

Six PPRs were chosen to be evaluated. The maximum PPR is 93 % to consider the electricity used for H_2 compression and transmission losses. Electrolyzer costs are according to the Figs. 5.4 and 5.6. Other costs (compressor, storage and O_2-related) are assumed to vary linearly with the size/capacity.

Each electrolyzer system is considered to be comprised of one electrolyzer module in Scenario 1, and therefore, the maximum and minimum production loads are the ones presented in Table 6.1. Fig.

6.7 shows the production behaviour for different plant power ratios in Scenario 1 (25.2 MW wind farm and capacity for 24 hour storage at rated load).

Table 6.1: Maximum and minimum electrolyzer's load for each PPR in Scenario 1.

PPR	5 %	20 %	35 %	50 %	**70 %**	93 %
Max. [MW]	1.26	5.0	8.82	12.6	**17.5**	23.9
Min. (20 %) [MW]	0.25	1.0	1.76	2.52	**3.5**	4.78

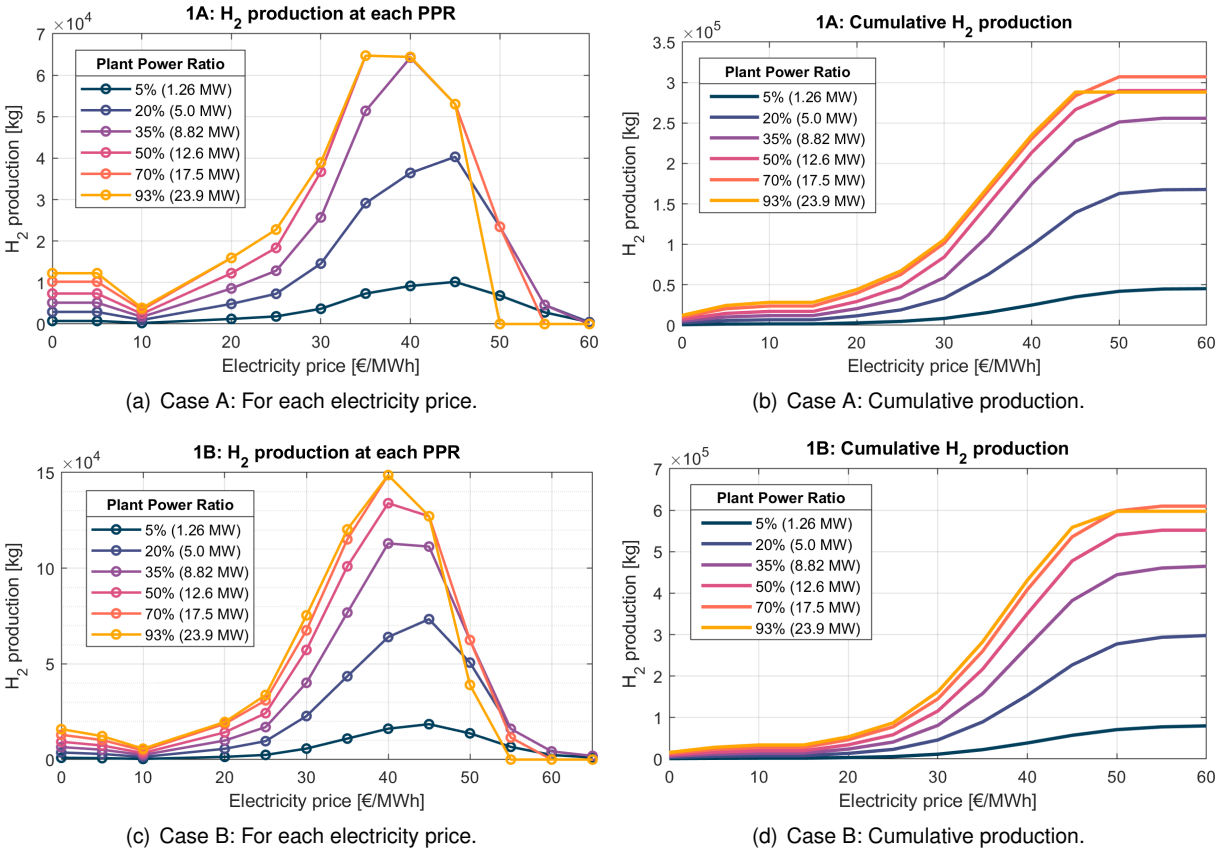

(a) Case A: For each electricity price.

(b) Case A: Cumulative production.

(c) Case B: For each electricity price.

(d) Case B: Cumulative production.

Figure 6.7: H_2 production for Scenario 1 (17.5 MW) and different H_2 system's load capacities.

Higher electricity prices are corresponded to lower wind production powers, therefore, for higher PPRs the minimum load necessary to produce hydrogen is not achieved at 55 or 60 €/MWh. This could be solved having a higher number of electrolyzer modules with lower capacity. However, to be consistent with the PPR of 70 % that has a *Silyzer 300* only-module, a single module is considered for all PPRs.

Computing the costs for each possibility, with and without O_2 production, Table 6.2 presents the specific H_2 production costs. The best case, highlighted in bold, corresponds to the PPR of 35 %, a system with a 8.82 MW module electrolyzer.

Same procedure was applied in Scenario 2, but now considering each system a set of eight electrolyzer modules. Table 6.3 shows the maximum system and module loads, and minimum loads considered for each electrolyzer system. Fig. 6.8 presents the respective hydrogen production behaviour for each PPR.

Electrolyzer's cost followed the same rule of previous scenario. Compressor's size varies linearly with

Table 6.2: Specific production cost of H_2 for Scenario 1 according to PPR.

Specific H_2 production cost [€/kg]: Scenario 1				
	Without O_2 production		With O_2 production	
	Case A	Case B	Case A	Case B
5% (1.26 MW)	6.88	5.23	6.48	4.76
20% (5.0 MW)	6.45	4.93	6.06	4.44
35% (8.82 MW)	**6.28**	**4.75**	**5.92**	**4.27**
50% (12.6 MW)	7.00	5.04	6.71	4.58
70% (17.5 MW)	8.47	5.78	8.28	5.37
93% (23.9 MW)	11.36	7.13	11.36	6.80

Table 6.3: Maximum and minimum system's load for each PPR in Scenario 2.

PPR	5 %	20 %	35 %	50 %	70 %	**93** %
Max. system [MW]	7.5	30.0	52.5	75.0	105.0	**140.0**
Max. module (1/8) [MW]	0.94	3.75	6.56	9.38	13.13	**17.50**
Min. (20 % of module) [MW]	0.19	0.75	1.31	1.88	2.63	**3.50**

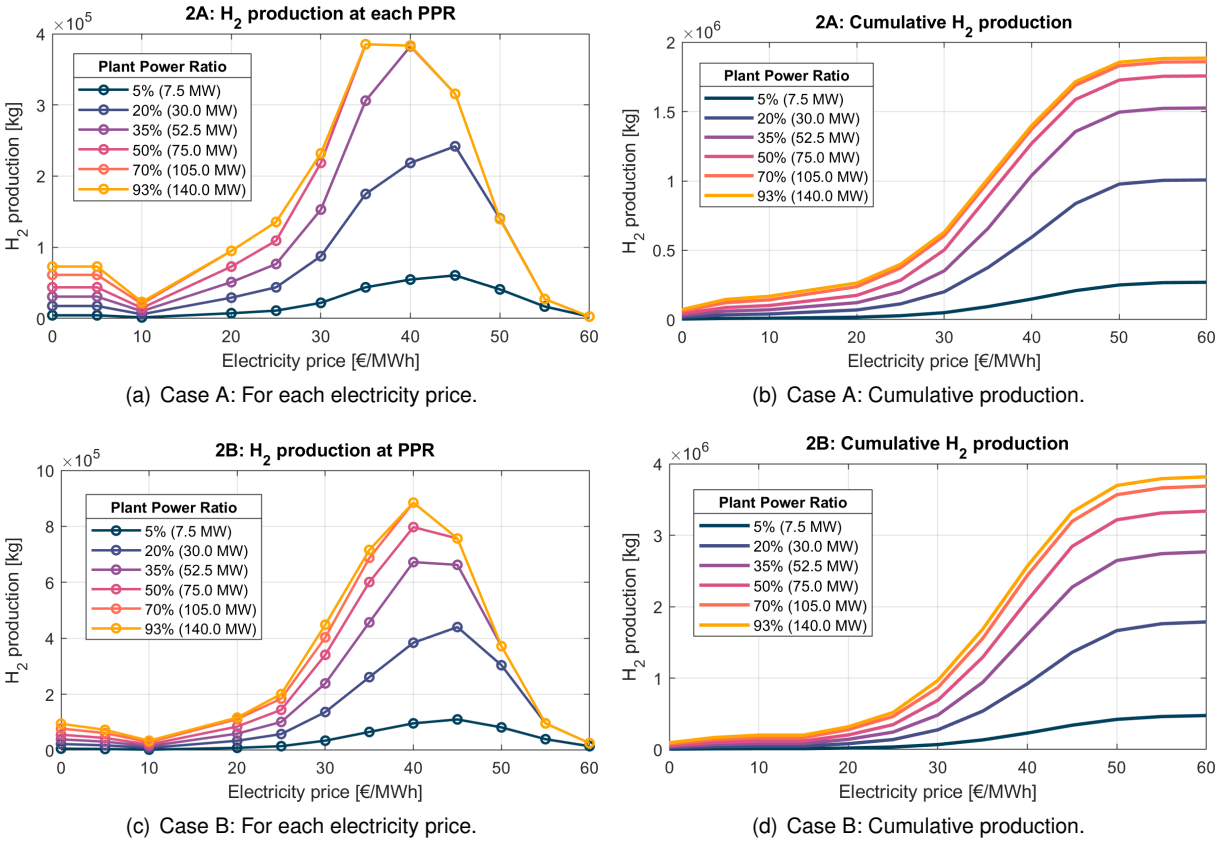

(a) Case A: For each electricity price.

(b) Case A: Cumulative production.

(c) Case B: For each electricity price.

(d) Case B: Cumulative production.

Figure 6.8: H_2 production for Scenario 2 $(140\ \mathrm{MW})$ and different H_2 system's load capacities.

maximum load production flow. Capacity of H_2 storage and O_2-related equipment were assumed to be the same as Scenario 1 since pipeline systems are considered to exist for the both products' distribution.

Table 6.4 represents the specific H_2 production cost results for Scenario 2. Best PPR for this scenario was achieved at $20\ \%$.

Table 6.4: Specific production cost of H_2 for Scenario 2 according to PPR.

Specific H_2 production cost [€/kg]: Scenario 2				
	Without O_2 production		With O_2 production	
	Case A	Case B	Case A	Case B
5% (7.5 MW)	4.25	3.52	3.50	2.76
20% (30.0 MW)	**3.83**	**3.25**	**3.07**	**2.49**
35% (52.5 MW)	3.97	3.30	3.23	2.54
50% (75.0 MW)	4.36	3.46	3.62	2.70
70% (105.0 MW)	5.08	3.78	4.35	3.03
93% (140 MW)	6.05	4.26	5.34	3.51

Summing up all the results for PPR, Fig. 6.9 is presented. Dashed line includes the sale of oxygen. The best power plant ratios are clearly the cases between 20 and 35 % and not the previous considered Scenario 1 of $17.5/25.2$ MW ($\mathrm{PPR} = 70$ %) or Scenario 2 of $140/150$ MW ($\mathrm{PPR} = 93$ %).

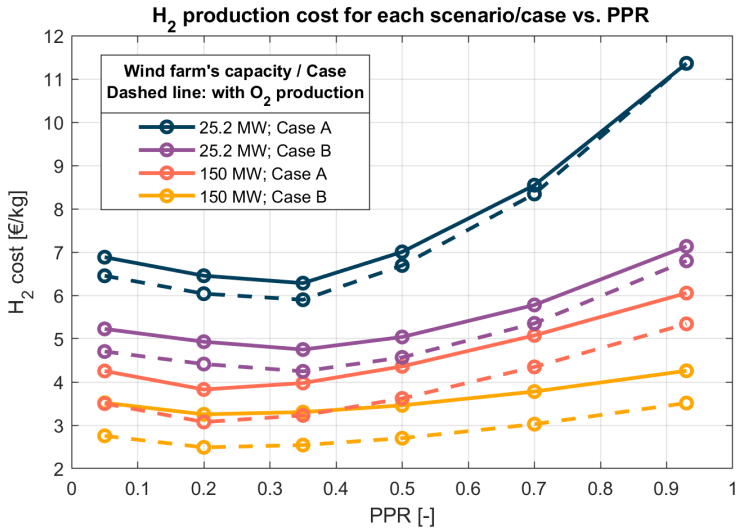

Figure 6.9: H_2 production costs for all considered H_2 system's load capacities. O_2 is included in dashed curves.

6.3 Economic Feasibility of the Project

To better understand the feasibility of a H_2 production project, some economic and financial indicators are evaluated on the results:

- **Levelized cost of H_2 (LCOH).**

  To compare with other technologies of H_2 production, LCOH must be calculated since it represents the average net present cost of the hydrogen generation for a generating plant over its lifetime. Its formula is presented in Eq. 6.5 [43]:

$$\mathrm{LCOH}[€/\mathrm{kg}] = \frac{\sum_{t=1}^{n} \frac{\mathrm{CAPEX}_t + \mathrm{OPEX}_t}{(1+r)^t}}{\sum_{t=1}^{n} \frac{E_t}{(1+r)^t}} \tag{6.5}$$

Where E stands for yearly H_2 production [kg]; n the lifetime of the project [years]; and r the discount rate [-].

- **Net present value (NPV).**

  NPV is used to compare the profitability of various projects. It considers all cash flows over a time period and the value changes over time with r (Eq. 6.6). [43]

$$\mathrm{NPV}[€] = I + \sum_{t=1}^{n} \frac{C_t}{(1+r)^t} \tag{6.6}$$

  In Eq. 6.6, I stands for initial investment in year 0 and C_t the difference between inflows and cash out.

- NPV sensibility to the **income tax**.

  Income tax is the tax imposed on entities over their profits. For companies, this tax is known as corporate tax. In Portugal, the corporate tax is called IRC (*Imposto sobre o Rendimento de Pessoas Coletivas*) and it is $21\ \%$.

- NPV sensibility to the **CAPEX investment**.

  Different percentages of CAPEX investment are considered to understand how the NPV behaves in case of any subsidy.

- NPV sensibility to the **discount rate,** r.

  Discount rate corresponds to the minimum rate of return on an investment project, *i.e.* the return that an investor requires to develop a project. This rate is used to update the future cash-flows generated as of today and it consists of three components/rates (Eq. 6.7): $(\mathrm{R1})$ the desired actual return on equity; $(\mathrm{R2})$ the annual risk premium, which is indicative of the economic, financial, overall and sectoral development of the project, as well as the total amount involved in the project; and finally $(\mathrm{R3})$ the inflation rate. [97]

$$r = [(1+\mathrm{R1}) \times (1+\mathrm{R2}) \times (1+\mathrm{R3})] - 1 \tag{6.7}$$

For the LCOH and NPV it is assumed a discount rate of $10\ \%$, a typical return required by private investors on offshore wind or biomass projects [98]. Nevertheless, a sensitivity analysis is done to understand the NPV behavior for higher and lower discount rates.

This economic feasibility analysis is applied to Case B of both scenarios, assuming that all nights and afternoons are dedicated to producing hydrogen. The results for the two scenarios (1B and 2B cases) are presented side by side below.

Fig. 6.10 shows the LCOH results. Sale of oxygen was considered in Eq. 6.5 and subtracted from the costs. Case 1B would only be feasible if the H_2 selling price is $8.08\ €/\mathrm{kg}$ producing all days. The analysis of the cash-flows and the respective NPV calculation are represented in Tables 6.5 and 6.6.

Hydrogen is assumed to be produced with all electricity prices, *i.e.* produced during all days of the year.

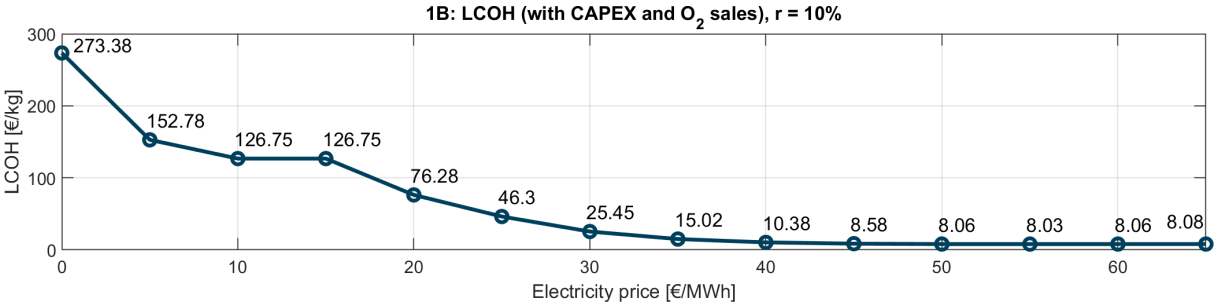

(a) Scenario 1 - Case B.

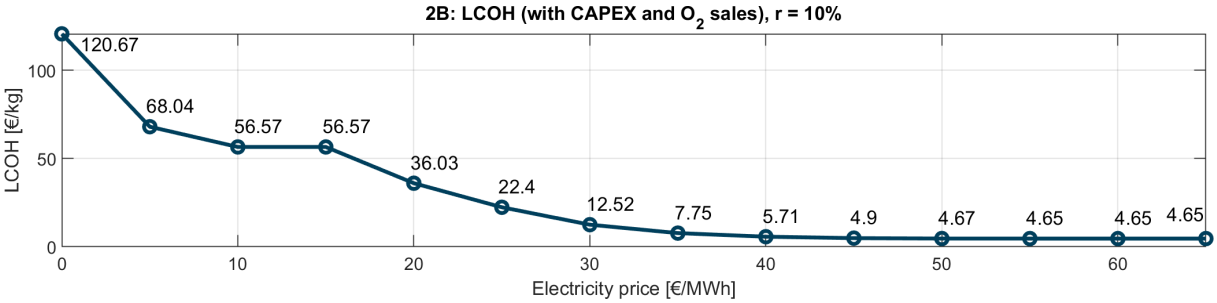

(b) Scenario 2 - Case B.

Figure 6.10: LCOH with $10\ \%$ of rate of return.

Table 6.5: Cash-flow analysis and respective NPV for Scenario 1 - Case B.

1B - Cash-Flow	[€]
H_2 Sales (8 €/kg)	$(+)\,4,878,062$
O_2 Sales (0.1 €/kg)	$(+)\,487,806$
Cost of Sales	$(-)\,2,677,461$
Depreciation $(-)$	$(-)\,1,163,963$
EBT	$1,524,444$
Taxes (21 %)	$(-)\,320,133$
EAT	$1,204,311$
Depreciation $(+)$	$(+)\,1,163,963$
C_t	$2,368,274$
Investment (100 %)	$23,279,269$
NPV (20 years, r=10 %)	$-3,116,820$

Table 6.6: Cash-flow analysis and respective NPV for Scenario 2 - Case B.

2B - Cash-Flow	[€]
H_2 Sales (8 €/kg)	$(+)\,30,584,044$
O_2 Sales (0.1 €/kg)	$(+)\,3,058,404$
Cost of Sales	$(-)\,13,427,933$
Depreciation $(-)$	$(-)\,3,152,147$
EBT	$17,062,368$
Taxes (21 %)	$(-)\,3,583,097$
EAT	$13,479,271$
Depreciation $(+)$	$(+)\,3,152,147$
C_t	$16,631,418$
Investment (100 %)	$63,042,939$
NPV (20 years, r=10 %)	$78,549,696$

As expected, due to the LCOH results, only in the 2B case the NPV is positive, considering the income tax. EBT and EAT stand for earnings before and after taxes, and C_t for the result of the cash flow (Eq. 6.6).

Fig. 6.11 shows the NPV sensibility to the income tax (IRC). Only electricity production and hydrogen production (with O_2 sales) are represented for both scenarios, either with or without IRC. Government incentives in the corporate tax may have a significant impact in the NPV. Choosing the selling price of 8 €/kg, the difference between the curves of H_2 production with and without IRC is about 2.7 million euros in 1B case, and about 30.5 million euros in the 2B case.

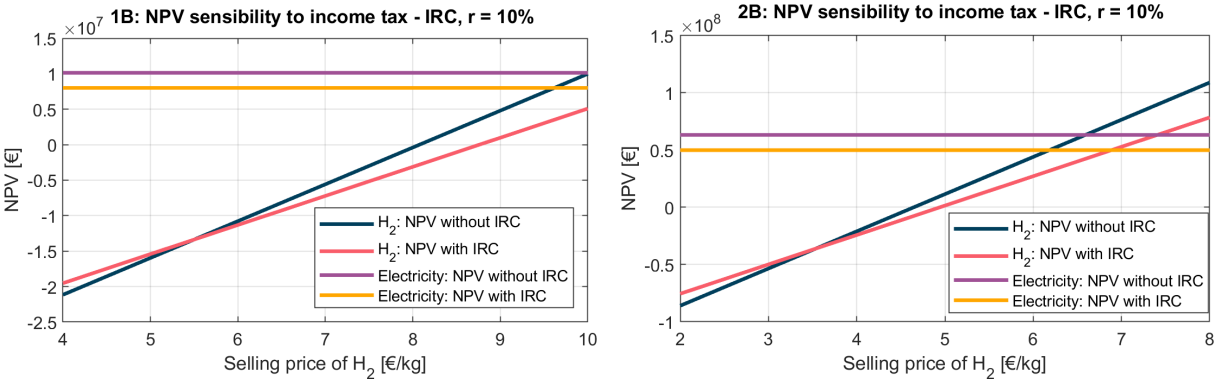

(a) Scenario 1 - Case B.

(b) Scenario 2 - Case B.

Figure 6.11: NPV sensibility to the corporate income tax (21 %), $r = 10$ %.

Other type of government incentives are the subsides. To analyze the impact of eventual incentives in the CAPEX investment, Fig. 6.12 presents the NPV sensibility for different percentages of investment (0, 25, 50, 75 and 100 % of the CAPEX). Considering again a H_2 selling price of 8 €/kg, the project is only feasible when comparing with electricity sales if at least 50 % of the CAPEX is subsidised in 1B case. For 2B case, the project is feasible even without any subsidy (100 % investment).

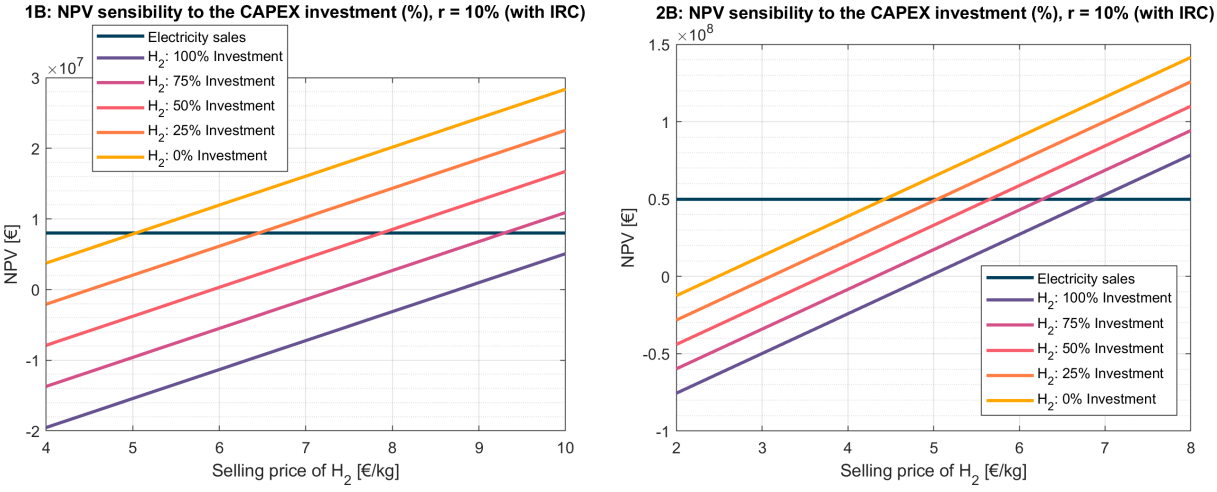

(a) Scenario 1 - Case B.

(b) Scenario 2 - Case B.

Figure 6.12: NPV sensibility to the percentage of CAPEX investment, with IRC, $r = 10$ %.

Finally, Fig. 6.13 depicts the NPV sensibility to the discount rate. Investors require a return of investment based on already mentioned factors, such as the risk and cost of opportunity. From this analysis one can see in which project the discount rate should be a decision variable or not. The discount rate of a given project for which the NPV equals 0 is called internal rate of return (IRR). For projects with high IRR values (> 20 %), the discount rate does not have an impact in the investor decision. From

both cases, the only two situations where the discount rate may take an important weight in the investor decision is the 100 and 75 % of CAPEX investment of 1B case, whose IRR values are about 8 % and 12 %, respectively.

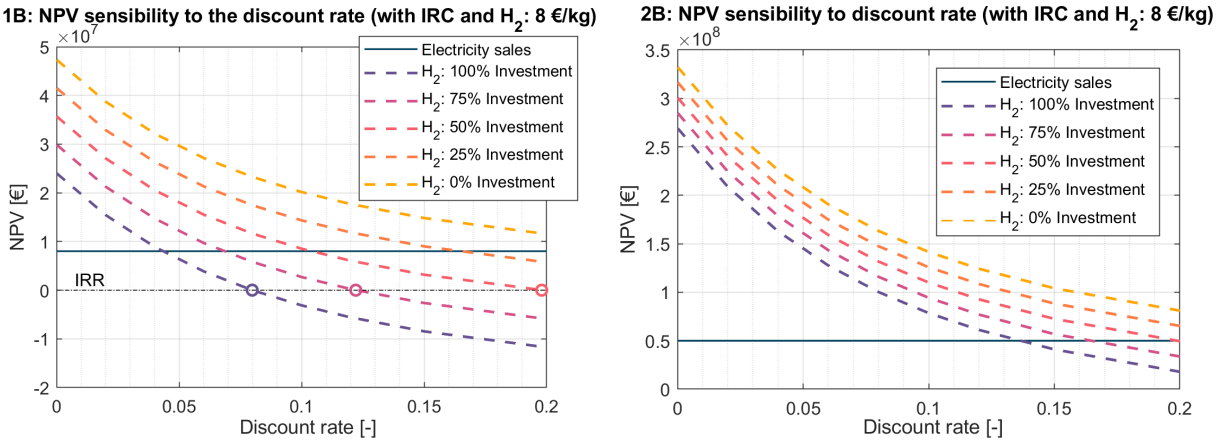

(a) Scenario 1 - Case B.

(b) Scenario 2 - Case B.

Figure 6.13: NPV sensibility to the discount rate (H_2 = 8 €/kg). In 1B case (a), internal rate of return (IRR) of the 100 %, 75 % and 50 % of investments are depicts on the graph.

6.4 Discussion of Results

Costs are one of the main considered parameters for the results above. Currently, there is limited information about electrolyzer plant costs and how it varies with size. Operational costs are not detailed and are assumed as a fixed cost, although a relation with number of operating hours would be expected. Only the stack replacement costs were considered to vary with operating hours.

Scenario 2 considers lower capital and operational costs (for 2050) as expected in a long-term scenario, whereas the electrolyzer model is the same as in Scenario 1 (with same efficiency and module capacity). Indeed, it is expected that the electrolyzer models themselves will also improve and present better efficiencies. Thus, as *Silyser 300* model is also assumed in Scenario 2, the efficiency is considered constant in both scenarios.

From Section 6.1, capacity factor is shown as one of the main factors to have in consideration to achieve low specific H_2 production costs. Figs. 6.1 and 6.2 clearly show that relation. The derivative of H_2 production cost with respect to annual operating hours is high for low operating hours, and hydrogen production should be avoided until 2000 - 4000 operating hours (about 23 - 45 % capacity factor) depending on the CAPEX investment and the scenario.

In fact, the amount of CAPEX investment can also have a significant impact in the H_2 production cost. In Scenario 1 (Fig. 6.1), at very low capacity factors (< 28 %), the cost of hydrogen is high (with high derivative) regardless of investment. Considering an intermediate capacity factor (between 28 and 75 %) a subsidy that would reduce the CAPEX investment would cause an impact of about 0.50 to 1 €/kg in the H_2 cost. For higher capacity factors (> 75 %) the CAPEX causes an impact lower than 0.50 €/kg. However, in Scenario 2, for capacity factors higher than 28 % (about 2500 hours at full load), the difference between considering or not the CAPEX has a impact lower than 0.50 €/kg.

In practice, the electrolyzer will not always work at full load considering a system where the electricity source is exclusively the offshore wind farm. For that reason, the wind production load was related with the electricity prices. However, the analyzes presented in Sections 4.4 and 6.2 have some limitations.

The electricity prices have other variables beyond the time of the day, season and renewable production. The Iberian market of electricity is under a system of free competition, *i.e.* the interconnections (importations/exportations), regional transmission capacities and different weather conditions within Portugal and Spain may influence electricity prices. Coefficients of determination of correlations (R^2) are lower than 0.5 in general, renewable/wind production data is only from Portugal and import balance is assumed to be null.

Then, the assumption of uniform wind production load capacity in all the country is also an approximation that distances itself from reality. Wind varies throughout the country and lower wind production in some parts does not mean lower wind production throughout country. In the present study, an overall, national relation between wind and electricity prices is applied in a specific wind farm.

Afterwards, the H_2 production cost calculation is conducted considering the assumptions above and the number of events of each electricity price in 2019. This is another limitation, since the only studied year is 2019, and the deployment of cheap renewable technologies tends to lower market electricity prices for the coming years.

Scenario 2 achieves lower H_2 production costs than Scenario 1 due to the lower capital and operational costs of the electrolyzer. The assumption of a developed economy with pipelines for distribution has an impact on the H_2 cost. Nevertheless, observing the results of the intermediate scenario in Appendix B, where the capital and operational costs are the same as Scenario 1, the results are the worst ones and it is more expensive to produce H_2. It would be expected to have lower specific production costs in the intermediate scenario when compared to Scenario 1, since specific costs related to storage are lower. The difference of plant power ratios between both scenarios (93 % and 70 %) may explain why hydrogen production is more expensive in the intermediate scenario.

Case 2 also presents better results than Case 1. Despite of more expensive electricity price events during afternoon, this difference is not so significant as the increase of the capacity factor, since Case 2 presents lower H_2 production costs.

The analysis done afterwards on which is the best power plant ratio shows that neither Scenario 1 or 2 have the best PPR. Best PPR, *i.e.* minimization of H_2 specific cost, is achieved about 35 and 20 % in Scenarios 1 and 2, respectively. These values mean a 8.82 MW eletrolyzer system in Scenario 1 and a 30 MW system in Scenario 2.

Finally, from the economic analysis results obtained for Case B of both scenarios (1B and 2B), assuming the H_2 selling price of 8 €/kg, the sale of oxygen, the 10 % discount rate and the corporate tax of 21 %, only 2B case is a feasible project, even when compared to the sales of the electricity to the market. At these conditions, 1B case only would be feasible with government incentives such as subsidies and corporate tax reduction.

Chapter 7

Conclusions

Main achievements obtained throughout this research work are presented in Section 7.1 and some ideas for future work are given in Section 7.2.

7.1 Achievements

The major insights and achievements of the present work are given below:

- Currently, there are three main technologies of electrolyzers: alkaline, proton exchange membrane (PEM) and solid oxide electrolyzer (SOEC). A PEM electrolyzer (Silyzer 300) was chosen for the calculations due to its better operational flexibility to the intermittent wind production and higher theoretical efficiency when compared to an alkaline electrolyzer.
- Wind turbulence does not affect the expected mean generated power but produces significant standard deviations in the instantaneous power around the rated wind speed. Due to the fluctuations, power generation presents the same behavior before nominal wind turbine load is reached. Controller delay may also create some standard deviation and justify it between the rated and cut-out wind speeds.
- Electricity wholesale market prices present a correlation with renewable production, and consequently wind production. An analysis was done for the two periods with lower energy consumptions: nights (3 to 8 a.m.) and afternoons (3 to 7 p.m.). Winter and Summer semesters are the considered season periods for the results. Afterwards, to consider the 2019 year in the case-study, expected wind production for each electricity price was obtained considering uniform wind production in all country, rainy winters and no importations or exportations.
- Two scenarios are considered for analysis. The first (Scenario 1), using electricity from the pre-commercial phase of $25.2\ \mathrm{MW}$ WindFloat Atlantic, H_2 plant capacity of $17.5\ \mathrm{MW}$, and compression and storage capacity. The second (Scenario 2), using electricity from the long-term WindFloat Atlantic commercial phase of $150\ \mathrm{MW}$, H_2 plant capacity of $140\ \mathrm{MW}$, compression, a existing H_2 pipeline for distribution and the same storage capacity of Scenario 1. The possibility of O_2 capture and sales is also considered.

- H_2 production cost is firstly calculated regardless the 2019 year, but depending on the scenarios, capacity factor (number of operational hours at full load), electricity price and O_2 capture for sales. Considering CAPEX or not is also represented. Higher electricity prices and lower capacity factors produce more expensive hydrogen. Scenario 2 achieves better production costs. Production costs are also reduced considering O_2 sales or subsidies for the CAPEX investment.
- Considering the 2019 year and its electricity prices, each one associated to a given wind production load, and a H_2 selling price of 8 €/kg, Scenario 1 and Case A (nights) is not feasible, reaching a minimum production cost of 8.47 €/kg. Other scenarios are feasible considering all year production (higher capacity factor). Scenario 1 and Case B (nights and afternoons) has a minimum H_2 production cost of 5.71 €/kg. Scenario 2 and Cases A and B present production costs of 6.05 €/kg and 4.25 €/kg, respectively. Excluding the non-feasible first case (1A), all other cases show that O_2 must be sold to achieve better profits.
- Applying a discount rate of 10 % and an income tax of 21 % to 1B and 2B cases, and a H_2 selling price of 8 €/kg again, only the 2B case is feasible. 1B case shall be feasible with government incentives on the investment and taxes.
- Analyzing the plant power ratio ($[\mathrm{H_2\ production\ rated\ load}]/[\mathrm{wind\ farm's\ rated\ load}]$), the electrolyzer system in Scenario 1 should have a load capacity of 8.82 MW ($\mathrm{PPR} = 35$ %) and in Scenario 2 a load capacity of 30 MW ($\mathrm{PPR} = 20$ %). These PPRs are substantially different from what was considered in the scenarios.

7.2 Future Work

A few ideas for future work are presented below:

- Instead of being limited to the 2019 year, extend the case-study analysis to the expected electricity market prices in next years.
- Study other H_2 production configurations, such as using electricity from the grid when there is not enough wind power to produce H_2 at maximum capacity load (increasing the capacity factor).
- Integrate also a solar power plant as a complement to the wind energy.
- Instead of onshore H_2 production, study its production integrated in offshore wind platforms installed in places far from the coast where there are higher wind speeds.
- Make a more in-depth study of the H_2 market in Portugal and understand more accurately the selling prices and demand for each end-use (industry, refuelling stations, etc).
- Study more accurately the storage and transportation options, and all associated costs to understand what is the H_2 cost for the end-user.
- To better understand the environmental impacts, a life-cycle assessment for all stages shall be done.

Bibliography

[1] Eurostat. Shedding light on renewable energy in the EU - A guided tour of Energy Statistics 2020, 2020. ISBN: 978-92-76-18199-6.

[2] APREN. Produção. URL https://www.apren.pt/pt/energias-renovaveis/producao. (Accessed on 15-09-2020).

[3] APREN. 2019 Yearbook - Portugal need our energy!, 2019. URL https://www.apren.pt/contents/documents/anuario-2019-aprenebook-v2-5562.pdf. (Accessed on 15-12-2020).

[4] IRENA. Global Energy Transformation: A Roadmap to 2050 (2019 edition). Technical report, International Renewable Energy Agency, Abu Dhabi, 2019. URL www.irena.org. ISBN: 978-92-9260-059-4.

[5] European Union. 2050 long-term strategy. URL https://ec.europa.eu/clima/policies/strategies/2050_en. (Accessed on 22-08-2020).

[6] European Union. Going Climate-Neutral by 2050: A strategic long-term vision for a prosperous, modern, competitive and climate-neutral EU economy. Technical report, European Commission, 2019. doi:10.2834/813032.

[7] D. R. Dias. Análise da Integridade Estrutural duma Fundação Flutuante para Energia Eólica Offshore. Master's thesis, IST, Instituto Superior Técnico, Nov. 2017.

[8] J. Cruz and M. Atcheson. *Floating Offshore Wind Energy: The Next Generation of Wind Energy*. Green Energy and Technology. Springer International Publishing, 1 edition, 2016. ISBN 978-3-319-29396-7,978-3-319-29398-1.

[9] EWEA. Deep water: The next step for offshore wind energy. A report by the European Wind Energy Association, July 2013. ISBN:978-293-0670-04-1.

[10] Global Wind Energy Council (GWEC). Global Offshore Wind: Annual Market Report 2020. Technical Report August, Brussels, 2020.

[11] Windfloat. URL https://www.principlepowerinc.com/en/windfloat. (Accessed on 28-08-2020).

[12] Windfloat atlantic project. URL https://www.power-technology.com/projects/windfloat-atlantic-project/. (Accessed on 28-08-2020).

[13] M. Aneke and M. Wang. Energy storage technologies and real life applications – A state of the art review. *Applied Energy*, 179:350–377, June 2016. doi:10.1016/j.apenergy.2016.06.097.

[14] República Portuguesa. EN-H2: Estratégia Nacional para o Hidrogénio (Draft), 2020.

[15] M. Lappalainen. Techno-economic feasibility of hydrogen production via polymer membrane electrolyte electrolysis for future Power-to-X systems. Master's thesis, Tampere University, March 2019.

[16] Air Products and Chemicals, Inc. Safetygram 9: Liquid Hydrogen, 2007.

[17] International Energy Agency. Technology Roadmap: Hydrogen and Fuel Cells. Technical report, OECD/IEA, Paris, 2015.

[18] M. F. Ruth, P. Jadun, N. Gilroy, E. Connelly, R. Boardman, A. J. Simon, A. Elgowainy, and J. Zuboy. The Technical and Economic Potential of the H2@Scale Concept within the United States. Technical Report October, NREL, 2020. NREL/TP-6A20-77610.

[19] Hydrogen Council. Path to hydrogen competitiveness: A cost perspective. Technical report, Jan. 2020.

[20] B. Zhang, L. Wang, and R. Li. *Bioconversion and chemical conversion of biogas for fuel production*. Elsevier Inc., 2019. ISBN 9780128179413. doi:10.1016/B978-0-12-817941-3.00010-3.

[21] Communal News. Hydrogen electrolyzer market charging into the future. URL `https://communalnews.com/hydrogen-electrolyzer-market-charging-into-the-future/`. (Accessed on 20-08-2020).

[22] A. Ursúa, L. M. Gandía, and P. Sanchis. Hydrogen production from water electrolysis: Current status and future trends. *Proceedings of the IEEE*, 100(2):410–426, Feb. 2012. doi:10.1109/JPROC.2011.2156750.

[23] A. Buttler and H. Splietho. Current status of water electrolysis for energy storage, grid balancing and sector coupling via power-to-gas and power-to-liquids : A review. *Renewable and Sustainable Energy Reviews*, 82:2440–2454, Sept. 2017. doi:10.1016/j.rser.2017.09.003.

[24] P. Lettenmeier. White paper: Efficiency - Electrolysis. *Siemens*, Jan. 2019. URL `https://assets.new.siemens.com/siemens/assets/public.1558704999.139de890-44e1-453b-8176-c3d45c905178.white-paper-efficiency-en.pdf`.

[25] K. Meier. Hydrogen production with sea water electrolysis using norwegian offshore wind energy potentials: Techno-economic assessment for an offshore-based hydrogen production approach with state-of-the-art technology. *International Journal of Energy and Environmental Engineering*, 5 (104):1–12, May 2014. doi:10.1007/s40095-014-0104-6.

[26] Energiepark Mainz. Technical data about the Energiepark, 2018. URL `https://www.energiepark-mainz.de/en/technology/technical-data/`. (Accessed on 20-06-2020).

[27] Greenlysis. Hydrogen and oxygen production via electrolysis powered by renewable energies to reduce the environmental footprint of a WWTP, 2008. Project reference: LIFE08 ENV/E/000118.

[28] M. D. Esteban, J. J. Diez, J. S. López, and V. Negro. Why offshore wind energy? *Renewable Energy*, 36:444–450, 2011. doi:10.1016/j.renene.2010.07.009.

[29] J. S. Hill. Hywind Scotland, World's First Floating Wind Farm, Performing Better Than Expected. URL https://cleantechnica.com/2018/02/16/hywind-scotland-worlds-first-floating-wind-farm-performing-better-expected/. (Accessed on 08-11-2020).

[30] IRENA. Hydrogen: A renewable energy perspective. Technical report, Abu Dhabi, 2019. URL www.irena.org. ISBN: 978-92-9260-151-5.

[31] Green Car Congress. Air Liquide selects Hydrogenics for 20MW electrolyzer for hydrogen production; largest PEM electrolyzer in world, Feb. 2019. URL https://www.greencarcongress.com/2019/02/20190226-airliquide.html. (Accessed on 10-11-2020).

[32] Direção-Geral de Energia e Geologia. Roteiro e Plano de Ação para o Hidrogénio em Portugal, 2020. ISBN: 978-972-8268-51-0.

[33] Bundesministerium für Wirtschaft und Energie. Gewinner des Ideenwettbewerbs „Reallabore der Energiewende“ – Steckbriefe –, 2019.

[34] P. de Laat. Overview of Hydrogen Projects in the Netherlands. TKI Nieuw Gas, 2020.

[35] A. Lee. Japan opens world's largest green-hydrogen plant near Fukushima disaster site, 2020. URL https://www.rechargenews.com/transition/japan-opens-worlds-largest-green-hydrogen-plant-near-fukushima-disaster-site/2-1-769361. (Accessed on 10-11-2020).

[36] J. Arias. Hydrogen and fuel cells in Japan. EU-Japan Centre for Industrial Cooperation, Oct. 2019.

[37] S. Djunisic. Western Australia govt okays 15-GW wind, solar mega-project, Oct. 2020. URL https://renewablesnow.com/news/western-australia-govt-okays-15-gw-wind-solar-mega-project-717875/. (Accessed on 10-11-2020).

[38] Port Lincoln Times. Port Lincoln hydrogen project is key to state's export plan, Sept. 2019. URL https://www.portlincolntimes.com.au/story/6403770/port-lincoln-hydrogen-project-is-key-to-states-export-plan/. (Accessed on 10-11-2020).

[39] Green Car Congress. Gigastack renewable hydrogen from offshore wind project advances to next phase; 100MW electrolyzer system, Feb. 2020. URL https://www.greencarcongress.com/2020/02/20200219-gigastack.html. (Accessed on 10-11-2020).

[40] A. Thomas. Exclusive: 'World first' floating green hydrogen project coming to Aberdeen, Sept. 2020. URL https://www.energyvoice.com/renewables-energy-transition/267583/world-first-floating-green-hydrogen-project-aberdeen/. (Accessed on 10-11-2020).

[41] A. Cabrita-Mendes. Corrida ao hidrogénio: Quatro projetos para Portugal que vale a pena conhecer, July 2020. URL https://jornaleconomico.sapo.pt/noticias/corrida-ao-hidrogenio-quatro-projetos-para-portugal-que-vale-a-pena-conhecer-617665. (Accessed on 11-11-2020).

[42] IRENA. Hydrogen from renewable power: Technology outlook for the energy transition. Technical report, International Renewable Energy Agency, Abu Dhabi, 2018. URL www.irena.org. ISBN: 978-92-9260-077-8.

[43] K. Lindblad. An economic feasibility study of hydrogen production by electrolysis in relation to offshore wind energy at Oxelösund. Master's thesis, KTH Royal Institute of Technology, 2019.

[44] L. Grond, P. Schulze, and J. Holstein. Systems analyses Power to Gas: A technology review. DNV KEMA, June 2013.

[45] M. David, C. Ocampo-Martínez, and R. Sánchez-Peña. Advances in alkaline water electrolyzers: A review. *Journal of Energy Storage*, 23:392–403, Jan. 2019. doi:10.1016/j.est.2019.03.001.

[46] M. Carmo, D. L. Fritz, J. Mergel, and D. Stolten. A comprehensive review on PEM water electrolysis. *International Journal of Hydrogen Energy*, 38:4901–4934, 2013. doi: 10.1016/j.ijhydene.2013.01.151.

[47] S. Shiva Kumar and V. Himabindu. Hydrogen production by PEM water electrolysis – A review. *Materials Science for Energy Technologies*, 2:442–454, Mar. 2019. doi:10.1016/j.mset.2019.03.002.

[48] M. Boudellal. *Power-to-Gas, Renewable Hydrogen Economy*. Walter de Gruyter GmbH, Berlin/Boston, 2018. ISBN 978-3-11-055881-4.

[49] M. Lehner, R. Tichler, H. Steinmüller, and M. Koppe. *Power-to-Gas: Technology and Business Models*. SpringerBriefs in Energy. Springer International Publishing, 1 edition, 2014. ISBN 978-3-319-03994-7.

[50] A. Godula-Jopek, P. Millet, N. Guillet, J. Laurencin, J. Mougin, C. Bourasseau, and B. Guinot. *Hydrogen Production by Electrolysis*. Wiley-VCH Verlag GmbH & Co., Germany, 2015. ISBN:978-3-527-33342-4.

[51] T. Smolinka, E. T. Ojong, and T. Lickert. *PEM Electrolysis for Hydrogen Production: Principles and Applications*. CRC Press, 2016. ISBN: 978-1-4822-5232-3.

[52] R. Moradi and K. M. Groth. Hydrogen storage and delivery: Review of the state of the art technologies and risk and reliability analysis. *International Journal of Hydrogen Energy*, 44:12254–12269, Mar. 2019. doi:10.1016/j.ijhydene.2019.03.041.

[53] G. Sdanghi, G. Maranzana, A. Celzard, and V. Fierro. Review of the current technologies and performances of hydrogen compression for stationary and automotive applications. *Renewable and Sustainable Energy Reviews*, 102:150–170, Nov. 2019. doi:10.1016/j.rser.2018.11.028.

[54] H. Barthelemy, M. Weber, and F. Barbier. Hydrogen storage: Recent improvements and industrial perspectives. *International Journal of Hydrogen Energy*, 42:7254–7262, Mar. 2017. doi:10.1016/j.ijhydene.2016.03.178.

[55] R. van Gerwen, M. Eijgelaar, and T. Bosma. Hydrogen in the electricity value chain. DNV GL, Mar. 2019.

[56] J. O. Abe, A. P. Popoola, E. Ajenifuja, and O. M. Popoola. Hydrogen energy, economy and storage: Review and recommendation. *International Journal of Hydrogen Energy*, 44:15072–15086, Apr. 2019. doi:10.1016/j.ijhydene.2019.04.068.

[57] G. Chisholm and L. Cronin. *Hydrogen From Water Electrolysis*. Elsevier Inc., 2016. doi:10.1016/B978-0-12-803440-8/00016-6.

[58] Fuel Cell Electric Buses. General Hydrogen Safety Facts. URL `https://www.fuelcellbuses.eu/wiki/safety-framework/general-hydrogen-safety-facts`. (Accessed on 14-11-2020).

[59] NASA. Safety Standard for Hydrogen and Hydrogen Systems: Guidelines for Hydrogen System Design, Materials Selection, Operations, Storage and Transportation. Technical report, NASA, USA, Sept. 1997.

[60] MHI VESTAS Offshore Wind. Final turbine sails to WindFloat Atlantic project site for installation. URL `https://mhivestasoffshore.com/final-turbine-sails-to-windfloat-atlantic-project-site-for-installation/`. (Accessed on 18-11-2020).

[61] J. George. WindFloat design for different turbine sizes. Master's thesis, IST, Instituto Superior Técnico, Sept. 2014.

[62] Noctula. Projeto Windfloat Atlantic: O primeiro Parque Eólico Marítimo em Portugal. URL `https://noctula.pt/projeto-windfloat-atlantic-primeiro-parque-eolico-maritimo-em-portugal/`. (Accessed on 14-11-2020).

[63] WindPlus S.A. The windfloat project, 2010. URL `http://www.portugalglobal.pt/en/general/documents/windfloatproject.pdf`. (Accessed on 18-11-2020).

[64] DTU Wind Energy. Global Wind Atlas. URL `https://globalwindatlas.info/`. (Accessed on 14-11-2020).

[65] E. Cheynet, J. B. Jakobsen, and C. Obhrai. Spectral characteristics of surface-layer turbulence in the North Sea. *Energy Procedia*, 137:414–427, Oct. 2017. doi:10.1016/j.egypro.2017.10.366.

[66] J. Jonkman. Dynamics Modeling and Loads Analysis of an Offshore Floating Wind Turbine. Technical report, Nov. 2007. NREL/TP-500-41958.

[67] WindGURU. Daily Archive. URL `https://www.windguru.cz/archive.php`. (Accessed on 14-11-2020).

[68] S. Li, P. W. Chan, and D. Chen. Empirical Correction Ratio and Scale Factor to Project the Extreme Wind Speed Profile for Offshore Wind Energy Exploitation. *IEEE Transactions on Sustainable Energy*, 9(3):1030–1040, July 2018.

[69] A. Cordle and J. Jonkman. State of the art in floating wind turbine design tools. *Proceedings of the International Offshore and Polar Engineering Conference*, Oct. 2011. ISBN:9781880653968.

[70] J. Jonkman and B. Jonkman. FAST v8.16.00a-bjj User's Guide, July 2016.

[71] J. M. Jonkman and M. L. Buhl Jr. FAST User's Guide. Technical report, Aug. 2005. NREL/EL-500-38230.

[72] B. Jonkman. TurbSim User's Guide: Version 1.50. Sept. 2009. NREL/TP-500-46198.

[73] M. Türk and S. Emeis. The dependence of offshore turbulence intensity on wind speed. *Journal of Wind Engineering and Industrial Aerodynamics*, 98:466–471, 2010. doi:10.1016/j.jweia.2010.02.005.

[74] C. Allen, A. Viselli, H. Dagher, A. Goupee, E. Gaertner, N. Abbas, M. Hall, and G. Barter. Definition of the UMaine VolturnUS-S Reference Platform Developed for the IEA Wind 15-Megawatt Offshore Reference Wind Turbine. July 2020. URL `https://www.nrel.gov/docs/fy20osti/76773.pdf`. NREL/TP-5000-76773.

[75] NREL. ROSCO. Version 1.0.0, 2020. URL `https://github.com/NREL/rosco`.

[76] E. Gaertner, J. Rinker, L. Sethuraman, F. Zahle, B. Anderson, G. E. Barter, N. J. Abbas, F. Meng, P. Bortolotti, W. Skrzypinski, G. N. Scott, R. Feil, H. Bredmose, K. Dykes, M. Shields, C. Allen, and A. Viselli. Definition of the IEA 15-Megawatt Offshore Reference Wind. Mar. 2020. URL `https://www.nrel.gov/docs/fy20osti/75698.pdf`. NREL/TP-5000-75698.

[77] E. Díaz-Dorado, J. Cidras, C. Carrillo, and A. F. O. Montaño. Review of power curve modelling for wind turbines. *Renewable and Sustainable Energy Reviews*, 21:572–581, Jan. 2013. doi:10.1016/j.rser.2013.01.012.

[78] Mercado Ibérico da Energia Elétrica – MIBEL. URL `https://www.mibel.com/`. (Accessed on 15-05-2020).

[79] OMIE. *Funcionamento do Mercado Diário*. Operador del Mercado Ibérico de Energía – Polo Español, S.A., .

[80] J. G. A. Ribeiro. Previsão de preços de eletricidade para o mercado MIBEL. Master's thesis, FEUP, Faculdade de Engenharia da Universidade do Porto, June 2014.

[81] REN. SISTEMA DE INFORMAÇÃO DE MERCADOS DE ENERGIA. URL `https://www.mercado.ren.pt/pt/Paginas/default.aspx`. (Accessed on 22-11-2020).

[82] OMIE. OMIEData: Resultados de mercado, . URL `https://www.omie.es/pt/`. (Accessed on 22-11-2020).

[83] IPMA. Monitorização da Seca - Índice PDSI - Evolução. URL https://www.ipma.pt/pt/oclima/observatorio.secas/pdsi/monitorizacao/evolucao/. (Accessed on 24-11-2020).

[84] T. W. May, Y. M. Yeap, and A. Ukil. Comparative evaluation of power loss in HVAC and HVDC transmission systems. *2016 IEEE Region 10 Conference (TENCON)*, pages 637–641, Nov. 2016. doi:10.1109/TENCON.2016.7848080.

[85] Siemens. Silyzer 300: The next paradigm of PEM electrolysis, 2018. URL https://www.siemens.com/silyzer. (Accessed on 20-06-2020).

[86] Águas do Alto Minho, S.A. Tarifário 2020: Abastecimento de Água e Saneamento de Águas Residuais. URL https://www.cm-pontedelima.pt/cmpontedelima/uploads/writer_file/document/4962/tarifario_adm_2020.pdf. (Accessed on 20-06-2020).

[87] G. Schneider. Power2Hydrogen: Electrolysis, Silyzer, Oct. 2019. URL https://assets.new.siemens.com/siemens/assets/api/uuid:33ef5476-2a47-4421-802b-e48564d210ac/version:1595233590/2019-10-23-power2x-silyzer-gernot-schneider.pdf;. (Accessed on 25-11-2020).

[88] W. Priest. Future Mining Energy Solutions – Hydrogen Hybrid Remote Area Power Systems (RAPS)., June 2019. URL https://australia.energyandmines.com/files/Case-Study-Opportunities-and-Challenges-of-Integrating-Hydrogen-into-a-Mining-Hybrid-Warner-Priest-Siemens.pdf. (Accessed on 25-11-2020).

[89] V. d. Laag. Large Scale PEM Electrolysis for Industrial Applications, June 2019. URL https://www.co2neutraalin2050.nl/wp-content/uploads/Van-der-Laag.pdf. (Accessed on 25-11-2020).

[90] T. D. (Hydrogenics), M. D (Colruyt), M. M. (Sustesco), V. d. L. W., and F. I. (WaterstofNet). Power-to-gas: Roadmap for Flanders, Oct. 2016.

[91] C. van Leeuwen and A. Zauner. D8.3 Report on the costs involved with PtG technologies and their potentials across the EU. *Innovative large-scale energy storage technologies and Power-to-Gas concepts after optimisation*, Apr. 2020.

[92] J. G. Maciel. The WindFloat Project, May 2010. URL https://www.unioviedo.es/ate/manuel/varios/11_Joao_Maciel.pdf. (Accessed on 28-11-2020).

[93] A. Baccioli, E. Bargiacchi, S. Barsali, A. Ciambellotti, D. Fioriti, R. Giglioli, and G. Pasini. Cost effective power-to-X plant using carbon dioxide from a geothermal plant to increase renewable energy penetration. *Energy Conversion and Management*, 226:113494, Sept. 2020. URL https://doi.org/10.1016/j.enconman.2020.113494. doi:10.1016/j.enconman.2020.113494.

[94] Alibaba. Low Price Compact used Cryogenic Oxygen Tank for Liquid oxygen. URL https://www.alibaba.com/product-detail/Low-Price-Compact-used-Cryogenic-Oxygen_60723852129.html. (Accessed on 28-11-2020).

[95] D. Bellotti, M. Rivarolo, L. Magistri, and A. F. Massardo. Feasibility study of methanol production plant from hydrogen and captured carbon dioxide. *Journal of CO2 Utilization*, 21:132–138, July 2017. doi:10.1016/j.jcou.2017.07.001.

[96] G. Matute, J. M. Yusta, and L. C. Correas. Techno-economic modelling of water electrolysers in the range of several MW to provide grid services while generating hydrogen for different applications: A case study in Spain applied to mobility with FCEVs. *International Journal of Hydrogen Energy*, 44:17431–17442, May 2019. doi:10.1016/j.ijhydene.2019.05.092.

[97] J. P. Esperança, L. M. Martins, P. Andrez, P. Baião, and V. Batista. *Finanças com Confiança - Tudo o que precisas de saber sobre as finanças do teu negócio.* Territórios Criativos, Oct. 2019. ISBN:978-989-20-9884-5.

[98] J. Pankhania, J. Palmer, and T. Tran. Renewable energy discount rate survey results – 2018, Jan. 2019.

Appendix A

Spreadsheet and Formulas

A spreadsheet extract and the main formulas for the step "$5\ €/\mathrm{MWh}$" of the case 1B are shown in Fig. A.1.

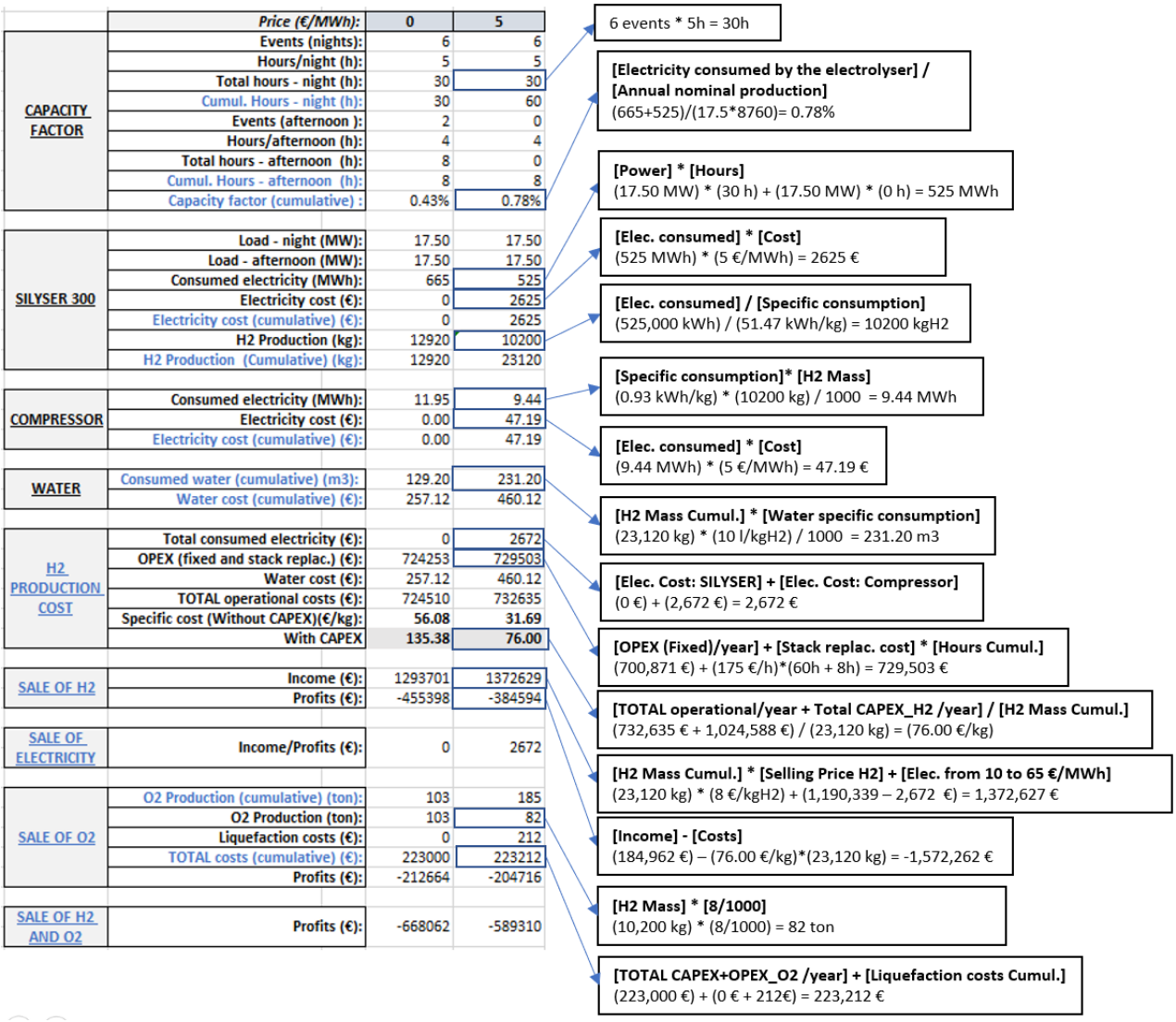

Figure A.1: 1B, "$5\ €/\mathrm{MWh}$" (extract from the spreadsheet and formulas).

Appendix B

Intermediate Scenario

Results for the intermediate scenario and Case A and B are depicted in Fig. B.1.

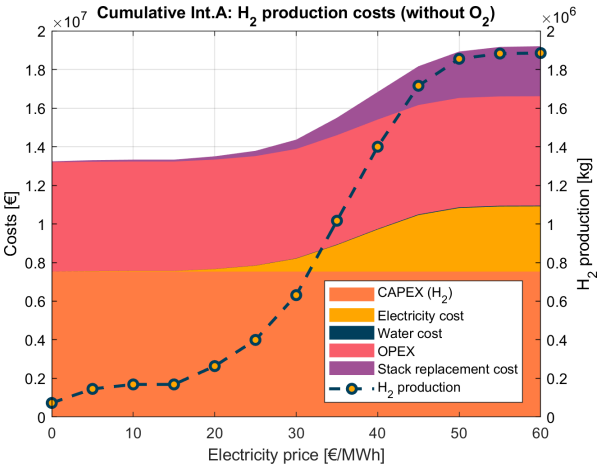

(a) Case A: Cumulated production costs (€) and quantity of produced H_2 (kg).

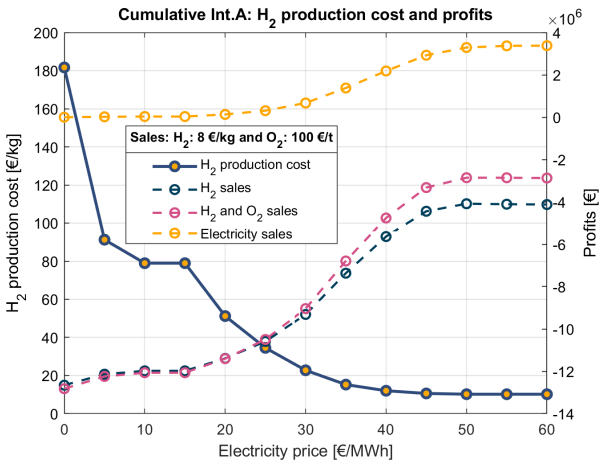

(b) Case A: H_2 specific cost and profits by selling H_2, H_2 and O_2 or electricity to the grid.

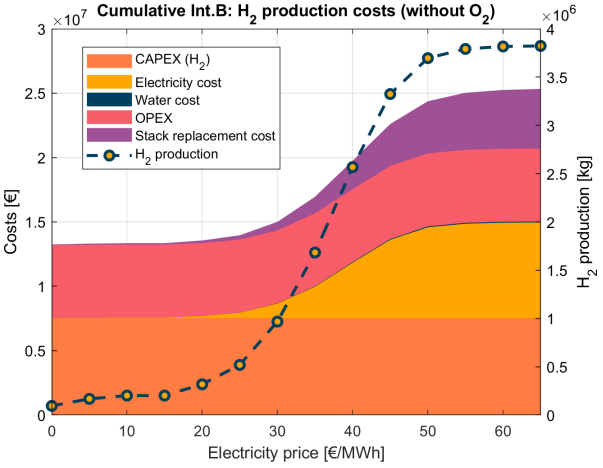

(c) Case B: Cumulated production costs (€) and quantity of produced H_2 (kg).

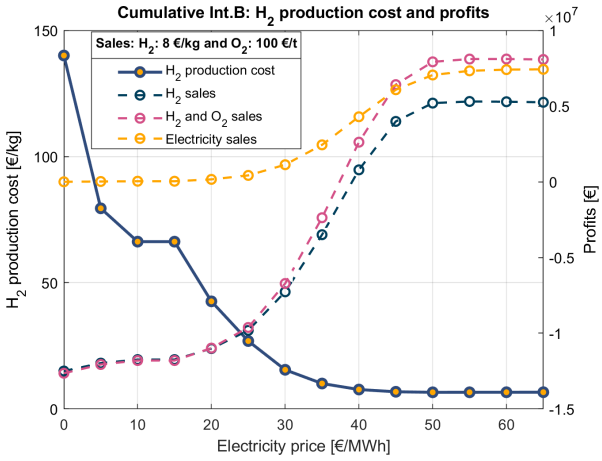

(d) Case B: H_2 specific cost and profits by selling H_2, H_2 and O_2 or electricity to the grid.

Figure B.1: H_2 production analysis for the intermediate scenario and both cases.

In Case A, the minimum H_2 production cost is 10.18 €/kg. In Case B, the minimum of 6.59 €/kg is achieved. These values do not include O_2 production.